UNIVERSITÀ
DEGLI STUDI
DI PADOVA

Sede Amministrativa: Università degli Studi di Padova
Dipartimento di Processi Chimici dell'Ingegneria

SCUOLA DI DOTTORATO DI RICERCA IN INGEGNERIA INDUSTRIALE
INDIRIZZO: INGEGNERIA METALLURGICA
XXIII° CICLO

INNOVATIVE STEELS FOR STRUCTURAL AND CORROSION RESISTANCE APPLICATIONS

ACCIAI INNOVATIVI PER APPLICAZIONI STRUTTURALI E RESISTENTI ALLA CORROSIONE

Direttore della Scuola: Ch.mo Prof. Paolo F. Bariani
Coordinatore d'indirizzo: Ch.mo Prof. Maurizio Magrini
Supervisore: Ch.mo Prof. Irene Calliari

Dottorando : Silvia Baldo

Gennaio 2010

PREFACE

The work presented in the present doctoral thesis has been carried out during three years full-time research and studies at the University of Padua from January 2008 to December 2010.
The experimental work was developed at the Department of Engineering's Chemical Processes (DPCI), Padua (Italy) under the main supervision of Professor Irene Calliari and Professor Emilio Ramous, and at the Department of Materials Science and Engineering (ATT) of the Budapest University of Technology and Economics (BME), Budapest (Hungary) in collaboration with Professor István Mészáros and Dr. János Dobránszky.

The thesis consists of an introductory part and a section including the following six published papers:

I. Analysis of phase stability in Cr-Ni and Cr-Mn DSS
I.Calliari, M. Pellizzari, S. Baldo, M. Zanellato, E. Ramous
Proceedings of Duplex World International Conference, Beaune (FR) 2010

II. Effect of Aging on the Fracture Behavior of Lean Duplex Stainless Steels
G. Straffelini, S. Baldo, I. Calliari, E. Ramous
Published in Metallurgical and Materials Transactions A (2009) v 40A, p 2617

III. Effect of cold rolling on microstructure and magnetic properties in a metastable lean duplex stainless steel
S. Baldo, I. Mészáros
Published in Journal of Materials Science (2010) v 45, p 5339-5346

IV. Effect of micro-alloying elements Nb and V on microstructural and mechanical properites of HSLA forming steels
M. Merlin, S. Baldo, G.L. Garagnani
Proceedings of 32° AIM National Conference, Ferrara 2008 (translated in English)

V. Fatigue characterization and fractographic analysis of a forming Nb-V alloyed HSLA steel
S. Baldo, M. Merlin
Proceedings of IGF Workshop, Forni di Sopra (Udine) 2009 (translated in English)

VI. ***The effect of braze-welding speed on the microstructure and mechanical properties of dual phase steel***
I. Rampin, M. Piazza, S. Baldo, A.F. Miranda Perez, K. Brunelli, I. Calliari, F.A. Reyes Valdès
Proceedings of Super-High Strength steels, International Conference, Peschiera del Garda (Verona), 2010

OTHER RELATED PAPERS AND ACTIVITIES NOT INCLUDED IN THE THESIS

In addition to the papers included in the thesis, further publications are listed below:

Trasformazioni strutturali di un duplex a basso nichel
S. Baldo, K. Brunelli, I. Calliari, M. Dabalà, L. Nodari, M. Zanellato, R.Bertelli
Proceedings of 32° AIM National Conference, Ferrara 2008

Analisi FEM dell'effetto dimensionale sulla precipitazione di fasi secondarie a raffreddamento in un acciaio inossidabile Duplex 2205
S. Baldo, M. Zanellato, I. Calliari
Proceedings of 22° AIM Heat Treatments National Conference, Salsomaggiore (Parma) 2009.

Different metallurgical methods to measure secondary phases precipitation in duplex stainless steels
Calliari, S. Baldo, M. Zanellato
Published on line, (2009) Icasi

Phase transformations in a Super Duplex Stainless Steel after isothermal and continuous cooling treatments
S. Baldo, M. Zanellato, I. Calliari
Presented in the oral session at European Congress and Exhibition on Advanced Materials and Processes EUROMAT, Glasgow (UK) 2009

Welding process parameters impact on the corrosion susceptibility of Advanced High Strenght Martensitic Steels (AHSS) used in the automotive industry
F.A. Reyes-Valdés, V.H. López-Cortéz, G.Y. Pérez-Medina, V. García-Custodio, I. Calliari, S. Baldo, K. Brunelli
Proceedings of the IIVV International Congress in Central and East Europe Region, High Tatra (SK) 2009

Caratterizzazione magnetica e micro strutturale dell'acciaiao duplex 2101 dopo deformazione a freddo
S. Baldo, G. Fassina, I. Calliari, E. Ramous, I. Meszaros,
Presented in the poster session at the 33° AIM National Conference, Brescia 2010

Phase transformation in 2101 DSS after cold rolling
S.Baldo, I.Calliari, M. Zanellato, and I. Mészáros
key-note lecture at the Duplex World International Conference, Beaune (FR) 2010.

The following M.S thesis have been supervised:

G. Fassina, ***Effects of cold rolling on austenite to α'-martensite transformation in 2101 lean duplex stainless steel***, supervisors: I. Calliari, I. Mészáros, S. Baldo, A.A. 2009-2010

M. Piazza, ***Piastre di acciaio Dual Phase saldo brasate: effetto della velocità di saldatura sulle caratteristiche microstrutturali***, supervisors: I. Calliari, S. Baldo, I. Rampin, A.A. 2009-2010

Moreover, in November 2010 she obtained the 'Felice De Carli' Prize for young metallurgists published by The Italian Association of Metallurgy (AIM).

CONTENTS

SUMMARY

The attention towards innovative steels at limited cost increased significantly in the last years. The research focused mainly in the development of new high strength steels where a combination of elevated mechanical properties, good formability and weldability is required and of duplex stainless steels if high corrosion resistance and mechanical properties are demanded. The possibility to design new light components thanks to the higher strength of such steels, the substitution of expensive raw elements and the new specific production processing have permitted to achieve a global costs saving. However a deep knowledge about the critical aspects of these two classes of steels is of fundamental importance to avoid problems in service and eventually catastrophic failures.

The aim of this study was to analyze the effects of metallurgical features and phase transformations on the properties of duplex stainless steels (DSS), high strength low alloy (HSLA) steels and advanced high strength dual phase (DP) steels. A detailed review on the state of art of the innovative steels considered has been carried out.

The experimental work has been organized into two sections dealing with the critical aspects of duplex stainless steels and high strength steels.

In the section concerning DSS, an overall study about secondary phase precipitation occurring during heat treatments of different DSS grades was performed. Then a deeper investigation on lower alloyed DSS, the so called Lean DSS, and their behavior was analyzed. In particular a relation between the morphology of intermetallics precipitation and the fracture toughness was found and compared for two Lean DSS. To reduce the costs, strong austenite phase stabilizers such as Ni are substituted with less stabilizing element as Mn, leading to a certain austenite phase (γ) instability which eventually transforms into ferromagnetic lath martensite (α') during plastic deformation. This phase transformation can potentially affect the properties of the material. Therefore the possible $\gamma \rightarrow \alpha'$ evolution during cold rolling was evaluated mainly through magnetic and X-ray diffraction techniques.

The second section focused on the influence of microstructure on the mechanical properties and weldability of high strength and advanced high strength steels. Fatigue behavior and weldability are of extreme importance in these two types of steels, especially if designed for structural automotive applications. Hence the role of microllaoying elements and thermo-mechanical processing on fatigue properties and fracture was revealed for different micro-alloyied HSLA steels, whereas the influence of braze-welding parameters on microstructural and mechanical properties was highlighted in a DP steel.

SOMMARIO

Nel corso degli ultimi anni la ricerca si è focalizzata sulla messa a punto di acciai innovativi a costo contenuto. Grande interesse è stato posto sullo sviluppo di nuovi acciai alto resistenziali in grado di avere una buona combinazione di elevate proprietà meccaniche, formabilità e saldabilità, e sullo sviluppo di acciai inossidabili bifasici nelle applicazioni richiedenti alta resistenza a corrosione e proprietà meccaniche. Inoltre la possibilità di progettare con materiali più leggeri, grazie all'elevata resistenza meccanica che presentano, il risparmio dovuto alla sostituzione di elementi costosi e all'utilizzo di nuovi processi produttivi hanno permesso una riduzione globale dei costi. Al fine di evitare problemi in esercizio con eventuali rotture catastrofiche si è resa necessaria una approfondita conoscenza degli aspetti critici di queste tipologie di acciai di ultima generazione, considerato il potenziale ampio utilizzo di tali materiali anche in applicazioni di uso comune.
L'obiettivo di questa tesi è di analizzare gli effetti da un punto di vista metallurgico sulle proprietà principali caratterizzanti gli acciai inossidabili Duplex (DSS), gli acciai basso legati ad alto limite di snervamento (HSLA) e gli acciai alto resistenziali avanzati Dual Phase. Per una maggiore completezza della ricerca e una migliore interpretazione dei risultati ottenuti nello studio sperimentale è stata condotta una dettagliata ricerca bibliografica sullo stato dell'arte delle categorie di acciai considerati.
Il lavoro sperimentale è stato diviso in due parti nelle quali sono stati messi in luce gli aspetti critici degli acciai inossidabili duplex e degli acciai alto resistenziali.
La sezione riguardante gli acciai inossidabili duplex comprende uno studio completo sui fenomeni di precipitazione di fasi secondarie che hanno luogo durante trattamento termico di diverse tipologie di tali acciai. In una fase successiva lo studio si è concentrato sui cosiddetti "Lean" Duplex, caratterizzati da un minore contenuto di elementi in lega. In particolare è stata rilevata una certa relazione tra la presenza e distribuzione di fasi infragilenti e le proprietà di tenacità di due acciai inossidabili "Lean" Duplex. Negli acciai "Lean" Duplex il contenuto di elementi costosi e volatili quali il Ni è ridotto per mantenere contenuto il loro costo. Il Ni viene sostituito principalmente dal Mn, avente tuttavia un minore potere stabilizzante nei confronti della fase austenitica (γ), che potenzialmente può evolvere in "lath" martensite ferromagnetica (α') con la deformazione a freddo. L'introduzione di questa nuova fase nel materiale può indurre cambiamenti nelle proprietà del materiale stesso. Pertanto la possibile trasformazione $\gamma \rightarrow \alpha'$ in seguito a laminazione a freddo è stata valutata mediante misure magnetica e diffrazione a raggi X.
La seconda parte del lavoro è stata incentrata sull'influenza della microstruttura sulle proprietà meccaniche e di saldabilità di acciai alto resistenziali. Le proprietà a fatica e la saldabilità sono di estrema importanza in questa classe di acciai, specialmente se destinati ad applicazioni nel campo auto motive. È stato quindi analizzato il ruolo che gli elementi microalliganti e gli specifici trattamenti termo meccanici rivestono sulle proprietà a fatica e sul relativo meccanismo di frattura in diverse tipologie di acciai HSLA. Inoltre sono stati valutati gli effetti della variazione dei parametri di saldobrasatura sulle proprietà microstrutturali e meccaniche di un acciaio DP.

PART 1

INTRODUCTION

1. GENERAL INTRODUCTION

The development of innovative steels in common applications, imposed by the financial crisis of the last years, is focused on costs reduction in terms of quantity of employed material, chemical composition and life cycle of the product. The growing use of high strength steels (HSS) and advanced high strength steels (AHSS), mainly in construction and automotive fields, and the use of duplex stainless steels (DSS) in applications where resistance corrosion and good mechanical properties were required, induced the technological and scientific research towards a deeper investigation about these classes of steels. One of the first targets to limited the costs was the "light" design. Therefore materials with high mechanical properties were realized in order to reduce the gauge section, without loss in safeness. This allowed a lightening of constructions and components, permitting an economic saving in the materials use and, concerning with automotive applications, in fuel consumption.

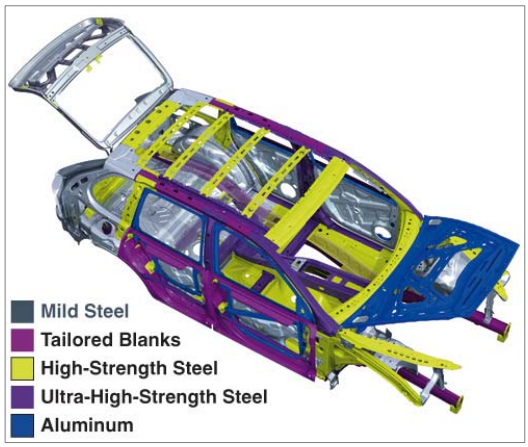

Fig. 1a. HSS and AHSS example of application
Source: www.i-car.com

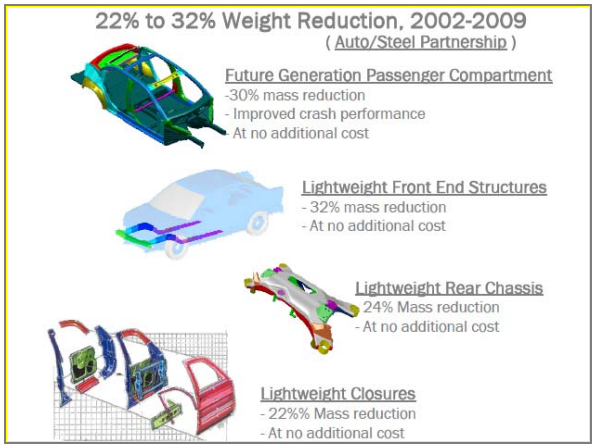

Fig. 1b. HSS and AHSS weight reduction
Source: www.autosteel.org

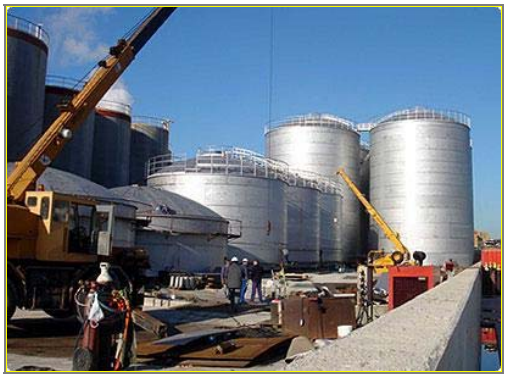

Fig. 2a. DSS example of application
Source: www.outokumpu.com

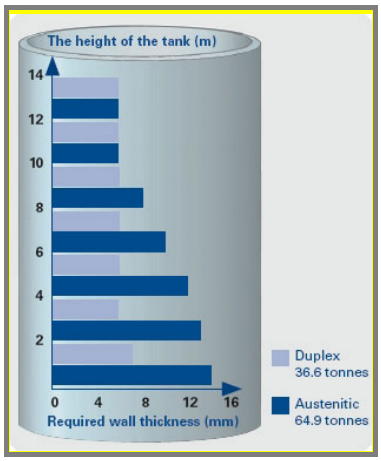

Fig. 2b. DSS weight reduction
Source: www.outokumpu.com

The strict control of chemical composition was another important aspect. The high fluctuation of elements such as Nickel, those market value is anyway high, and Cr-Fe alloys induced their substitution with less expensive elements with comparable metallurgical effects, leading to the development of new or modified alloys.

Fig. 3a. Ni price and fluctuations
Source: www.metalprice.com

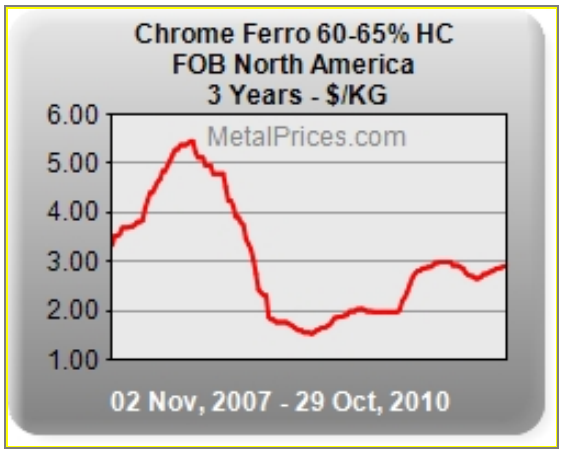

Fig. 3b. Cr-Fe alloy price and fluctuations
Source: www.metalprice.com

Moreover in the last years the concept of life cycle assessment (LCA) increased in importance. It considered not only the product realization charges but also the maintenance and eventually disposal ones. Hence an overall and more likely costs analysis was possible. Both high strength and duplex stainless steels, even if very different ones from each others, are examples of technological innovation which takes in account the economical aspects above mentioned. This became absolutely necessary due to the large area of applications covered by these categories of steels.

In some applications high strength steels and duplex stainless steels can be competitive. A typical field where both the steels are involved is the automotive sector. In this case innovative structural stainless steels assure equal or higher mechanical properties than structural carbon steels (e.g. TRIP/RA, DP), offering a pronounced increase in corrosion resistance and aesthetic quality. This new class of stainless steels are more expensive than carbon advanced high strength steels, but the replacement of expensive elements with cheaper ones could be a promising solution to decrease the total price.

Finally the production and applications of such alloys are doomed to increase in the next years, as it is noticeable by the forecast concerning the use of HSS and AHSS in the automotive field and by the forecast of the general use of stainless steels in which Ni is progressively substituted.

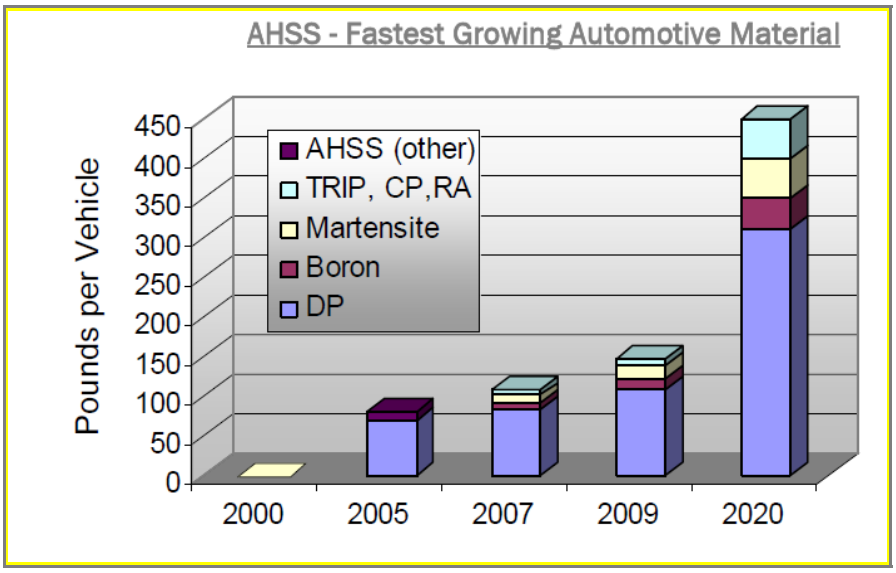

Fig. 4a. HSS and AHSS trend and forecast
Source: Ducker Worldwide

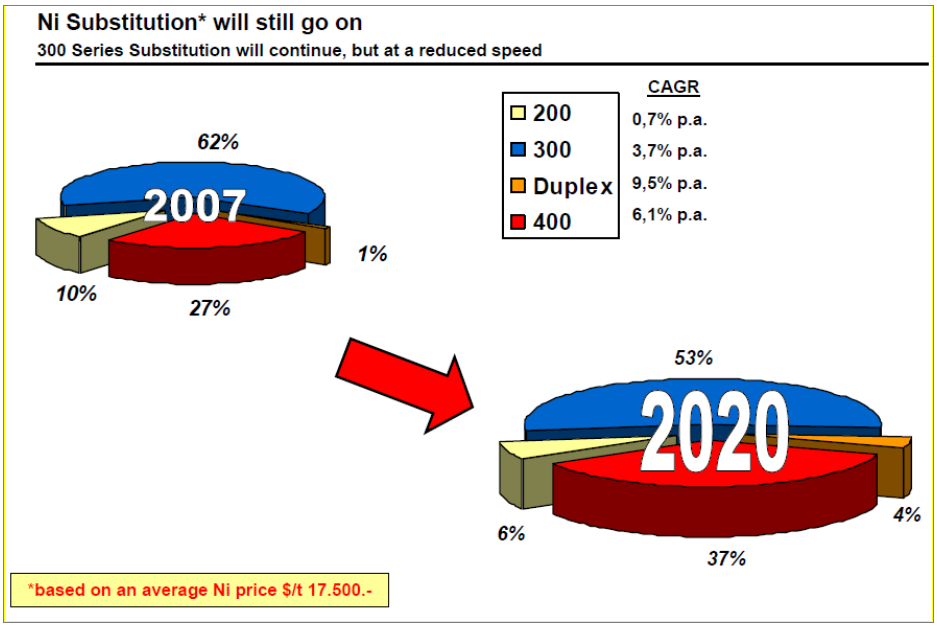

Fig. 4b. Stainless steels trend and forecast
Source: "Outlook for the stainless steel world market", M.A.Moll, Feinox 2008 Conference, Sao Paulo, Brazil

2. SECTION I. DUPLEX STAINLESS STEELS

2.1 HISTORICAL PERSPECTIVE AND CLASSIFICATION

2.1.1 General Introduction

Duplex stainless steels (DSS) are a particular category of stainless steels characterized by a biphasic microstructure with about equal proportions of austenite and ferrite.

The combination of properties, including high strength and excellent resistance to corrosion and chloride stress corrosion cracking (SCC), made DSS very attractive for many purposes.

The mixed ferrite/austenite microstructure leads to different advantages if compared with the unique structure of the austenitic and ferritic stainless steels. In fact, DSS show more toughness than most ferritic grades, improved SCC resistance than most austenitic grades, and higher strength than most grades of either type. DSS are also less expensive than austenitic stainless steels with similar corrosion resistance, due to a lower nickel content.

Moreover DSS optimize some other specific features proper of austenitic and ferritic stainless steels. Austenitic stainless steels have good weldability and low-temperature toughness, whereas their chloride SCC resistance and strength are comparatively poor; while ferritic stainless steels show opposite trend about chloride SCC but have poor toughness, especially in the welded condition. Therefore a duplex microstructure can emphasize some aspects better than others choosing an appropriate phase balance. For what concerns welding characteristics, DSS are more sensitive to minor variations in chemical composition or processing than are austenitic stainless steels.

Nowadays duplex stainless steels comprise almost 1% of all stainless steels production, however their sector is continuously growing. Some statistics reported the trend of DSS market during the last years. Research from the ISSF reveals that production increased from 6,000 metric tonnes a month in 2004 to 10,000 by 2005, and in 2008 reached 22,000. It is especially interesting to compare the standard grade, 2205, with the lean duplexes. Although production of grade 2205 increased in absolute terms, its market share decreased from around 67% in 2004 to around 47-48% in 2007-8. By contrast the market share of lean grade S32304, which was about 5% in 2006, grew up to 13% in 2007 and to 17% in 2008. The two super duplexes S32750 (SAF 2507) and S32760 (ZERON® 100) production remained more or less stable and always lower than 5% [1]. Even Gagnepain revealed the growth in DSS market, especially concerning with new grade DSS, as reported in fig.1 [2]. Lean duplex stainless steels seem to be the most attractive DSS in the recent years. The expansion of these DSS belongs to the lower content of expensive and volatile elements like nickel and molybdenum, without strong loss in corrosion resistance. In particular lean duplex grades have similar corrosion resistance properties of the common austenitic stainless steel 316L, but have a higher yield strength, permitting weight saving. Besides cost and strength-to-weight advantages, resistance to stress corrosion cracking is another important feature for lean DSS success. For these reasons they are used in many applications field including process industries, offshore, pulp and paper, desalination and other new segments such as biofuels, architecture and (waste)water [1].

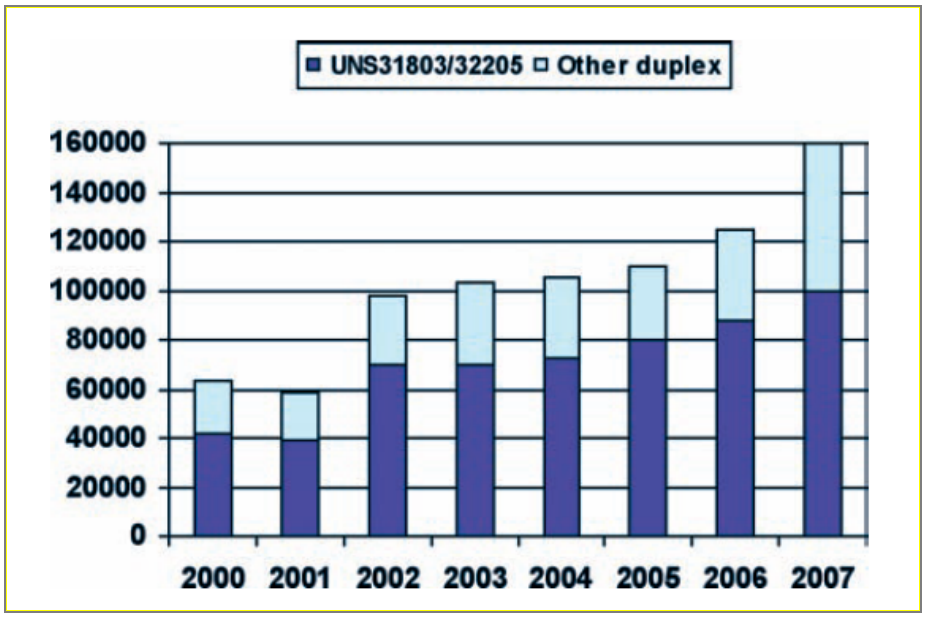

Fig. 5. Crude productions of duplex stainless steel according to global markets [2]

2.1.2 Historical Evolution

Duplex stainless steels have existed for more than 70 years [3].The first information to appear about DSS was the development of a two-phase stainless alloy by Bain and Griffith in 1927 [4]. The first commercial DSS, named 453E and whose chemical composition was about 25%Cr-5%Ni, seems to be made in 1929 by Avesta Jernverk [5].

Then duplex stainless steels in cast form were produced in Sweden in 1930 and were used in the sulfite paper industry [6]. These grades were developed to reduce the intergranular corrosion problems in the early high-carbon austenitic stainless steels. Duplex castings were produced also in Finland since 1930. In 1932 and 1933 a new DSS with modified 25%Cr-5%Ni-1%Mo composition was introduced under the name of 453S grade. Again in 1933 an error occurred during the melting of a 18%Cr-9%Ni-2.5%Mo grade at the Firminy works of the J. Holtzer Company in France led to a 20%Cr-8%Ni-2.5%Mo biphasic stainless steel [7]. This was an important discovery as the new steel, characterized by a high volume fraction of ferrite, was less sensitive to intergranular corrosion, caused by carbide precipitation, compared with high carbon austenitic grades [8-10]. Moreover it was found that a balance of ferrite and austenite had better resistance to chloride stress-corrosion cracking than a fully austenitic microstructure. One of the first duplex grades developed specifically for improved resistance to chloride stress corrosion cracking (SCC) was 3RE60. The improved corrosion resistance in different environments and the higher strength of such DSS encouraged French research [11]. A patent was granted in France in 1936 for the forerunner of the modern Uranus 50. In France, the UR 50 grade with 20-35% ferrite (UNS S32404) was marketed in different product for such industries as oil refinement, food processing, pulp and paper, and pharmaceutical. These steels were produced in high frequency induction furnaces using precisely weighed alloying additions. Partial vacuum ensured carbon removals, rudimentary de-oxidation and restricted nitrogen ingress [12]. However plate products remained sensitive to edge cracks [13]. AISI Type 329 became well established after World War II and was used extensively for heat

exchanger tubing for nitric-acid service. In subsequent years, both wrought and cast duplex grades have been used for a variety of processing industry applications including vessels, heat exchangers and pumps. These first-generation duplex stainless steels provided good performance characteristics but had limitations in the as-welded condition. The heat-affected zone (HAZ) of welds had low toughness because of excessive ferrite and significantly lower corrosion resistance than that of the base metal. These limitations confined the use of the first-generation duplex stainless steels, usually in the non-welded condition, to a few specific applications. The cost of DSS became relevant during and after the Korean war (1950-51), which imposed a nickel saving. Since these years DSSs with low nickel content were studied and developed. In order to improve toughness and ductility, the cast alloy CD4-MCu (UNS J93370, Tab. 1) marketed at the end of 1950s and containing about 70% of ferrite volume fraction was modified decreasing chromium content to 22-23% [14] and controlling carbon content (UNS S31500).

Standard 22% Cr											
J92205 (2205)	0.03	0.020	0.04	1.00	1.50	4.5–6.5	21.0–23.5	2.5–3.5	1.00	0.10–0.30	–
J93183 (KCR-D183)	0.03	0.03	0.040	2.0	2.0	4.0–6.0	20.0–23.0	2.0–4.0	1.0	0.08–0.25	0.5–1.5 Co
High alloy											
J93345 (Escoloy)	0.08	0.025	0.04	–	1.00	8.0–11.0	20.0–27.0	3.0–4.5	–	0.10–0.30	–
J93370 (CD-4MCu)	0.04	0.04	0.04	1.00	1.00	4.75–6.00	24.5–26.5	1.75–2.25	2.75–3.25	–	–
J93371 (3A)	0.06	0.040	0.040	1.00	1.00	4.00–6.00	24.0–27.0	1.75–2.50	2.75–3.25	0.15–0.25	–
J93372 (CD-4MCuN)	0.04	0.04	0.04	1.0	1.0	4.7–6.0	24.5–26.5	1.7–2.3	2.7–3.3	0.10–0.25	–
J93550 (KCR-D283)	0.03	0.03	0.040	2.0	2.0	–	23.0–26.0	5.0–8.0	1.0	0.08–0.25	0.5–1.5 Co
Superduplex											
J93380 (Zeron 100)	0.03	0.025	0.030	1.0	1.0	6.5–8.5	24.0–26.0	3.0–4.0	0.5–1.0	0.2–0.3	0.5–1.0W
J93404 (Alloy 958)	0.03	–	–	1.00	1.50	6.0–8.0	24.0–26.0	4.0–5.0	–	0.10–0.30	–

The chemical compositions listed are for information puposes only.
After 'Metal and Alloys in the Unified Numbering System', SAE/ASTM, September 1996.
Values are maxima unless range given.

Tab. 1. Common cast DSS grades listed in the Unified Numbering System [5]

During the late 1960s and early 1970s a further nickel shortage happened, strongly enhancing the price of austenitic steels. Moreover stainless steels with excellent corrosion properties in severe environment were required by the offshore oil industry in continuous expansion. The success of DSS grew in these circumstances, also thanks to the new improved steel production techniques with the introduction of the vacuum and argon oxygen decarburization (VOD and AOD) practices, allowing to produce much cleaner steels with a very low carbon level and well controlled nitrogen content. Moreover the improved hot workability and rolling, together with the introduction of continuous casting process in stainless steel production, [5], permitted the production of sheets and coils of many different size at lower cost and higher quality.

Since 1970 the addition of nitrogen and lowering of carbon content improved corrosion resistance austenite stabilization during welding process, being HAZ particularly sensitive to phase balance [15].

Finally the commonly known modern engineering duplex stainless steels were marketed in the early 1980s.

Modern Developments

Today the most common duplex grade is UNS S31803/S32205 (EN 1.4462) or commercially named 2205, characterized by a nominal chemical composition of 22% Cr, 5%Ni, 3% Mo, and 0.16% N. This steel is used for a wide area of applications. The 2205 alloy is a nitrogen enhanced duplex stainless steel alloy. The DSSs of the previous generation showed quite good resistance to general corrosion and chloride stress-corrosion cracking. Different behavior were revealed for the same alloys in the welded conditions, where corrosion resistance became critical.
The 2205 DSS provides corrosion resistance superior to that of AISI Type 304, 316 and 317 austenitic stainless steels in various media. 2205 DSS is commonly used as welded pipe and welded sheet product as well as tubular components for applications in environments where resistance to general corrosion and chloride stress corrosion cracking are important. Moreover 2205 DSS has higher mechanical properties than austenitic stainless steels, leading to a reduction in tube wall thickness and consequently in weight. However the cost of 2205 DSS still remained quite high.

Recently some new duplex grades have been introduced in the market following the aim to reduce alloying elements than 2205 grade and to maintain comparable corrosion resistance of the 304 and 316 austenitic stainless steels. For applications in more aggressive environments Mo, Cu and W alloying elements are added. The development of lean duplex with higher content of N and Mn to replace part of the expensive Ni, can certainly improve the progress of the duplex steels since it is possible to retain quality and reduce material cost. With this purpose Bergstrom *et al*. [16] proposed an economical alternative to the common 2205 DSS with lower alloy content, particularly nickel and molybdenum. Bergstrom's duplex stainless steel exhibits mechanical properties and resistance to pitting/crevice corrosion similar to 2205 DSS. Table 2 reports the main corrosion and mechanical properties of the new duplex steel created under the US Patent No. 6551420 B1 [16] in comparison with pre-existing stainless steels.

Alloy	Chemical Comp. (wt. %)		PCR	SCC	Mechanical Properties		
	Ni	Mo	CPT	CSCC	0.2 % PS	TS	El (%)
2205	4.5-6.5	2.5-3.5	35°C	20°C	450 MPa	620 MPa	25
Type 304*	8-10.5	--	--	-2.5°C	205MPa	515 MPa	40.0
Type 316*	10-14	2-3	15°C	-3°C	205 MPa	515 MPa	40.0
Type 317*	11-15	3-4	19°C	2°C	206 MPa	517 MPa	35.0
US6551420B1[a]	3.0 - 4.0	1.5 - 2.0	31°C	**	572 MPa	786 MPa	37

PCR: Pitting Corrosion Resistance; CPT: Critical Pitting Temperature (ASTMG-48A); CCCT: Crevice Corrosion Critical Temperature (ASTM G48B); 0.2%PS: 0.2% offset Proof Strength; TS: Tensile Strength;
* ASTM minimum. ** Not specified in the patent. [a] Ref. [11].

Tab. 2. Corrosion and mechanical properties of the US Patent No. 6551420 B1 and other common stainless steels [6]

Commercial Name	International steel N		Typical chemical composition [wt%]					
	EN	***ASTM***	***C***	***N***	***Cr***	***Ni***	***Mo***	***Others***
4301	1.4301	304	0.04	0.04	18.1	8.3	-	-
4404	1.4404	316L	0.02	0.04	17.2	10.2	2.1	-
4436	1.4436	316	0.04	0.05	16.9	10.7	2.6	-
904L	1.4539	N08904	0.01	-	20	25	4.3	1.5 Cu
2205	1.4462	S32205	0.02	0.17	22	5.7	3.1	-
SAF 2304®	1.4362	S32304	0.02	0.10	23	4.8	0.3	-
LDX 2101®	1.4162	S32101	0.03	0.22	21.5	1.5	0.3	5 Mn

Tab. 3. Chemical composition of the recent lean duplex stainless steels compared to other common stainless steels

An overview about lean DSS was presented by Alfonsson [17]. He focused especially on the main characteristics and applications of this new class of DSS.
Parallel to lean DSSs, higher alloyed DSS, the so called hyper duplex (HDSS) have been recently developed for long life and high temperatures applications or when a combination of excellent corrosion resistance and extra high strength are needed. Two examples of new advanced DSS are SAF 2707 HD and SAF 3207 HD- These alloys have nitrogen contents up to 0,5% and PRE-values close to 50. The new grades show both highest corrosion pitting resistance or highest critical pitting corrosion temperature CPT and highest strength among the existing modern DSS [18]. Other HDSS are reported in Tab. 4.

Alloy (USA)	Chemical Composition [wt%]							
	Cr	***Ni***	***Mo***	***N***	***Cu***	***Mn***	***Others***	***PREN***
S32906	29	6	2	0.4	0.5	1	-	42
S32707	27	7	5	0.4	0.3	1	0.76	50
S33207	30	8	4	0.5	1	1	-	51

Tab. 4. Chemical composition of recent hyper duplex stainless steels

The duplex family is now an industrial success and represents about 1% of the total stainless steel market. An annual growth of more than 10% is expected [19]

2.1.3 Classification

The modern duplex stainless steels can be divided into four groups:

- lean duplex as 2304 or as 2101, with 0.05-0.6 wt% of Mo.
- 2205, the most common grade which covers more than 80% of duplex use
- 25Cr duplex as Alloy 255 and DP-3
- superduplex, with 25-26 Cr and increased Mo and N compared with the 25 Cr grades, including grades such as 2507, Zeron 100, UR52N+, and DP-3W.

Tab. 5 shows the chemical composition of the modern wrought duplex stainless steels and includes also the first generation of duplex stainless steels as a point of reference.

Another way to classify DSS is to define the corrosion resistance of duplex grades by their pitting resistance equivalence number [5] (PREN) as defined by Eq. 1:

PREN = %Cr + 3.3%Mo + 16%N (1)

PREN does not provide an absolute value for corrosion resistance and is not applicable in all environments, it does provide an overview of the expected resistance to pitting corrosion in an aqueous chloride media. In some DSS the addition of W can increase corrosion resistance.

For these alloys, the pitting resistance is expressed as PREW, according to Eq. 2:

PREW = %Cr+3.3%Mo+1.65%W+16%N (2)

The PREN or PREW number is commonly used to classify the family to which an alloy belongs. In general, materials having a pitting resistance number in the low 30's or lower are classified as lean duplex grades, those with PRE's in the mid 30's such as 2205, are classified as standard duplex, and those with PRE's of 40 or more are known as superduplex stainless steels [20].

In Tab. 6 are summarized some examples of different stainless steels grades, i.e. duplex, austenitic and superaustenitic grades with their main alloying components and the PREN/W number. The superduplex grades with a pitting index PREN/W >40, contain 25% Cr, 6.8% Ni, 3.7% Mo and 0.27% N, with or without Cu and/or W additions (SAF 2507, UR52N, DP3W, Zeron100).

Grade	UNS	EN	C	Cr	Ni	Mo	Mn	N	Cu	W
First generation DSSs										
329	S32900	1.4460	0.08	23.0-28.0	2.5-5.0	1.0-2.0	1.0	not-defined	23.0-28.0	2.5-5.0
3RE60	S31500	1.4417	0.03	18.0-19.0	4.3-5.2	2.5-3.0	1.2-2.0	0.05-0.10	18.0-19.0	4.3-5.2
UR50	S32404		0.04	20.5-22.5	5.5-8.5	2.0-3.0	2.0	–	1.00-2.00	–
Modern DSSs										
2304	S32304	1.4362	0.03	21.5-24.5	3.0-5.5	0.0-0.6	2.5	0.05-0.20	–	–
2205	S31803	1.4462	0.03	21.0-23.0	4.5-6.5	2.5-3.5	2.0	0.08-0.20	–	–
2205	S32205	1.4462	0.03	22.0-23.0	4.5-6.5	3.0-3.5	2.0	0.14-0.20	–	–
DP-3	S31260		0.03	24.0-26.0	5.5-7.5	5.5-7.5	1.0	0.10-0.30	0.20-0.80	0.10-0.50
UR52N	S32520	1.4507	0.03	24.0-26.0	5.5-8.0	3.0-5.0	1.5	0.20-0.35	0.50-3.00	–
255	S32550	1.4507	0.04	24.0-27.0	4.5-6.5	2.9-3.9	1.5	0.10-0.25	1.50-2.50	–
DP-3W	S39274		0.03	24.0-26.0	6.8-8.0	2.5-3.5	1.0	0.24-0.32	0.20-0.80	1.50-2.50
2507	S32750	1.4410	0.03	24.0-26.0	6.0-8.0	3.0-5.0	1.2	0.24-0.32	0.50	–
Zeron100	S32760	1.4501	0.03	24.0-26.0	6.0-8.0	3.0-4.0	1.0	0.20-0.30	0.50-1.00	0.50-1.00

Tab. 5. Chemical composition of modern wrought DSS compared to first generation DSS [6]

Grade	UNS	C	Cr	Ni	Mo	W	Cu	N	$PRE_{N/W}$
Lean Duplex	S32101	0.03	21.5	1.5	0.3	-	-	0.22	25
	S32304	0.02	23	4	0.3	-	0.3	0.10	25
Standard Duplex	S31803	0.02	22	5.5	3.0	-	-	0.17	35
	S32205		22.5	5.8	3.2	-	-	0.17	36
Superduplex	S32750	0.02	25	7	4.0	-	0.5	0.27	43
	S32760	0.03	25	7	3.5	0.6	0.5	0.25	42
Superaustenitic									
904L	N08904	0.02	20	24.5	4.2	-	1.5	0.05	35
254 SMO	S31254	0.02	20	18	6.1	-	0.7	0.20	43
Austenitic									
304L	S30400	0.02	18.2	8.1	0.3	-	-	0.07	20
316L	S21600	0.02	16.3	10.1	2.1	-	-	0.07	24
317L	S31703	0.02	18.4	12.4	3.2	-	-	0.07	30

Tab. 6. Chemical composition and PRE number of the most common DSS and austenitic stainless steels

2.1.4 Applications

The typical sectors where DSS find application are mainly oil production, petrochemicals and desalination plants. DSS are used in oil production industry thanks to their resistance in conditions of SCC and localized corrosion [21-23]. For this reason DSS are frequently used in oil-refinery heat exchangers where the exposition to chloride-containing process streams, cooling waters or deposits is consistent. Superduplex S32750 are suitable in crude distillation cases. In this case the corrosive conditions are severe and complex, due by the possible ammonium chloride deposits and overheating. Therefore more alloyed DSS are required to prevent the risk of premature failure. In hydrotreating, the main purpose is to remove sulfur from the intermediate and final refinery products. Modern DSS S31803 and S32304 showed good performances avoiding corrosion failure for some years. This is mainly attributed to the use of advanced welding procedures introducing N in the shielding gas, lowering the risk for excessive ferrite in the welds. In general in petrochemical industry applications corrosion environments are less aggressive than the ones observed in oil refineries [21]. However the production of organic acids can cause corrosion problems, so duplex and superduplex, especially DSS S32803 / S32205 and S32750 were found to be suitable materials for such applications. DSSs are also used in desalination plants [24]. However, the high cost of alloying elements, such as nickel and molybdenum, has presented a need to look for more effective options. A solution to this problem could be the use of lean DSS. Specific DSS were developed for some critical media applications, like urea plants [25].

Since 2006 the application area covered by DSS became larger and larger. New usage fields were explored, thanks to product diversification. Recent statistic data states that traditional applications as oil and gas, offshore and petrochemical declines from 27% to 7%. There is a relative decline also in chemical, storage and transportation, while segments with increased market share include (waste)water (9% to 18%), construction and civil engineering (6% to 12%), power generation (1% to 7%) and other applications (presumably pulp & paper [26], ethanols, biofuels – 10% to 28%) [1].

DSS, and especially less expensive lean DSS, are of great interest also in lightweight automotive design. This is due to the advantageous combination of many

properties as corrosion resistance, surface quality, high strength and formability. Moreover high energy absorption in crash situation enhances the safe use this class of steels [27].
Lean DSS are also finding application in architecture, for example in bridges construction. Again the corrosion resistance, aesthetic quality, the load-bearing and weight saving properties of lean DSS are the key of their success.

2.2 PHYSICAL METALLURGY AND PROPERTIES

2.2.1 Solidification

A correct austenite/ferrite phase ratio is of extreme importance both for mechanical properties and corrosion resistance. The microstructure and, as consequences mechanical and corrosion properties, depends on the chemical composition and on the specific production process. A first approach to roughly predict the DSSs microstructure is given by Schaeffler-DeLong diagram, mainly used for stainless steel weldments and casting [28]. The diagram (Fig. 6) is based on the chemical composition. In particular Cr-equivalent elements are alloying elements stabilizer of ferritic phase, while Ni-equivalents are stabilizer of austenitic phase [28].

$$Cr - equivalent - Cr + Mo + 1.5Si + 0.5Nb\ [wt\%] \quad (1)$$

$$Ni - equivalent = Ni + 30(C + N) + 0.5Mn\ [wt\%] \quad (2)$$

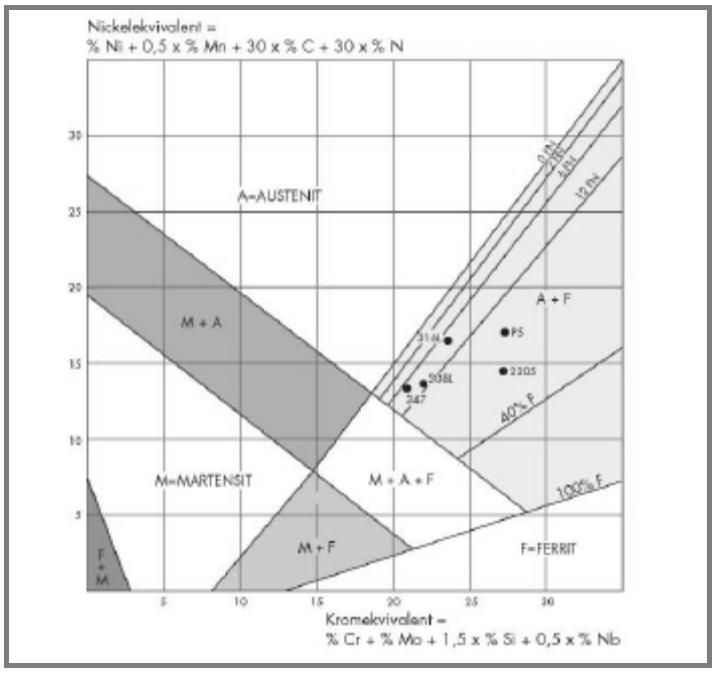

Fig. 6. Schaeffler-DeLong diagram

DSSs are usually characterized by almost the same amount of ferrite and austenite, which can be obtained by hot working followed by solution annealing and water quenching [29].

To study the DSSs solidification and solid phase transformation thermodynamic diagrams are used. The DSSs are based on the ternary Fe–Cr–Ni phase diagram (Fig. 7a).

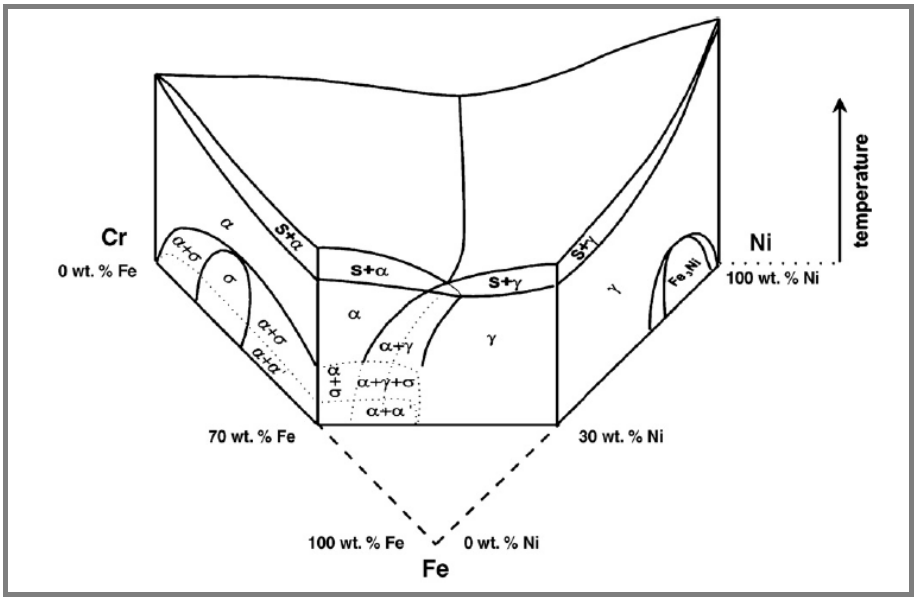

Fig. 7a. Ternary Fe–Cr–Ni phase diagram

The microstructural evolution is easier to analyze using a section of the ternary diagram. The section at 70% iron shows the quasi-binary phase diagram, representing the DSS (Fig. 7b) [30].

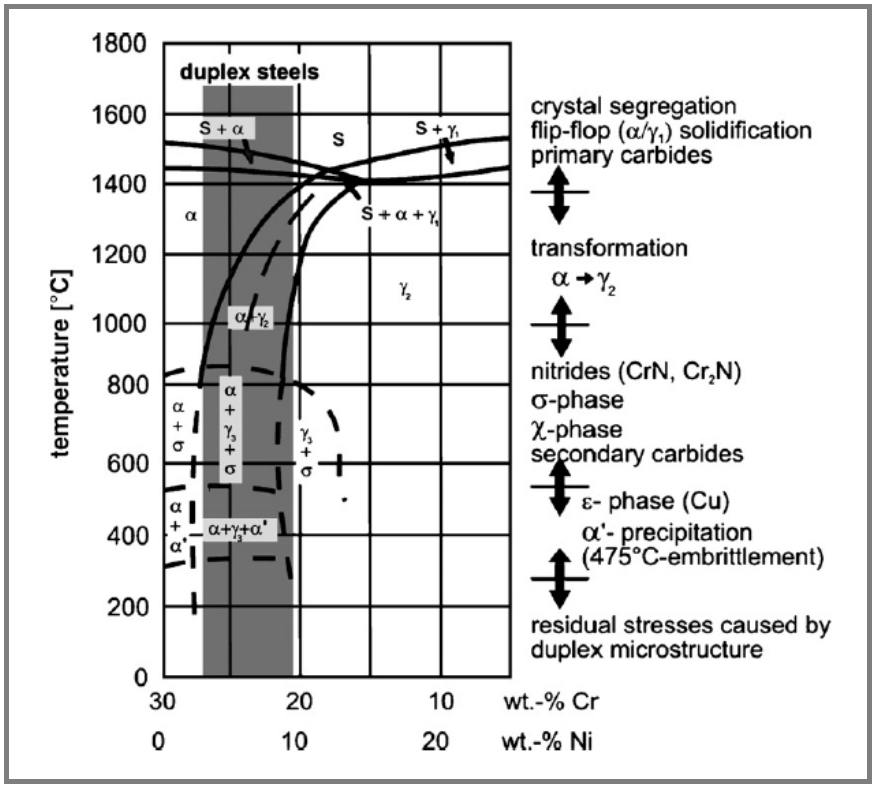

Fig. 7b. Quasi-binary phase diagram used for DSS

The DSS solidify ferritically. At lower temperature ferrite partially evolves to austenite by a solid state transformation. Therefore the phase balance can be modify at

temperature over 1000°C, depending to the content of alloying elements. As highlighted by the quasi-binary diagram, DSS are sensitive to complex precipitation phenomena, which are strictly connected with mechanical and corrosion properties.

2.2.2 Phase transformation

Many undesirable secondary phases can form during isothermal or improper heat treatments in the critical temperature range 300-1000°C [30]. The precipitation is mainly connected to the ferritic phase, due to the larger amounts of Cr and Mo, lower solubility of N and C and faster diffusion within the BCC lattice than austenitic phase. The decomposition of ferrite leads to the formation of many different secondary phases, as σ phase, , χ phase, carbides M_7C_3 and $M_{23}C_6$, nitrides Cr_2N and CrN, secondary austenite, *R* phase, *π* phase and spinodal decomposition in the range of 300-500°C [30-32].Typical phase precipitation diagrams of different DSSs grades are presented together with the effect of some alloying elements in Fig 8**.** Secondary phases precipitation are favoured by higher Mo, Cr and W contents (*Paper I*, pp. 67-79).

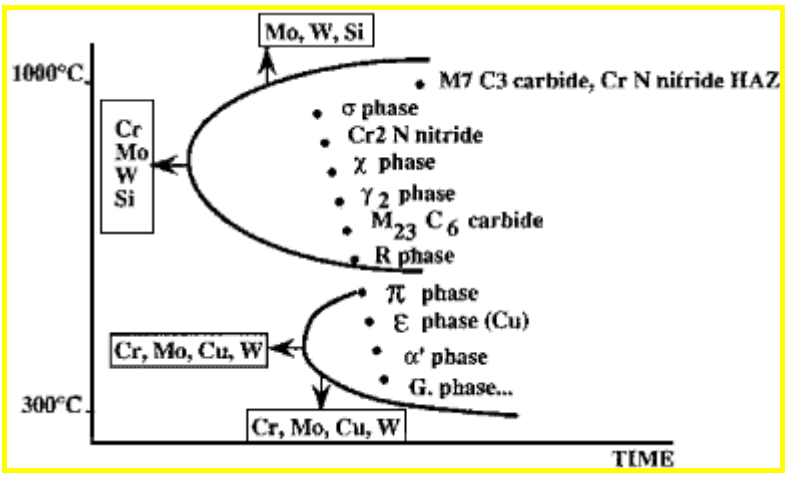

Fig. 8. TTT diagram and elements effect on secondary phases precipitation

Further details about temperatures precipitation, lattice parameters, crystal structure are reported in Tab. 7.

Type of precipitate	Nominal chemical formula	Temperature range in DSS, °C	Space group	Lattice parameter, nm	Ref.
Ferrite (δ)	...	...	*Im*3*m*	$a = 0{\cdot}286–0{\cdot}288$	...
Austenite (γ)	...	...	*Fm*3*m*	$a = 0{\cdot}358–0{\cdot}362$	...
σ	Fe–Cr–Mo	600–1000	$P4_2/mnm$	$a = 0{\cdot}879$, $c = 0{\cdot}454$	16
Chromium nitride	Cr_2N	700–900	*P*31*m*	$a = 0{\cdot}480$, $c = 0{\cdot}447$	17
Chromium nitride	CrN	...	*Fm*3*m*	$a = 0{\cdot}413–0{\cdot}447$	...
χ	$Fe_{36}Cr_{12}Mo_{10}$	700–900	*I*43*m*	$a = 0{\cdot}892$	18
R	Fe–Cr–Mo	550–650	*R*3	$a = 1{\cdot}090$, $c = 1{\cdot}934$	19
π	$Fe_7Mo_{13}N_4$	550–600	$P4_132$	$a = 0{\cdot}647$	20
τ	ND	550–650	*Fmmm*	$a = 0{\cdot}405$, $b = 0{\cdot}484$, $c = 0{\cdot}286$	21
M_7C_3	...	950–1050	*Pnma*	$a = 0{\cdot}452$, $b = 0{\cdot}699$, $c = 1{\cdot}211$	22
$M_{23}C_6$	...	600–950	*Fm*3*m*	$a = 1{\cdot}056–1{\cdot}065$	23

ND not determined.

Tab. 7. Lattice parameters and critical temperature range of phases precipitation in DSS [33]

Sigma (σ) phase is the most investigated intermetallic phase as it can precipitate in high volume fractions thus strongly affecting mechanical and corrosion properties [34-37]. Super duplex stainless steels with high additions of Cr and Mo are most prone to sigma precipitation. Quantitative chemical analysis has, in fact, revealed that σ phase is rich in chromium, molybdenum, and silicon [37].
The typical temperature range for sigma phase precipitation is between 600 and 1000 °C. However the fastest precipitation rate can be found between 850 and 900 °C [38,39]. The mechanism of precipitation is a eutectoid transformation of ferrite into austenite and sigma phase. Sigma phase usually nucleates at grain ferrite-ferrite grain boundaries and triple points, growing into ferritic grains. The morphology of sigma phase was found to change depending on transformation temperature: from a coral-like shape at lower precipitation temperatures of 750 °C to bigger and more compact structure at higher temperatures [40].
Sigma precipitation phenomenon can be modify by solution annealing temperature. Increasing solution treatment temperature, the volume fraction of ferrite increases with a consequent elements dilution which permits to avoid high quantity of sigma phase till theoretically complete suppression [34,35].
The cooling rate is also an important factor, as if it increases the precipitation of sigma phase is hindered.

Chi (χ) phase precipitates at lower temperatures than sigma phase and it is often difficult to separate the detrimental contribute of each phase. Typical precipitation temperature range for χ phase is 700-900 °C [30] when diffusion is slower [41]. Moreover, χ contains larger amount of Mo [36]. Due to its high Mo content, the formation of the x phase is even more affected by the restriction of the time for diffusion; therefore, the x phase appears only during precipitation conditions with the longer time allowing diffusion: isothermal aging and the lowest cooling rates.
Some authors [42,43] suggest that χ particles could act as precursor of σ phase. It means that the former precipitation of χ phase can assist following σ phase precipitation that finally proceeds at expense of χ.

Nitrides (Cr_2N, CrN) precipitate in the range of temperature of 700-900 °C during rapid cooling or isothermal heat treatment in different form. Cr_2N nitrides formed from high solution temperature followed by fast cooling rate precipitated mainly intragranularly in elongated shape. While Cr_2N belonging to isothermal heat treatment in the range 700-900°C are intergranular [30].

Carbide ($M_{23}C_6$, M_7C_3). Carbide type $M_{23}C_6$ is the most common and precipitates at temperatures below 950°C, while M_7C_3 has higher precipitation temperature (950-1050°C). However the problems connected with carbides have almost completely be solved in modern duplex stainless steels due to the strong limitation and control in C addition [30].

Secondary austenite may form from ferrite decomposition through three different mechanisms [30]:

I. by the eutectoid reaction δ→σ+γ"
II. as WidmannsHitten precipitates
III. via a martensitic shear process.

Moreover it was find that local high carbides-nitrides precipitation cause a depletion in the surrounding ferrite grains that can evolve to secondary austenite. The secondary austenite is different from primary austenite not only for the different mechanisms of formation but also for the chemical composition. It was found that the secondary austenite has a higher Ni content and a lower Cr and Mo content compared to the primary austenite.

Other minor secondary phases

R phase has been observed in the super DSS SAF 2507 [44]. It is a phase rich in Mo and it forms in a temperatures range of 550-650°C.

Π phase, as R phase, has been found after isothermal heat treatments at 600°C. Both R phase and π phase contribute to embritt1ement and pitting corrosion in the DSSs heat treated at the critical precipitation temperatures.

The *spinodal decomposition of ferrite* in another type of embrittlement, which takes place at 475°C after long time [30]. It is connected to the decomposition of ferrite into two components: one richer in chromium and one richer in iron with a final increase in harndess and detrimental effect on toughness.

2.2.3 Mechanical properties

Many authors have studied the relation between mechanical properties and microstructure in DSS [45-48].
The yield strength of DSS is two- three times that of AISI 304 austenitic stainless steel. The higher strength properties are related to the presence of ferrite, which is, for the same interstitial content, stronger than austenite. However ferrite has also lower ductility. In the DSS the presence of ferrite is not the only reason for high strength properties. It has been found that DSS has stronger ferrite than those of common ferritic stainless steels. This is due to the smaller grain size in DSS that contributes to enhance the strength, according to Hall- Petch relation. The effect of both the volume fraction of ferrite and grain size was extensively analyzed by Floreen and Hayden [46].
Moreover in super DSS a further contribution to the total strengthening is given of solid solution hardening of substitutional elements as chromium and molybdenum, and of interstitial elements as nitrogen [30].
A comparison of the mechanical properties of four duplex grades can be found in Tab. 8 [31].

Grade	$R_{p0.2}$ [MPa]	R_m [Mpa]	A_5 [%]
2304 [31]	400	600	25
LDX 2101 [45]	450	650	30
2205 [31]	450	620	25
2507 [31]	550	795	15

Tab. 8. Mechanical properties of different DSS grades

Finally it was found that yield strength, tensile strength and hardness are improved after cold rolling, with a slight loss in elongation [31].

The fatigue strength of DSSs is directly related to the yield strength [47]. DSSs are, in the solution annealed condition, characterized by high fatigue crack propagation resistance with crack propagation micromechanism that are mainly ductile [48]. Hayden and Floreen [46] assessed the relation between grain size and fatigue strength, stating that better fatigue properties were reached with duplex structure than with single phase. In solution annealed DSSs the ferrite and the austenite are plastically deformed during fatigue test and short cracks can nucleate inside the grains of both phases. Grain boundaries act as obstacle to cracks propagation [49]. Low fatigue resistance can be enhanced both by N additions thus increasing austenite volume fraction, which avoid brittle fracture [50]. In high cycle fatigue tests the failure mechanism was mainly governed by ferritic phase [51].

While tensile properties were find to be mainly controlled by ferrite presence and quantity, toughness resistance is related to the austentic phase that has beneficial effects, retarding brittle fracture of ferrite. Cold deformation seems to have slight effects on toughness at low temperatures [31], as shown by Fig. 9.

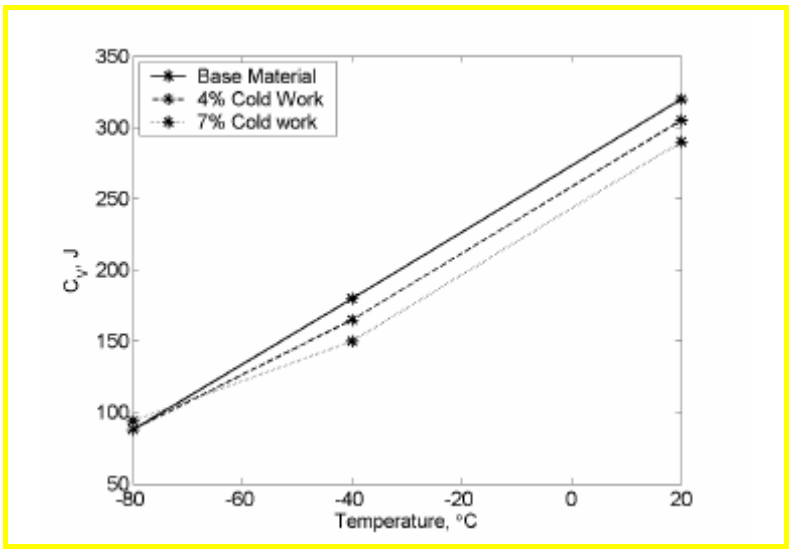

Fig. 9. Effect of cold working on toughness properties in DSS [31]

Influence of secondary phase precipitation on mechanical properties: critical aspects

Whereas tensile properties are slightly affected by the precipitation of secondary phase, toughness properties can be drastically reduced [48]. Several authors [30,37] found that even small amounts of brittle intermetallic phases can severely compromise the toughness of the DSSs, if treated in the critical range of temperatures for secondary phases precipitation. The decrease of fracture energy is noticeable just with 1% of secondary phases content, as shown in Fig. 10. In this case a small amount of plastic deformation is required at the notch root to have brittle fracture. The combination of a high volume and a large size of intermetallic phases produces a high density of microcracks leading to brittle fracture [37]. Pohl et al. found also a relation between the precipitation temperature and the embrittling effect of secondary phase. This was related to the morphology of sigma phase [40].

The loss of toughness is often related to the presence of σ phase, however it is difficult to separate the embrittling contribution of each secondary phase to the complex precipitation phenomena, even in the same range of temperatures (*Paper II*, pp. 81-92). Another decrease of the toughness is caused by the spinodal decomposition of ferrite at 475°C [52].

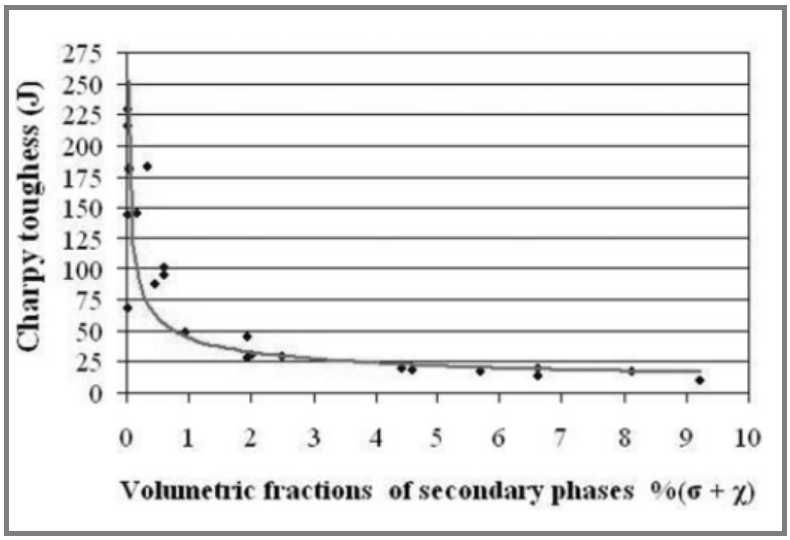

Fig. 10. Loss of toughness due to secondary phases in 2205 DSS grade [37]

The presence of secondary phases affects also fatigue resistance and fatigue crack mechanism of the DSSs. Ageing treatments have influence to crack grow rate, which is definitively higher with higher secondary phase content. Even the behavior of fatigue crack propagation is different in aged DSS than in the solution annealed material. In aged DSS the plastic deformation is mainly supported by the austenitic phase with a consequent stress concentration and local fracture in the ferritic grains [49].

Machinability

DSS present some difficulties towards machine operations. This is due to the higher strength if compared with common austenitic stainless steels and the strict control and limit of non-metallic inclusions for resistance corrosion purpose [30]. Carlborg et al. investigated the beneficial effect of sulphur addition in 2205 grade DSS [53]. Despite the good machinability the presence of sulphur inclusions showed a decrease in both toughness and corrosion resistance. Hence a compromise is needed to have good corrosion properties and acceptable machinability. Machinability is also influenced by alloying elements. Higher content of alloying elements, especially Mo, has detrimental effect on machine operations.

2.2.4 Corrosion Properties

The main attractive characteristic of DSSs, besides mechanical properties, is their behavior towards different types of corrosion as pitting corrosion, stress corrosion and intergranular corrosion. DSSs corrosion resistance in many critical environments is comparable or higher than that of common austenitic stainless steels. The corrosion

properties of DSS are strongly influenced by chemical composition, phase ratio and partitioning of alloying elements, especially in the case of pitting corrosion [54]. Ferritic phase contains higher content of chromium and molybdenum, whereas austenite is more enriched of nickel and nitrogen. Nitrogen is of particular interest as it strongly influences electrochemical mechanisms during corrosion attacks, enhancing pitting resistance in DSSs [55]. Phase balance, which determine elements partitioning, is determined by the parameters of thermo-mechanical processing, heat treatment and eventually welding. In particular, as the ferrite volume fraction increases with temperature, its content in Cr and Mo decreases due to the elements dilution. The optimal pitting resistance is reached with PREN similar for both ferrite and austenite, obtained through a proper solution annealing treatment [56]. However DSSs is generally characterized by slight differences of PREN values between the two phases. For the most common DSSs local the PREN of austenite is lower than that in ferrite. Only in lean DSSs containing high level of N and low content of Cr and Mo an opposite behavior was observed, with higher PREN in the austenitic phase [57]. The PREN differences between the two phases can caused preferential selective dissolution of the weakest phase.
PREN, or PREW in case of W addition, and critical pitting temperature (CPT) are useful indexes for pitting corrosion resistance evaluation of a DSS in chloride media. In Fig. 11 corrosion properties evaluated through CPT index are graphed together with yield strength for some common austenitic and duplex stainless steels.

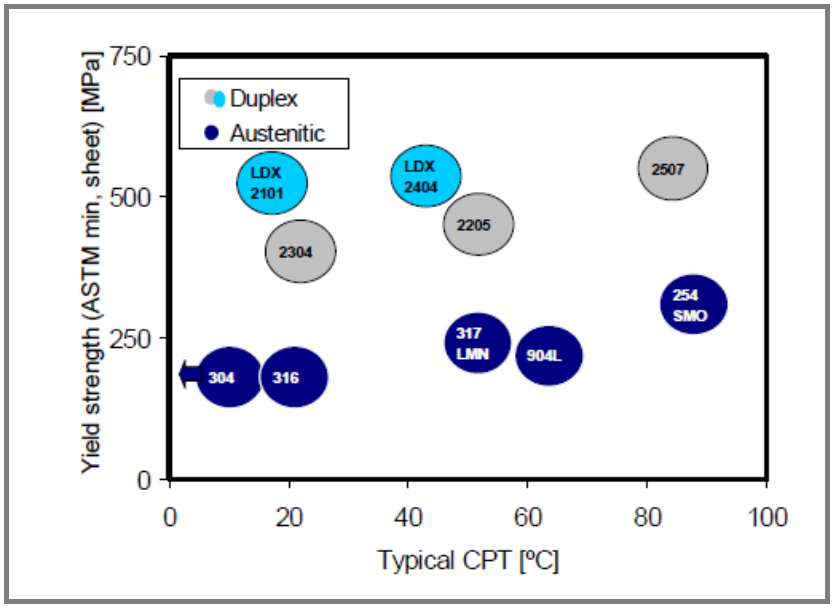

Fig. 11. Pitting corrosion properties and yield strength of different DSS grades and austenitic stainless steels [58]

Pitting behavior is more influenced by chemical composition rather than phase balance. In particular it is well known [56] that nitrogen, chromium and molybdenum improve the resistance to pitting corrosion in DSSs.
Stress corrosion cracking (SCC) is a damage phenomenon due to the combination of both mechanical and corrosive components. As pitting resistance, SCC is influenced by chemical composition and phase ratio, even if this last aspect seems to prevail [30]. SCC resistance increases with increasing in Cr and Mo content.

Furthermore DSSs are less sensitive to SCC if compared with common moderate Ni alloyed austenitic stainless steels. The reason stands in the increased amount of ferrite phase that is characterized by higher yield strength. Cracking limits based on constant load testing at the proof stress and practical experience are reported in Fig. 12 for different stainless steel grades and different chloride concentrations.

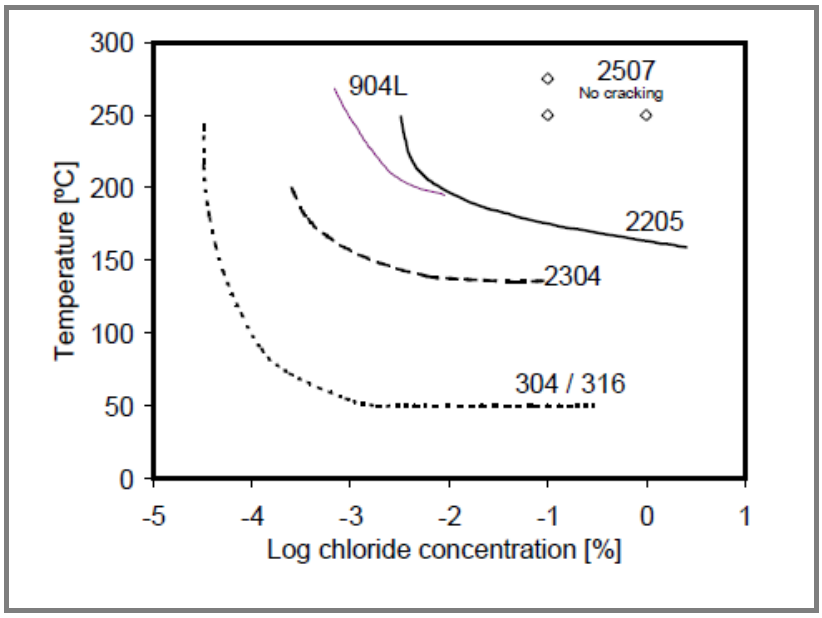

Fig. 12. Cracking limits of DSS compared to austenitic stainless steels

Influence of secondary phase precipitation on corrosion properties: critical aspects

The secondary phases precipitation affects the mechanical properties as well as the corrosive properties in a rather extensive way. Due to their high content of alloying elements, DSSs are prone to form chromium and/or molybdenum-rich phases when thermal treated in critical range of temperatures. Such elements are the most effective in preventing pitting therefore when a secondary phase precipitates local depletion in the surrounding area may occur with associated passivity breakdown. In particular the passivity breakdown can be explained by associated local chromium gradients. Typical polarization curves showing the influence of sigma phase precipitation on corrosion resistance are reported in Fig. 13.

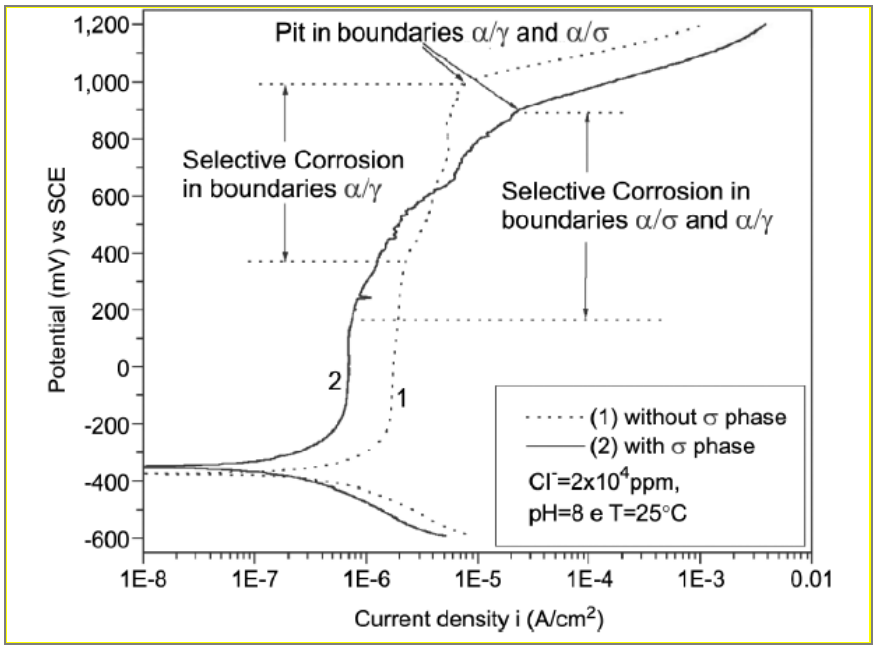

Fig. 13 Influence of sigma phase on corrosion resistance [60]

The Cr and Mo depletion is mainly related to ferrite phase due to the high diffusion rate in this BCC phase [61] leading to a very low PREN value and unstable phase which can evolve to secondary austenite. Experimental results proved that this depletion is sufficient to start selective attack of secondary austenite. This is of particular importance if this steel grade is applied in highly corrosive media, such as desulphurization plants. The lower molybdenum and chromium content is not the only factor affecting localized corrosion. The neighbor more noble phases enhances the anodic dissolution of weaker secondary austenite [62] through galvanic corrosion.

2.3 LEAN DUPLEX STAINLESS STEELS

2.3.1 Lean Duplex stainless steels benchmark

The recent fast growth of the price of raw materials as nickel and molybdenum (and in the last period of chromium too) forced stainless steel companies causing to switch away from austenitic stainless steels (304, 316, 317LMN) and super austenitic stainless steels to alternative less expensive grades. Fig. 14 compares the prices of several austenitic and duplex stainless steels, on the basis of high cost elements content. In addition to their interesting combination of mechanical and corrosion properties, the more stable price of duplex grades make them very attractive in the current market situation.

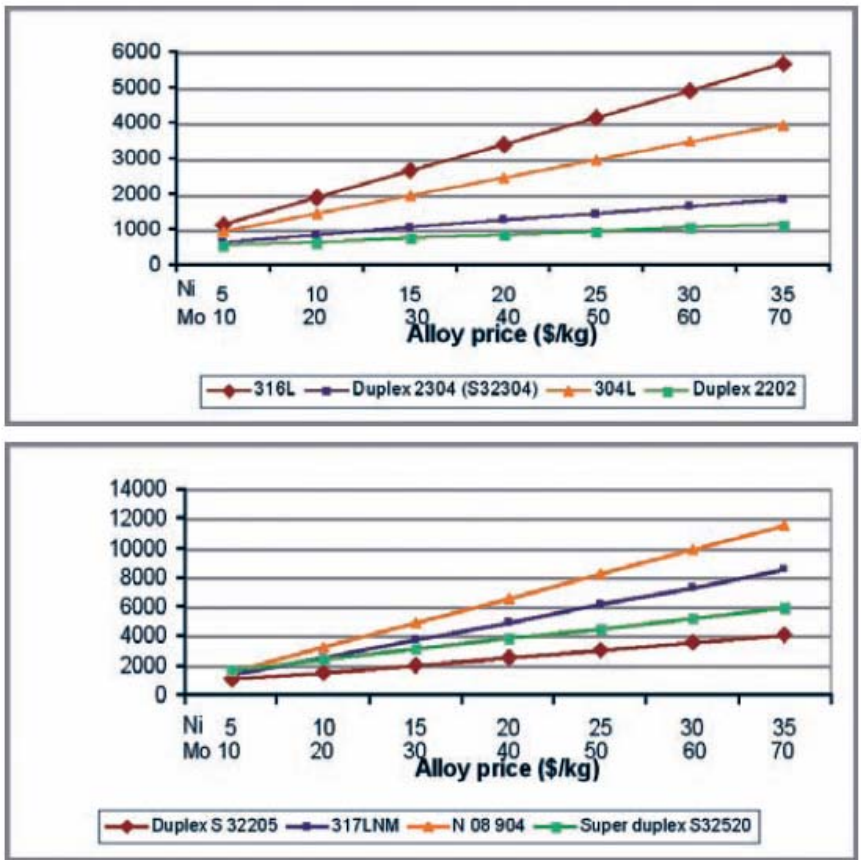

Fig. 14. DSS prices compared to that of common austenitic stainless steels
Source: J.C. Gagnepain, Stainless Steel World America 2008 Conference & Expo

With the aim to replace more expensive austenitic stainless steels many different duplex grades were developed, on the basis of corrosion resistance and applications: new lean duplex 2101 or 2202 as an alternative to 304, 2304 as an alternative to 316L, 2205 and super duplex SS as alternatives to 317LMN or super austenitic stainless steels. In the following table (Tab. 9) the chemical composition and PREN of new lean duplex grades are reported together with the possible common austenitic stainless steels to replace.

USA Designation	Cr	Ni	Mo	N	Cu	Mn	PREN
304L	18	9	-	-	-	1	18
316L	17	10-14	2.5	-	-	1	24
S32001	20	1.7	0.3	0.15	0.3	5	23
S32101	21.5	1.5	0.3	0.2	0.3	5	26
S32202	22.7	2	0.3	0.21	0.2	1.3	26/27
S32003	20	3.5	1.7	0.15	-	2	28

Tab. 9. Chemical composition [%wt] and PREN of the newest lean DSS

LDX 2101® (UNS S3201), produced by Outokumpu, and the lean duplex grades UNS S32001 (promoted by e.g. AK Steel and Acerinox), S82011 (AL2102 by ATI) and S32202 (UR/DX2202 by Arcelor Mittal) are all mainly aimed to be used as substitutes for 304 types and carbon steel. They all contain low contents of nickel and all but UNS S32001 have a maximum nitrogen content exceeding than of 2205 (UNS S31803/S32205). UNS S32003 (AL 2003 by ATI) has been developed primarily to replace 316 types and has a higher alloy elements content. Compared to the previously existing 2304 (UNS S32304) it contains less chromium, has a lower maximum content of nickel and a higher maximum content of nitrogen. The newest duplex grade is LDX 2404™, which combines a pitting resistance well exceeding that of 316 types with a higher minimum yield strength than for 2205 [20].

2.3.2 Lean Duplex grade UNS S3201

The lean duplex grade LDX 2101® was firstly developed by Outokumpu in the late ’90 aiming to offer the market a stainless steel for light-weight constructions, suitable for use in environments where the corrosion resistance of 2205 grade is not required. 2101 grade lean DSS combines mechanical properties typical of DSSs and corrosion resistance similar or superior to AISI 304/EN1.4301. The main reason for the success of 2101 grade is the lower cost and the better price stability than standard austentic grades. This was possible thanks to the substitution of expensive and volatile elements such as Ni and mo with N and Mn, which stabilize austenite and contribute to enhance mechanical and corrosion resistance at lower cost. Some users replace 304 austenitic grade with lean DSS 2101 for saving purposes without loss in corrosion properties, while many others also utilized the superior technical properties, in particular the mechanical strength, to achieve more competitive constructions. The result is a fast volume growth of lean DSS grade, which is nowadays an established member of the duplex family with a market demand of several 10,000 tonnes per year [20]. The range of application is very wide and includes general purpose applications and environments, buildings and constructions such as bridges, pipe lines and flexible pipes in oil and gas industry, storage tanks, reinforcement bars, water heaters but new uses are still being explored. DSS 2101 grade, like all the other DSSs, has a balanced microstructure which contains approximately equal amounts of ferrite and austenite after solution annealing at 1050°C.

Mechanical properties

Lean DSS 2101 has higher mechanical strength than common austenitic stainless steels due to its duplex microstructure and high nitrogen content. In Table x the mechanical properties values, according to EN standard, of 2101 grade are compared with the most common duplex 2205 and austenitic grades. It can be seen that lean DSS 2101 has comparable mechanical strength to 2205 grade and more than twice values if compared to austenitic grades (Tab. 10) [63].

Grade	$R_{p0.2}$, N/mm^2	R_m, N/mm^2	A_5, %
LDX 2101[1]	450	650	30
2205	450	655	25
1.4307	200	500	45
1.4404	220	520	45

Tab. 10. Mechanical properties. Comparison between 2101 DSS grade, common 2205 DSS grade and austenitic stainless steels [63]

Lean duplex grades has lower impact strength than 2205 at sub-zero temperatures as lower nickel addition does not contribute to high impact toughness at such temperatures, as noticed in Tab. 11 where impact toughness minimum values in J on transverse direction are reported according to EN 10028 [20] .

Temperature, °C	LDX 2101*	2304	2205
20	60	60	60
-40	27	40	40

*Values from internal specification, AM611

Tab. 11. Impact toughness of lean DSS 2101 grade compare to that of other common DSS [20]

The strengthening effect of N in lean DSS 2101 has been studied by Zhang Wei et al. [63]. The results showed that the yield strength improved 80 MPa if nitrogen content was increased from 0.12% to 0.26%, whereas the elongation remained constant. They also confirmed that the substitution of Ni by N reduced the impact energy values at low temperature proportionally to the Ni content reduction.

Machinability

Recently Bergqvist and Olsson presented the results about machinabilty of LDX 2101® [64]. They assessed that LDX 2101® had superior machinability if compared to other traditional stainless steels. This result was found without the addition of alloying elements to improve machinability of the lean DSS thus without loss in corrosion resistance. The reason for the good machinability shown by LDX 2101® is in the well balanced chemical composition. Beside the excellent combination of mechanical properties, corrosion resistance and price, the possibility to also reduce the machining cost makes lean DSS 2101 grade even more attractive for a number of applications.

Corrosion properties

The corrosion properties of lean DSS 2101 grade are generally good and comparable to those of 304 austenitic stainless steel grade and in some cases as good as Cr-Ni-Mo grades such as 4404.

Uniform corrosion. Different medias have been used to test uniform corrosion of lean DSS 2101, including inorganic, organic and alkaline solutions. The results highlight a better corrosion resistance in all test solutions of lean DSS 2101 than AISI 304 austenitic stainless steel, with the exception of an almost water-free mixture of acetic acid and acetic anhydride, in which all austenitic grades tested performed better than duplex or ferritic grades [65].

Pitting corrosion. The resistance localized corrosion in chloride solutions increases with chromium, molybdenum and nitrogen addition. Despite low Mo content the resistance of lean DSS 2101 is good thanks to the higher nitrogen content. Typical CPT values, according to ASTM G48 Method E standard, are presented in Tab.12 [20].

Steel grade			CPT,°C
Outokumpu	EN	ASTM	
LDX 2101®	1.4162	S32101	15
2304	1.4362	S32304	25
2205	1.4462	S32205	40
4307	1.4307	304L	10
4404	1.4404	316L	20
4432	1.4436	316L	25

Tab. 12. CPT values of different DSS grades and austenitic stainless steels [20]

Stress corrosion cracking. As all duplex stainless steels, even lean DSS 2101 grade shows higher resistance to SCC than common austenitic grades [66].

Secondary phases precipitation

The lower content of Mo and Cr of lean duplex 2101 grade compared to other DSSs makes this steel less prone less prone to the precipitation of secondary phases rich of such elements like sigma and chi phases. To study phases precipitation Liljas et al. performed isothermal heat treatments in a wide range of temperatures, finding that the formation of intermetallic phase as very sluggish. However precipitation of nitrides and carbides was revealed after exposure in the temperature range 600 to 800°C, with detrimental consequences on mechanical and corrosion properties [67].

Other authors [63,68] confirmed Liljas et al. results stating that the nose temperature of precipitation is at about 700°C. The heat treatment at 700°C produced high chromium intermetallic precipitates along the α/γ and α/α boundaries. Lihua Zhang et al. found also secondary austenite areas close to the precipitates, due to chromium depletion [68].

Moreover lean DSS 2101 seems to be also sensitive to 465°C embrittlement after long time treatments, due to probable ferrite spinodal decomposition [69]

Influence of secondary phase precipitation on mechanical properties: critical aspects

First studies [63,67] reveal a drop in thoughness values of heat treated lean DSS 2101 in the critical range of temperature for intermetallics precipitation.

Influence of secondary phase precipitation on corrosion properties: critical aspects

The high chromium precipitates and the consequent depleted surrounding areas after heat treatments of lean DSSs 2101 have deleterious effects on pitting corrosion resistance.
Both pitting potential and critical pitting temperature drastically drop even after short time isothermal heat treatments at 700 °C. Pit initiation was found to be around the precipitates due to the selective dissolution of weaker chromium depleted area. Once initiated, these pits grew into the ferrite phase [68].
Comparing to common DSS 2205 grade, higher susceptibility to ferrite grain selective corrosion was revealed in lean DSS 2101 after sensitization at 475°C, probably due to the spinodal decomposition mechanism. Moreover the lower Ni and Mo content of lean DSS 2101 seems to make the austenite more sensitive to corrosive attack developing from ferrite grains selective corrosion [69].

Austenite stability

The substitution of Ni with a combination of N and Mn can lead to a less stable austenite, which can evolve into martensite phase after heat treatment or plastic deformation (*Paper III*, pp. 93-105). The deformation-induced martensite has been studied by many authors for lower Ni alloyed austenitic stainless steels such as AISI 302 and 304 [70-77]. Moreover it was found that DSS 2205 grade is prone to austenite-martensite transformation as well as austenitic stainless steels [78-80]. Thus the same microstructural evolution can also involve lean DSSs, especially due to the less austenite stabilizing effect of Mn than that of Ni. In austenitic stainless steels the presence of deformation-induced martensite has different effects. It can cause problems, such as delayed cracking of deep-drawn components [81], or it can has beneficial effects, for example enhancing the rate of work hardening thus improving the formability [82]. Controversial opinions still remain for the influence of martensite on corrosion behavior.

2.4 MARTENSITIC TRANSFORMATION

2.4.1 General behavior of martensitic transformation

The term martensitic transformation is general and can be referred to various materials. Deformation-induced martensitic (α'-martensite) transformation may occur in metastable austenitic stainless steels, where the metastable austenite phase evolvs to the thermodynamically more stable α'-martensite phase due to the plastic deformation. Many authors agrees on the transformation of austenite to lath martensite via an adifussional process, promoted by dislocations and twins accumulations introduced in the material during plastic deformation. The martensitic transformation takes place with a cooperative movement of atoms crating a very precise orientation relationship between the parent austenite and the product martensite. Bain was the first to introduce a theory to explain the martensitic transformation from face centered cubic (fcc) austenite, to the body-centered cubic (bcc) or body centered tetragonal (bct) martensite with a minimum of atomic movement (Bain, 1924). Later new theories were proposed taking in account both the shape change and a twinning shear according to experimental observations, since it was found that the Bain distortion was not complete, since it did not produce any invariant plane (habit plane). On the basis of experimental observations on an austenitic stainless 18/8 steel Reed [83] revealed an habit plane coincident to {225}, but other habit planes have also been observed.
The commonly accepted crystallographic relationship between the austenite and martensite phases has been determined [84] and differs one from each other of about 5° around [111]:

$(111)\ ||\ (011)$ and $[\bar{1}01]\ ||\ [1\bar{1}1]$ (Kurdjumov and Sachs)
$(111)\ ||\ (011)$ and $[1\bar{1}0]\ ||\ [101]$ (Nishiyama-Wasserman)

However the experimental results were found to follow a theory which includes both the Bain distortion and the presence of an invariant plane. In the so called phenomenological theory the martensitic transformation is accomplished by the Bain distortion and a shear deformation, slip or twinning, at the interface between austenite and martensite. Fig. 15 represents the stages of the martensitic transformation: the shape change following Bain's theory (a), the shear at the interface between parent austenite and new martensitic phase (b) and the twinning at the interface between austenite and martensite (c).

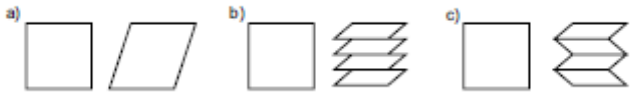

Fig. 15. Martensitic transformation: shape change following Bain's theory (a), shear at the interface between parent austenite and new martensitic phase (b) and twinning at the interface between austenite and martensite (c)

The transformation occurs in a quasi-instantaneous way as the speed of transformation is extremely fast and equal to 1100 m/s [85].
The basis to martensitic transformation stands on the introduction of defects in the material, their arrangements and interactions. In particular the formation of

deformation-induced martensite is related closely to shear bands, which are planar defects associated with the overlapping of stacking faults on {1 1 1}γ [86]. Twins, the ε martensite or stacking fault bundles generate depending on the way of the overlapping. Twins form when stacking faults overlap on successive {1 1 1} planes, the ε martensite when the overlapping of stacking faults occurs on alternate {1 1 1} planes whereas stacking fault bundles originates from the irregular overlapping of stacking faults. Moreover the susceptibility to strain-induced martensite transformation increases with the decrease of stacking fault energy (SFE) [71,87].

Two different types of deformation-induced martensite can form from metastable austenite. In the first steps of cold deformation and at low levels of strain hcp, paramagnetic ε-martensite seems to be favoured; while at higher levels of strain bcc, ferromangnetic α'-martensite predominates. The increasing amount of α'-martensite with increasing of deformation and the contemporary decreasing till complete disappearance of ε-martensite led to suppose the following sequence of martensite transformation from metastable austenite: γ→ε→α' [74,75,78]. However in some case only direct γ→α' transformation seems to take place through a dislocation reaction [87]. Recent studies [88,89] have assessed that both the transformations may occur in the same stainless steel. Many authors stated that during the γ→ε→α' evolution, the ε martensite seems to act as the precursor phase of α' [90,91] in both metastable austenitic stainless steels and high N austenitic stainless steels [92]. Preferential sites for α'-martensite nucleation could be the intersections of ε martensite [88], but single ε-martensite plate [92], the intersections between ε martensite and slip bands (or twins or grain boundaries) [93], intersections between mechanical twins and shear bands [94] were found to be other sites for α'-martensite first embryos as well.
On the contrary Hedstrom et al. [95] suggested that α' first plates nucleate at the dislocations pile-ups in a stepwise transformation behavior after reached a critical value. Through X-ray diffraction (XRD) the lattice parameters of the different structure were determined, revealing for fcc austenite a lattice parameter a_γ = 0.36 nm, for both bcc δ-ferrite and α'-marteniste $a_{\delta,\alpha'}$=0.287 nm and for hcp ε-martensite a_ε=0.254 nm and c_ε=0.416 nm [77]. Moreover changes in magnetic properties due to the formation of α' is also usable for its detection.

Strain induced martensitic transformation is sensitive to many factors. External factors that may affect the transformation are temperature, strain rate [75], mode of deformation [96].
Talonen et al. stated that an increase of strain rate and temperature suppressed the formation of strain-induced α'-martensite, due to the temperature-dependence of the stacking fault energy [75]. The temperature at which the deformation is carried out also influences the spatial distribution of the martensitic phase [93].
Even the internal structure in terms of grain size and orientation can modify the evolution and the amount of the transformed phase. In particular coarser grain size of prior austenite leads to higher amount of α'-martensite phase [97].
Nevertheless, as mentioned in the previous section, the chemical composition has a strong influence on austenite stability and consequently on martensitic transformation.

2.4.2 Effects of martensite on mechanical properties

Both ε and α'-martensite enhance the strength in austenitic stainless steels. Talonen et al. proposed two alternative strengthening mechanisms of the α'-martensite. For α'- martensite content till 30%, the α'-martensite particles dispersion harden the

softer austenite phase, and the plastic deformation is accommodated mainly by the austenite phase. Whereas over 30%, the α'-martensite forms clusters so the material can deform only if also the α'-martensite phase is deformed, with a further increase in the work-hardening rate. Moreover the presence of α'-martensite may affect the uniform elongation through its influence on the work-hardening rate [75].

2.4.3 Effects of martensite on corrosion properties

There is still some controversies about the effects of deformation-induced martensite on corrosion properties. For example the dissolution in acidic solution of metastable austenitic stainless steels was found to be higher [98], lower or unaffected [99] by the cold deformation applied. The repassivation potential behavior appears very irregular as well since it depends of many factors such as cold rolling [100], chemical composition and the chloride concentration in the solution. However the main opinion is that α'-martensitehas deleterious effect on corrosion resistance. Peguet et al. studied the effect of cold rolling and martensitic formation on pitting corrosion resistance in an AISI 304 stainless steel, revealing a decrease of repassivation potential and a less stable passive film in the steel in the cold rolled conditions [101]. For AISI 301LN and AISI 316L austenitic grades the presence of α'-martensite, till a maximum level of cold deformation equal to 50%, negatively affects both generalized corrosion and pitting corrosion. The reasons for the decrease of pitting corrosion resistance with the increasing amount of α'-martensite were attributed to the presence of residual stresses resulting from the 4% volume expansion associated to the γ→α' transformation and to a change in composition and compactness of the passive film caused by the new martensitic phase introduced [102]. Kumar et al. confirmed a decrease of pitting potential due to residual stresses but only at low deformation levels.
At higher cold deformation the stainless steel considered in their investigations was characterized by an increase of the pitting potential due to the high density close-packed planes structure which seems to have favored the formation of Cr-rich passive film [103].

3. SECTION II. HIGH STRENGTH STEELS

3.1 HISTORICAL PERSPECTIVE AND CLASSIFICATION

3.1.1 General Introduction

In the last 50 years high strength steels have been used in a wide range of applications where the economical benefits of weight saving together with other specific characteristics such as wear resistance, atmospheric degradation resistance, fracture toughness and weldability can be simultaneously realized. The strict control of chemical composition together with the development of thermo-mechanical technological processes (TMCP) have permitted to gain high mechanical properties at limited costs if compared with common mild carbon steels [104,105]. The new concept TMCP processing technique not only gives economic advantages avoiding additional heat treatments, but also has a beneficial environmental impact due to the reduction in energy consumption. The most common applications for high strength steels are in the structural, automotive, mining and oil and gas industries. In particular the aim to use light materials, thus decreasing consumption and gas emission along with increasing in passenger safety, has made this class of materials attractive and has forced to further development.
In the two last decades a new classes of high strength steels has been carried out, permitting to increase both resistance and toughness properties than those of conventional high strength steels. The transformation hardened steels (the so-called Advanced High Strength Steels) along with High Manganese Austenitic Steels are some of the new classes developed [106]. In conventional HSS such as high strength low alloy steels (HSLA), grain refinement and/or precipitation are the typical strengthening mechanisms, whereas in AHSS phase transformations mechanisms are the main hardening method. The most known class of AHSS are: Dual Phase, TRIP, Martensitic, Complex Phase steels. Depending on the microstructure and its components, a wide range of properties can be reached just adjusting the balance of the phases.

3.1.2 Historical Evolution

The first HSS, a carbon steel with low amount of Nb, was developed in the 1963, when the fine precipitation of Nb carbides was found to markedly increase mechanical properties of the material. In 1963 the theory and practice of microalloying with strong carbonitride forming elements (V, Nb, Ti) started to be developed extensively [107]. Since this moment high strength steels with low alloy of Nb, V, Ti elements received more and more attention especially for construction applications. In the 1970s a new technological process, the controlled rolling, permitted to reach higher and higher mechanical properties of HSLA at lower costs and with good weldability. For these reasons HSLA were used in many industrial fields including oil and gas pipelines, construction and farm machinery, storage tanks.
From 1960 to 1980, the microalloyed steels were characterized by a ferrite-perlite (F-P) structure with low hardenability steels and yield strengths up to about 420 MPa, resulting from the effect of microallying elements added, controlled rolling followed by air cooling processes. The first solution to increase mechanical properties, as required by both pipe lines and automotive companies in the first years of the ‘80s, was to refine F-P grain structure. However higher strength and toughness were still demanded. For this purpose new steels with mixed hard and soft microstructure were developed. In the

end of the ‘70s the first type of AHSSs was introduced, i.e. the *dual phase* carbon steels. They were developed for cold drawn of automotive components and they were characterized by a bi-phasic structure made of a mixture of ferrite and martensite, obtained through rapid cooling. The combination of higher hardenability and higher cooling rates permitted to obtain such microstructure. From the processing point of view this was possible using water cooling after hot rolling. A further development in technological processing was introduced in the mid-1980s by interrupted accelerated cooling (IAC) and interrupted direct quenching (IQD) for plates production [108].

Parallel to the mixed microstructure high strength steels, the interstitial free steel was introduced in the ‘80s. They are another interesting class of microalloyed steel developed in order to have better cold formability of the current HSLA.
Fig. 16 reported the historical evolution of high strength steel grades and production technologies. It can be noticed how, in 1970, thermo-mechanical rolling processes replaced distinct phases of hot rolling and normalizing. Hence the possibility to produce X70 from steels that are microalloyed with niobium and vanadium and have reduced carbon content. By the same technique even higher strength materials like X80 was processed, having a further reduced carbon content and excellent weldability. More recently the additions of molybdenum, copper and nickel enable the strength level to be raised to that of grade X100, when the steel is processed to plate by thermo-mechanical rolling followed by modified accelerated cooling.

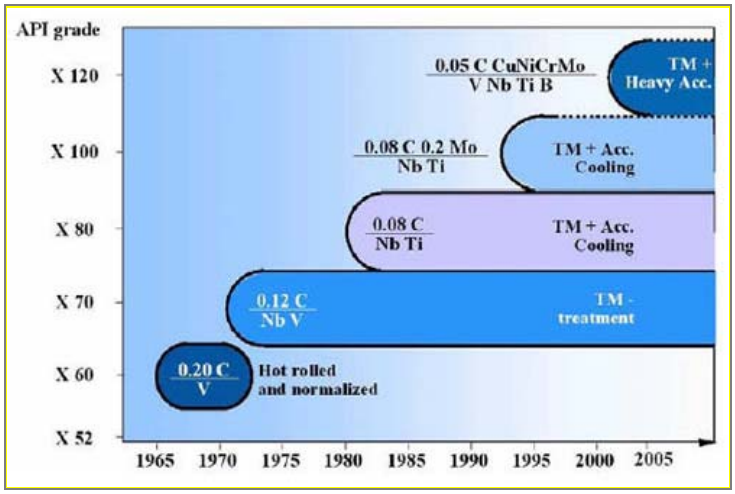

Fig. 16. Historical evolution of high strength steel grades and production technologies
Source: www.keytometals.com

The effects of processing and alloy design changes on microstructure and properties of plate steels for large diameter pipe lines are shown in Fig. 17.

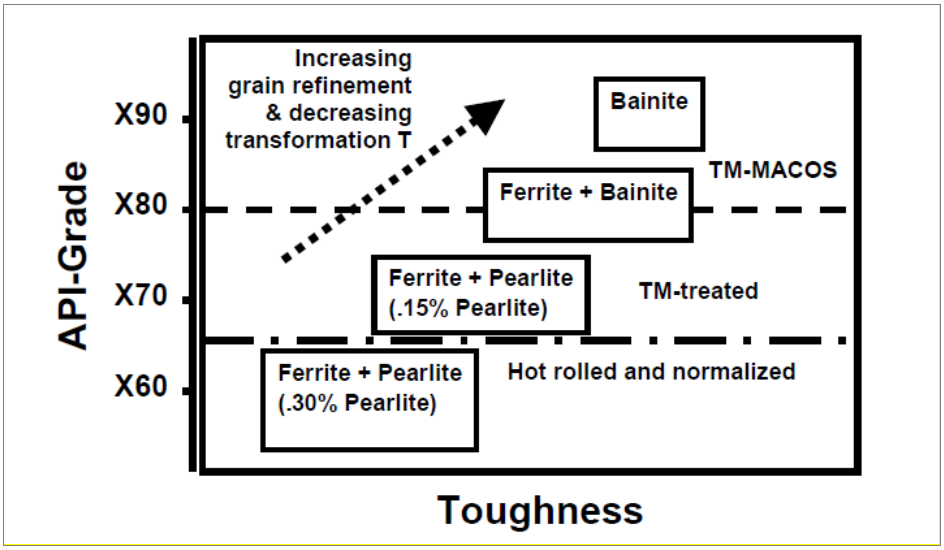

Fig. 17. Effects of processing and alloy design on microstructure and properties of plate steels
Source: M. K. Graff et al., Accelerated Cooling of Steel, TMS-AIME USA (1986)

Only in the last years many new different AHSS, as TRIP and TWIP steels, were developed and are still under investigation.
On the other hand, even if the level of understanding of the effect of microalloying additions such as Nb, V, and Ti to high strength low alloy steels on the austenite (γ) to ferrite (α) transformation and concomitant precipitation reactions during thermo-mechanical processing is well established [109-112], special attention is till reserved to the behavior of microalloying additions from one type of thermo-mechanical processing to another.

3.1.3 Classification

A first classification was given for older high strength steels, mainly concerning HSLA. This classification is divided into six categories as follows:

- *Weathering steels*, characterized by small contents of alloying elements such as copper and phosphorus to increase atmospheric corrosion resistance and solid-solution strengthening.
- *Microalloyed ferrite-pearlite steels*, containing very small (generally, less than 0.10%) additions of strong carbide or carbonitride forming elements such as niobium, vanadium, and/or titanium for precipitation strengthening, grain refinement, and possibly transformation temperature control.
- *As-rolled pearlitic steels*, which may include carbon-manganese steels but which may also have small additions of other alloying elements to enhance strength, toughness, formability, and weldability.
- *Acicular ferrite (low-carbon bainite) steels*, which are low-carbon (less than 0.05% C) steels with an excellent combination of high yield strengths (as high as 690 MPa, or 100 ksi) weldability, formability, and good toughness.
- *Dual-phase steels*, which have a microstructure of martensite dispersed in a ferritic matrix and provide a good combination of ductility and high tensile strength.

- *Inclusion-shape-controlled steels*, with improved ductility and through-thickness toughness through slight additions of calcium, zirconium, or titanium, or rare earth elements so that the shape of the sulfide inclusions is changed from elongated stringers to small, dispersed, spherical globules.

However the introduction of many types of new high strength steels with improved mechanical properties, the AHSSs, required a novel classification especially concerning the main applications sector which is automotive. Automotive steels can be ordered in different categories, based on the metallurgical features, on technical characteristics for part designers or on the mechanical properties or forming parameters. The first distinction is between conventional HSS and AHSS. The principal difference between conventional HSS and AHSS is their microstructure. Conventional HSS are single phase ferritic steels, whereas AHSS are multi-phase steels. Different amounts of ferrite, martensite, bainite, and/or retained austenite are present in such steels.
The classification based on the metallurgy provides low-strength steels (interstitial-free and mild steels), conventional HSS (carbon-manganese, bake hardenable, high-strength interstitial-free, and high-strength, low-alloy steels), AHSS (dual phase, transformation-induced plasticity, complex phase, and martensitic steels) and the newer even higher strength steels including ferritic-bainitic, twinning-induced plasticity, nano, hot-formed, and post-forming heat treated steels.
An useful designation for designers is based on different steel strength levels. Particularly High-Strength Steels (HSS) has yield strength values between 210 and 550 MPa and tensile strength values between 270 and 700 MPa, while Ultra-High-Strength Steels (UHSS) steels have yield strengths higher than 550 MPa and tensile strengths higher than 700 MPa [113].
The possibility to obtain, through balanced microstructure characterized by very different phases, a wide range of mechanical properties makes necessary to organize these different steels on the basis of such mechanical or forming properties. For instance some types of AHSS, due to their phase balance, have a higher strain hardening capacity thus better strength ductility than conventional high strength steels, whereas others have ultra-high yield and tensile strengths and are characterized by bake hardening behavior. The different strength of low strength traditional steels (dark grey), common HSS (light grey) and newer AHSS (coloured) are reported together with their total elongations in Fig. 18 [113].

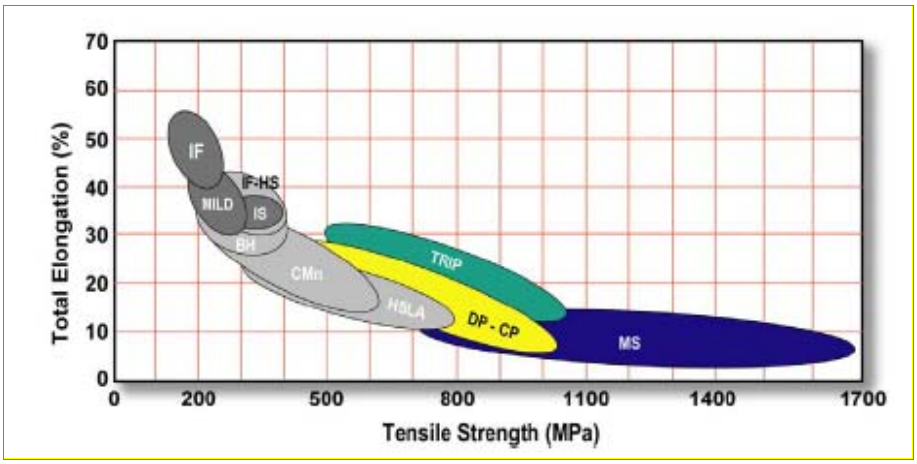

Fig. 18. Comparison of mechanical properties between traditional C steels, HSS and AHSS

Even if many different designations have been chosen by different companies, the easiest way to give a complete description of a steel is to identify it by metallurgical type, yield strength (in MPa), and tensile strength (in MPa). As an example, DP 500/ 800 means an AHSS dual phase steel type with 500 MPa minimum yield strength and 800 MPa minimum ultimate tensile strength [113].

3.1.4 Applications

The choice of a particular high-strength steel depends on the requirements needed by the specific application, including thickness reduction, formability, weldability, surface quality and in specific cases corrosion resistance. The most attractive characteristic of high strength steels is the favorable strength-to-weight ratio compared with that of traditional mild steels. Therefore HSS and AHSS find their main use in the automotive sector. HSLA and DP are the most applied steels in a wide range of automotive components construction. However due to the increasing demands for occupant safety and fuel efficiency, further strengthening of DP steels without a loss in ductility is often required. The application of AHSS martensitic type is limited on hot stamping process, in which sheet is heated to obtain a complete austenitic structure, then it is formed in press and quenched in the water-cooled stamping tool. The resulting martensitic microstructure leads to reach high strength values while the hot forming process limits residual stresses and spring back effect, compared to cold formed components [114]. The current and the ideal combinations of steel in car components are showed in Fig. 19. The mild and traditional microalloyed steels are replaced mainly by AHSS dual phase steels, due to their higher strength and toughness.

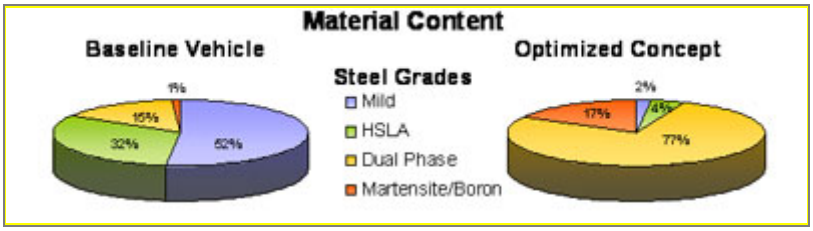

Fig. 19. J. Shaw et al., Steel Manufacturing Challenges and Reducing Vehicle Mass (2010)

The wide applications field of HSLA steels include also metallic structures in railway bridges, mine and railroad cars, industrial equipment, marine platform bases, storage tanks, high pressure vessels, large oil and gas pipe lines, etc. Particularly pipe lines construction was of one of the most attractive application of high strength steels due to high strength, favorable strength/weight ratio and good weldability typical of this class of steels. The benefits introduced by HSLA were the possibility to improve the transport efficiency by high pressure operation, to reduce pipe laying costs by the use of thinner- wall pipes, to guarantee good toughness also in the welded joints. Fig. 20 shows the weight saving produced by the introduction of HSS with higher strength values in pipe lines applications.

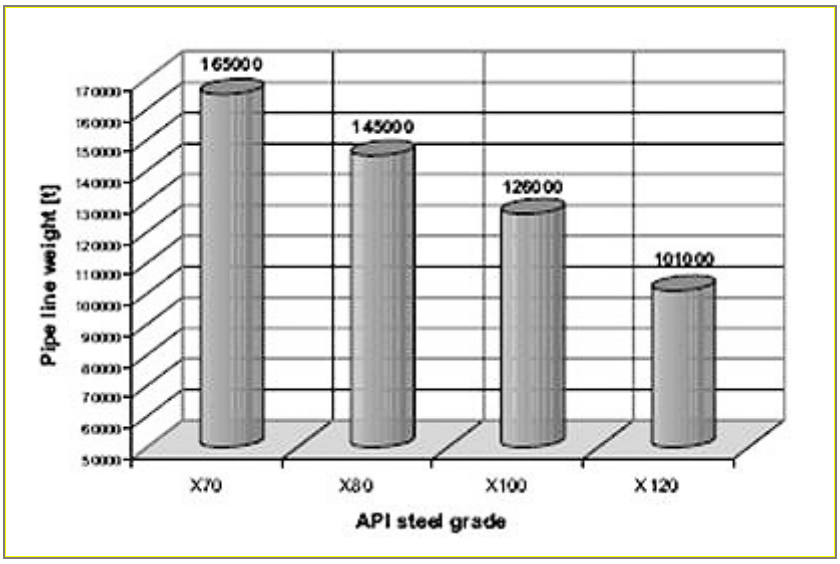

Fig. 20. Increasing mechanical properties and weight saving in pipe lines applications

3.2 PHYSICAL METALLURGY AND PROCESSING

Even if Carbon is the most important element for strengthening steel, it has deleterious effects on many technological properties such as weldability and formability. Hence the addition of C in high strength steels is limited. The development of high-strength steels for a number of applications at reduced costs was made possible through both the addition of other strengthening alloying elements and the introduction of different harder phases. As a result, an increase in strength is achieved while good toughness is generally maintained.
In order to deeply understand the advantages and the problems dealing with the introduction of HSS and AHSS, a brief description of the physical metallurgy and processing is provided, focusing on the specific steels discussed in the present dissertation.

3.2.1 HSS, High Strength Low Alloy (HSLA) Steels

The most used HSS are the HSLA steels. This group of steels are strengthened by the addition of micro-alloying elements such as Nb, V and Ti. In order to obtain a good combination of mechanical properties it is essential to have the most favorable microstructure in the steel. The superior properties exhibited HSLA steels has been associated with the precipitation of carbo-nitrides of small addition of alloying elements, such as Nb, V, Ti. These carbo-nitrides strength the material through different strengthening mechanism like precipitation hardening and grain refinement. The most important is grain refinement which leads to an improvement of both strength and toughness at the same time [109-112][115-121]. Microallying elements and thermo-mechanical processing have a synergic effect on the increase of mechanical properties. In microalloyed steels, strain-induced precipitation (SIP) of the microalloying elements during thermomechanical controlling processing (TMCP) plays an important role in controlling the final microstructure of the steel. [108].

Controlled rolling, which is a type of TMCP, was applied for the production of hot rolled low carbon HSLA steel with a refined microstructure (*Paper IV*, pp. 107-117). The schematic representation of a typical thermo-mechanical processing applied to HSLA steels is shown in Fig. 22.

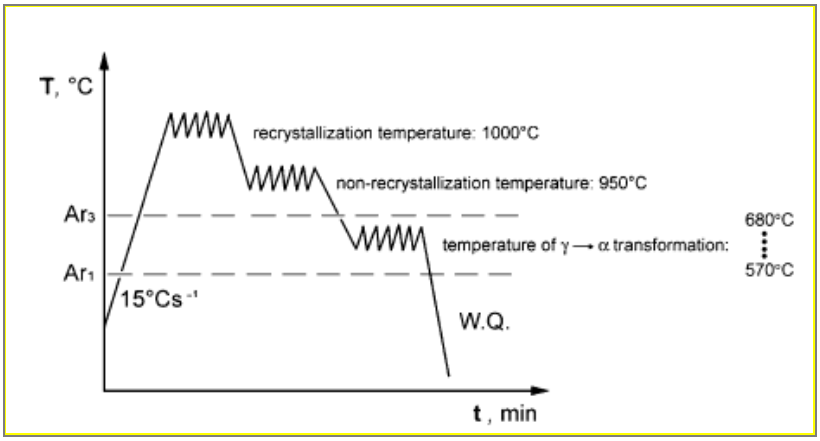

Fig. 22. Typical steps of a TMCP

The ferritic grain refinement is achieved by the maximization of the total interfacial area per unit volume of austenite grain before the γ→α transformation, realized by controlled rolling through the rolling passes and the retardation of austenite recrystallization. The retardation of austenite recrystallization seems to be caused by the inhibition of subgrain boundaries movement due to the strain-induced carbo-nitrides precipitation during deformation [119] or to grain boundary segregation of micro-alloying elements [123].
A strong grain refinement has been made possible through two alternative strategies of hot rolling of austenite in the finishing mill. In the first case, relatively high temperatures are used for steel rolling, with particular attention to avoid grain coarsening between the rolling passes and mainly between the finishing mill exit and the cooling section of the material. The rolling speed is set up to attain the aim finishing temperature, taking also in account the final strip thickness and width. The austenite grains are refined through repeated cycles of recrystallization with a consequent creation of large grain boundary and increasing of the number of potential nucleation sites during γ→α phase transformation [124].
In the second case, the choice of rolling parameters are set to extend the incubation period for recrystallization beyond the time intervals available in the given mill for the onset of recrystallization. Hot rolling of austenite is performed in a way to avoid any recrystallization during and between the rolling passes and after the finishing mill exit. Thus a strongly deformed austenite can be obtained. The so called pancaked austenite, characterized by high dislocation density, shear bands, deformation bands, increases the number of sites for ferrite nucleation leading to a strong refined structure [124]. This type of TMCP is commonly applied for Nb alloyed HSLA steels. The strip is rolled at relatively low temperatures to further suppress the recrystallization of austenite. The most important factor to be considered for the final microstructure and properties is the recrystallization behavior of austenite during and after hot deformation, determining also the type of rolling.
Nowadays many hot strip mills have the sufficient power to implement both of the strategies just described to produce HSLA steels. To obtain the optimal grain refinement and strengthening the finishing temperature, the coiling temperature and the cooling rate have to be controlled. The refinement of the ferrite is achieved by increasing the cooling rate in the run out table (ROT) and lowering the coiling temperature (CT), whereas the precipitation hardening is mainly influenced by the cooling path from the finish rolling temperature is critical [125].
Recent studies showed that a rapid transformation annealing (RTA) permits to realize both grain refinement and a substantial change in precipitate state. In particular more homogeneous fine grain structure and lower distance between extremely fine precipitates (<20 nm) have been found to increase significantly the strength of the material with a slight loss in formability [126].

Microalloying elements precipitation and effects

The effect of grain refinement caused by the precipitation of carbo-nitrides of alloying elements to the increase of strength can be quantified though the well known Hall Patch approach:

$$\sigma_{HP} = \sigma_0 + k_y d_{eq}^{-1/2} \quad (3)$$

where σ_o is the strength of the material considered as a single crystal in the annealed condition and $k_y d_{eq}^{-1/2}$ is the hardening contribute due to mean size of the grains.

Besides the grain refinement effects, the microalloying elements precipitates contributes to the overall strength through precipitation hardening. In micro-alloyed steels the dispersion strengthening is provided by NbC, VC, TiC or Nb(C,N), V(C,N), Ti(C,N) particles, depending on N addition [116][119-121]. Such particles mainly precipitated on crystalline defects in either the austenite or ferrite [125], as their crystal lattice does not permit a suitable location inside ferrite phase. The lattice mismatch for Nb and V precipitates in both austenite (fcc, a_0=0.35698 nm) and ferrite (bcc, a_0=0.28664 nm) was evaluated, revealing that the particles cannot be coherent due to the misfit strain (Tab.13) [125].

	NbC	NbN	VC	VN
Lattice Parameter, a_0, nm	4.4702	4.39	4.16	4.29
[100]ppt // [100]γ	25.22	22.98	16.53	20.17
[010]ppt // [010]γ	25.22	22.98	16.53	20.17
[001]ppt // [001]γ	25.22	22.98	16.53	20.17
[100]ppt // [100]α	55.95	53.15	45.13	49.67
[011]ppt // [010]α	10.26	8.28	2.61	5.81
[0-11]ppt // [001]α	10.26	8.28	2.61	5.81

Tab. 13. Lattice mismatches of Nb,V(CN)

This means that the mechanism of precipitation strengthening can be modeled by Ashby-Orowan formula that includes the contribution of the energy required for dislocations to pass between particles and of the energy required by the cross slipping of screw segments or climb of edge dislocation segments in bypassing the particles [125].

$$\Delta YS(ppt) = \{(M \cdot K \cdot G \cdot b) / < (\pi)^{1.5} >\} 1.2[< (f_V)^{0.5} > / d] \cdot [\ln(d / 2b)] \quad (4)$$

$$\text{or } \Delta YS(ppt) = 6982[< (f_V)^{0.5} > / d] \cdot [\ln(2d)]$$

The yield strength contribution due to Ashby-Orowan reinforcement mechanism can be simplified in the equation below reported where 3 is the Taylor factor, G the shear modulus (4 9 104 MNm^{-2}), b the Burgers vector (0.2 nm), m the Poisson ratio (0.3), d_{eq} the mean equivalent diameter of the particles and k_{eff} their mean lateral centre-to-centre spacing [123].

$$\sigma_{Or} = 3(0{,}81Gb/\left(2\pi(1-\nu)^{\frac{1}{2}}\right)\ln(\tfrac{d_{eq}}{b})/\lambda_{eff}) \quad (5)$$

The dependence of precipitation strengthening on precipitate volume fraction and size (X) has been compared for the experimental results and theoretical values calculated according to the Ashby-Orowan model, as highlighted in Fig. 23 [128].

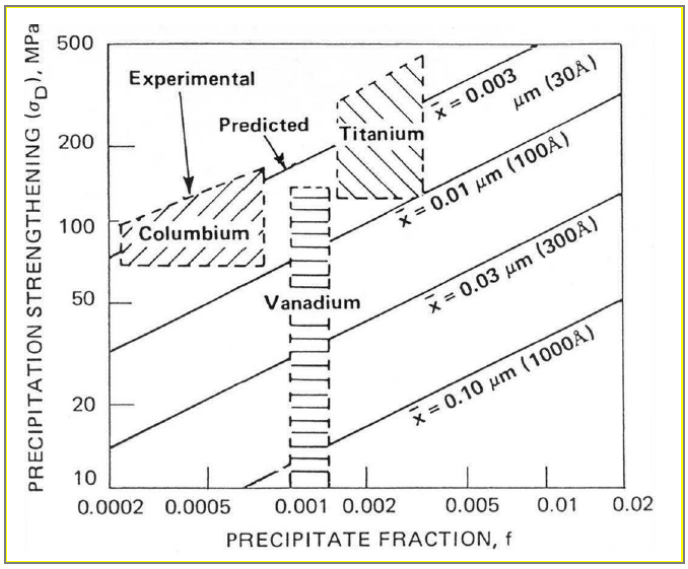

Fig. 23. Relation between precipitation strengthening and precipitate volume fraction

Combining the strengthening due to the grain refinement, according to Hall Patch approach together with precipitation hardening and the solid solution reinforcement component ($\Sigma k_i c_i$), the total strength of the material can be expressed as follows:

$$\sigma_{tot} = \sigma_0 + \sum k_i c_i + k_y d_{eq}^{-1/2} + 3\sigma_{Or} \quad (6)$$

As it can be seen in Fig. 24 the main contribute to total strength is given by grain refinement and precipitation hardening, while solid solution strengthening contribute is negligible.

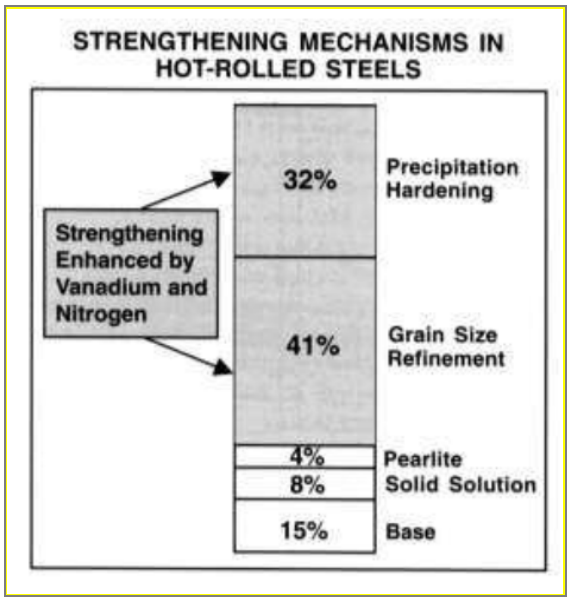

Fig. 24. Strengthening contributions due to different reinforcing mechanisms

Effect of Nb addition

Nb is considered the most potent microalloying element for the increase of both strength and toughness in HSLA steels. The addition of Nb has many different effects [113,114,124]. First of all it is the most effective element to retard and even suppress the austenite recrystallization prior to γ→α transformation through the strain-induced precipitation (SIP) of NbC. The mechanism of SIP has been analyzed by many researchers [118][132-134]. The first detailed study of mechanism and kinetics of SIP was developed by Dutta *et al* [115], who also introduced a mathematical model based on thermodynamics and experimental observation [132]. Since this moment other authors applied the Dutta model for SIP of Nb(C,N) in HSLA steels hot rolled in single pass [133] and multipass [134].
Moreover the presence of Nb in HSLA steels is beneficial also because it is an inhibitor of austenite grain coarsening during reheating and it enhance the strength of the steel through precipitation hardening due to the formation of NbCN in the low temperature transformation step of the thermo-mechanical processing. It has been found a bimodal grain structure in some Nb HSLA steel plates. Such bimodal distribution consists of abnormally large ferritic grains surrounded by other small ones. The phenomenon is associated with the micro-segregation of microalloying elements during solidification, so it is strongly sensitive to particular processing conditions and chemical compositions [135].

Effect of V addition

The effects of V in HSLA steels have been extensively studied, especially due to its lower cost if compared to Nb and Ti. V forms V(C,N) nanoparticles during cooling after hot rolling [136,137]. Similarly to Nb, V increases the strength of the material through both precipitation hardening and grain refinement. However V is stable at lower temperatures than Nb, so it has less grain refinement effect [138]. The strengthening effect is enhanced with higher N content [111,118].V is easily added to liquid steel and its solubility during reheating is very high.

3.2.2 AHSS, Dual Phase (DP) Steels

In HSS the increase of mechanical properties is achieved mainly by grain refinement and precipitation hardening in a single phase structure, obtained by small additions of elements such as Nb, V, Ti and suitable thermo-mechanical processing. In AHSS the reinforce mechanism is due to the introduction of other phases in the material. Types of AHSS include dual-phase (DP), TRIP, complex phase (CP) and martensitic (MART) steels. However DP and HSLA are usually competitive in their use in automotive components.

Dual-phase (DP) steels are characterized by a ferritic matrix and typically 5-30 vol.-% of hard martensite islands. The soft ferrite phase is generally continuous, giving these steels good ductility and formability [139,140]. The typical DP microstructure is schematized in Fig. 25 [113]. In DP steels, carbon is the main element used for the formation and strengthening of martensite at practical cooling rates. However the

addition of other elements such as chromium, molybdenum, vanadium, manganese and nickel also help to increase hardenability [113].

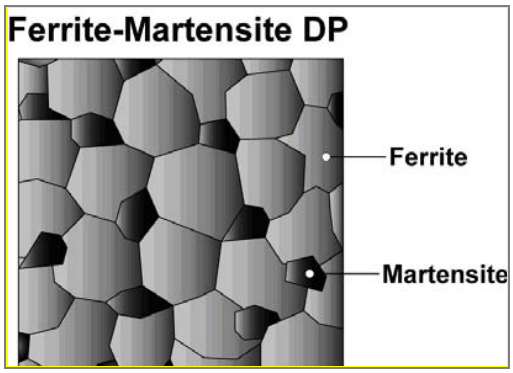

Fig. 25. Scheme of DP steel microstructure

Thanks to the mixed microstructure, DP steels exhibit an excellent combination of strength and ductility. When DP steels deform, strain is concentrated in the softer ferrite phase surrounding the islands of harder martensite, leading to high work-hardening. The work hardening rate together with high values of elongation contributes to lowering yield strength to ultimate tensile strength ratio.
Therefore DP steels much higher ultimate tensile strengths than conventional HSS steels of similar yield strength as it can be noticed in Fig. 26, where an AHSS DP and a HSS common HSLA with the same yield strength is compared [113].

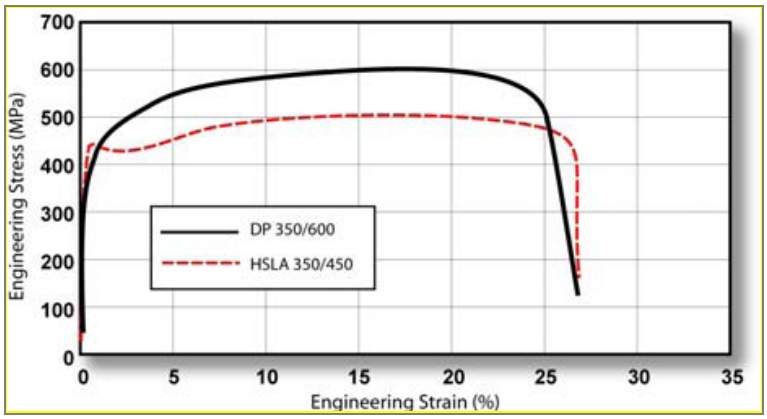

Fig. 26. Engineering stress-strain curves of a HSLA and a DP steels with the same yield strength

If compared with traditional carbon ferritic-perlitic steels, DP steels have higher uniform elongation. The martensitic phase is responsible to the high mechanical properties, thus increasing the volume fraction of hard second phases generally increases the strength. DP steels also show low brittle-ductile transition temperature, a good fatigue strength and a good weldability, related in the first instance to their low carbon content and carbon equivalent number [142].
The dual-phase steels found their main applications in automotive industries, due to their combination of high strength and formability. Therefore they are mainly produced as flat steel-mill products. In particular DP can be manufactured in the form of hot rolled hot-rolled and control-cooled steel hot strips or as intercritically annealed cold

strips, usually of thickness below 5 mm [142]. In the first case the flat products are produced by controlled cooling from the austenitic phase, whereas in the second case they are produced from a ferritic-austenitic two-phase structure to transform some austenite to ferrite before a rapid cooling transforms the remaining austenite to martensite. Hot-rolled steels can have a microstructure containing a significant amount of bainite, due to some variation in chemical composition and processing parameters to avoid stretching on a blanked edge [113].
Recently, due to the increasing demands for occupant safety and fuel efficiency, further strengthening of DP steels without a loss in ductility is needed. Several authors found grain refinement a possible tool to achieve this purpose [143,144]. Moreover there is an increasing interest in new application fields of DP steels such as fasteners, pinions, axles, requiring thicker starting materials with uniform and controlled microstructure and properties [142].

In addition to their high strength, the AHSS grades often show a large potential for bake hardening (BH). The BH effect is the increase in yield strength due to blocking of dislocations by carbon atoms and/or small carbides. It is activated by a controlled ageing at relative high temperature after a pre-straining of the material. The BH effect depends on the specific chemical composition, in particular on the amount of dissolved carbon atoms and other alloying elements as well, on the microstructure like the size of ferritic grains and thermal histories of the steels.

3.3 PROPERTIES OF HSLA AND DP STEELS

In this section the main mechanical properties together with formability and weldability are reported for both HSLA and DP steels. HSLA and DP steels are often competitive materials, hence a comparison between these two class of steels is given.

3.3.1 Mechanical Properties

A summary of the mechanical properties evolution from HSS (HSLA) to AHSS for automotive applications is highlighted in Tab. 14, showing the potentiality of DP and TRIP AHSS both in strength and elongation [113].

Steel Grade	YS (MPa)	UTS (MPa)	Tot. EL (%)
HSLA 350/450	350	450	23-27
DP 300/500	300	500	30-34
DP 350/600	350	600	24-30
TRIP 450/800	450	800	26-32
DP 500/800	500	800	14-20
CP 700/800	700	800	10-15
DP 700/1000	700	1000	12-17
MS 1250/1520	1250	1520	4-6

YS and UTS are minimum values
Tot. EL (Total Elongation) is a typical value for a broad range of thicknesses and gage lengths.

Tab. 14 Mechanical properties of DP and TRIP steels compared to a common HSLA [113]

In the previous section the correlation between microstructure and mechanical properties together with the influence of various reinforcing mechanism caused by microalligation has been reported for *HSLA* steels. For *DP steels* the connection between the mixed microstructure and mechanical properties has been shown as well.
An useful instrument to compare different steels or different grades of the same class of steels is given by the stress-strain curves. Ultimate tensile strength, yield strength, uniform elongation, total elongation can be derived from the engineering stress-engineering strain curves. Fig. 27a and Fig. 27b highlight the different behavior of different HSLA steels grades and DP steels grades, respectively. A mild steel is used for comparison [113].

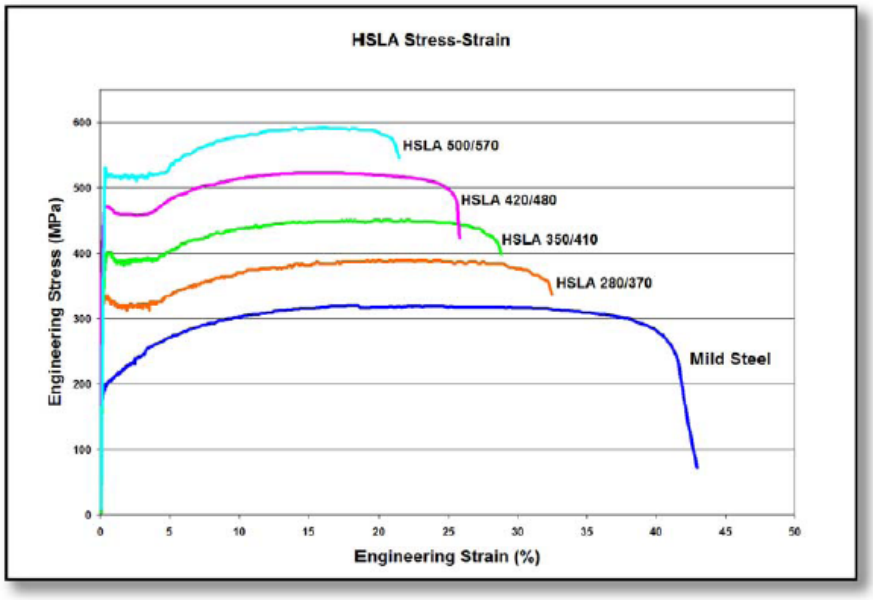

(a)

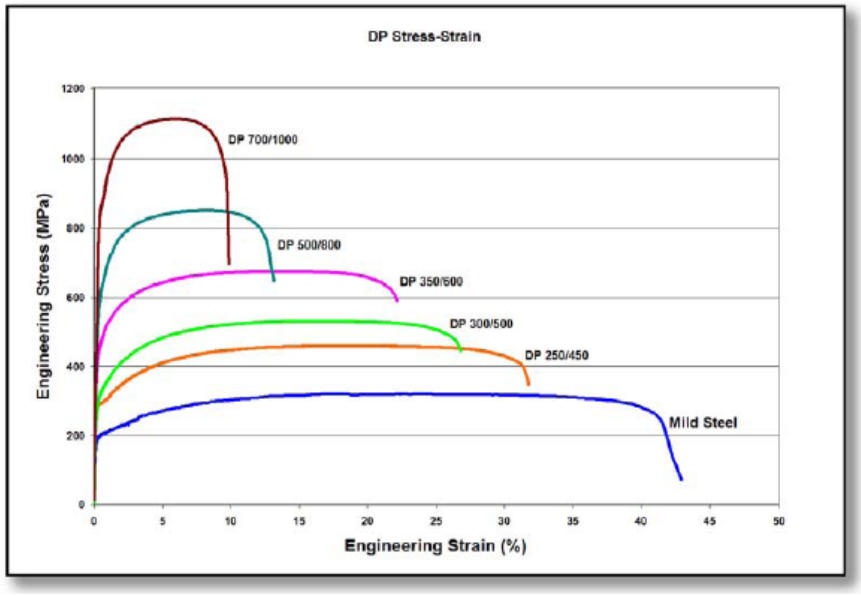

(b)

Fig. 27. Engineering stress-strain of different HSLA grades (a) and different DP grades (b)

The most important needs for automotive applications are formability and crash-energy absorption. DP steels, with their increased values of the work hardening exponent due to the particular balanced microstructure, can have greater stretchability and crash energy absorption than HSLA steels.

Stretching can be derived from the total elongation obtained in a standard tensile test. The DP steels are generally characterized by higher total elongations than HSLA steels of equal yield strengths and of equal tensile strength, as it can be noticed in Fig. 28a and Fig. 28b [113].

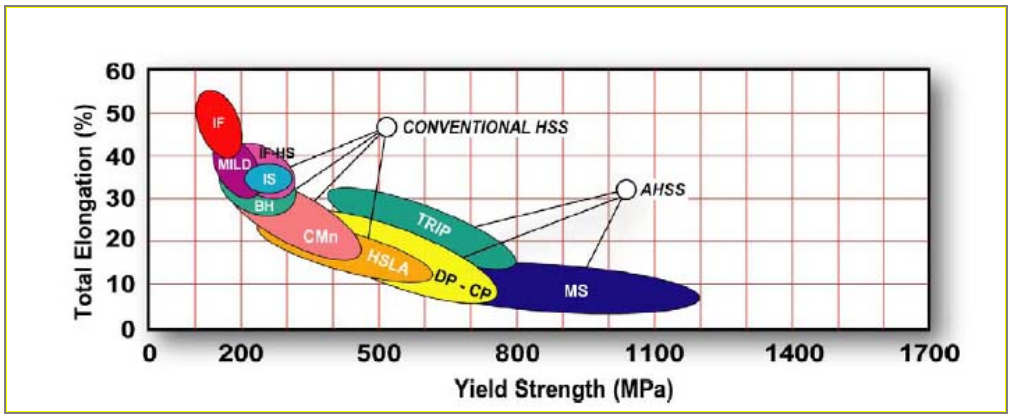

(a)

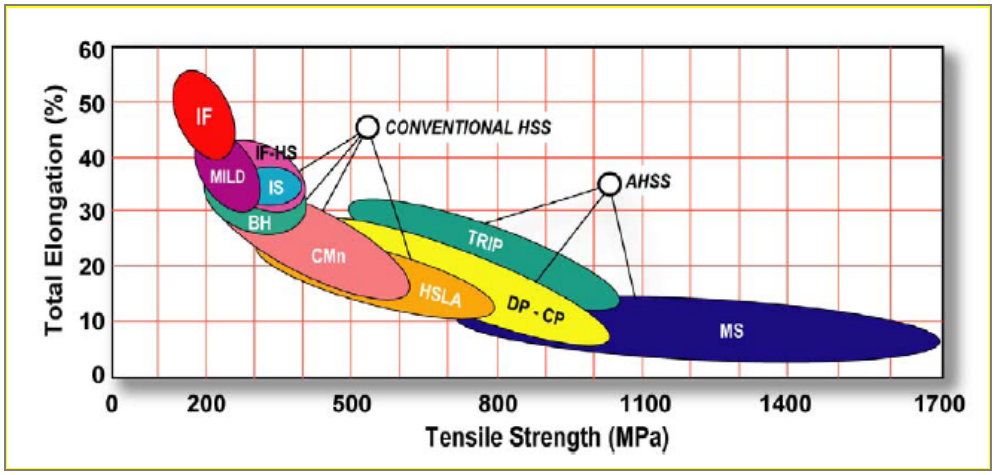

(b)

Fig. 28. Relationship between yield strength and total elongation (a) and between tensile strength and total elongation (b) for various types of steel

The stretchability is also strongly affected by the work hardening exponent or n-value, as it determines the ability of steel to distribute the strain more uniformly in the presence of a stress gradient. A higher n-value means a deeper part can be stretched for equal safety margins or a larger safety margin for equal depth parts. However conventional HSS have a decreasing n-value with increasing yield strength thus limiting the application of some HSS. DP steels have a different behavior, especially in the early stage of strain. In fact, as reported in Fig. 29, they show an increased of instantaneous n-values in the initial stages of deformation compared to HSS. These higher n-values lead to a more uniform deformation when a stress gradient is present. Therefore with the DP steels it is possible to reduce local thinning [144].

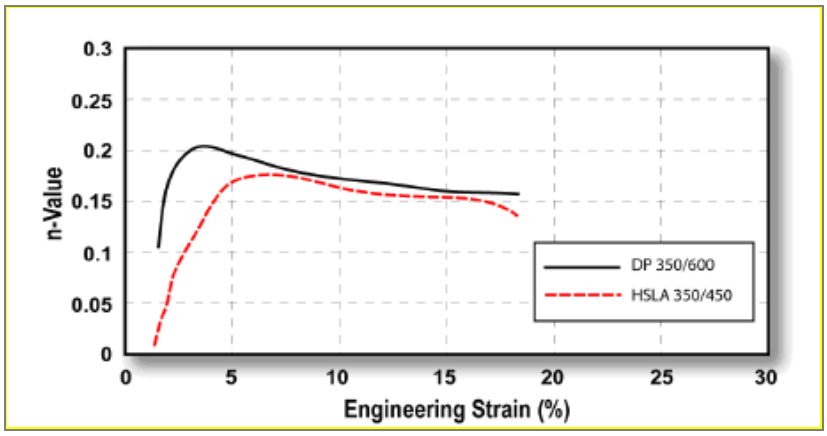

Fig. 29. Instantaneous n values versus strain for a DP and a HSLA steels with the same yield strength *[148]*

Another difference between HSLA and DP steels is the increase in yield strength caused by BH effects, as DP steels are subjected to this phenomenon whereas HSLA steels are not [113].
Also toughness properties are strongly affected by metallurgical features, as reported in Fig. 30 [145].

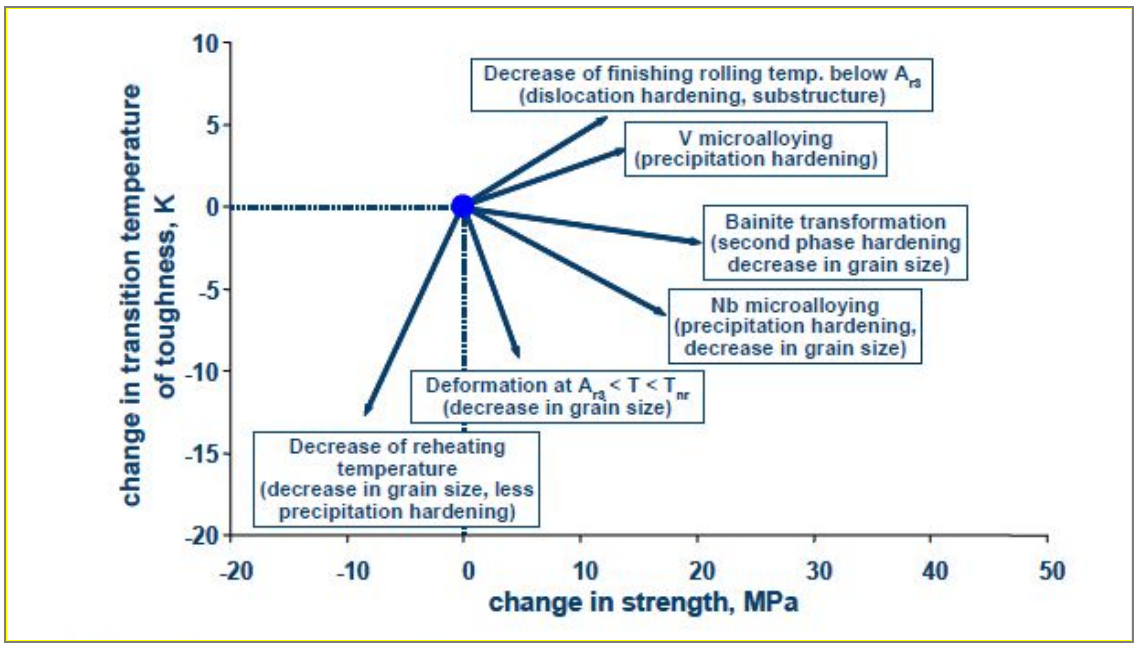

Fig. 30. Influence of microstructure and processing parameters on strength and transition temperature of toughness [145]

Fatigue properties are of crucial importance for safe long life components(*Paper V*, pp. 119-129).
HSLA steels were found to have comparable or superior fatigue properties than conventional mild steels. However the mechanisms of crack nucleation seem to be quite different. In HSLA steels an important role to the retard in crack nucleation and early propagation is played by slip bands. Some authors revealed a transgranular mechanism

of fracture differently from the traditional mild steels, in which fatigue crack started both in a trangranular and intergranular routes. Other studies highlighted the role of grain boundaries to hinder crack growth [146,147].
The fatigue limit of DP steels is higher than that of precipitation-hardened steels of similar yield strength, as noticeable in Fig. 31, where HSLA and DP steels are compared. The reasons for this better behavior is mainly metallurgical, as it was found that the dispersed fine martensite small islands retard the propagation of fatigue cracks [113,147].

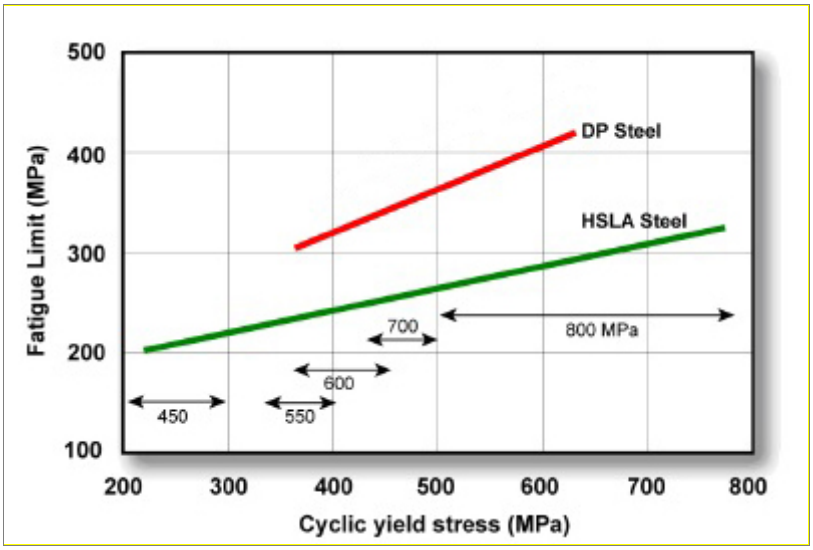

Fig. 31. Comparison between fatigue limits of a HSLA and a DP steels [147]

3.3.2 Formability

The formability is an essential property to know to optimize the product design and the production cycle of flat products. The formability of metal sheet is strictly related to the microstructure of the material. It can be determined through the strain hardening exponent *n*, the plastic strain ratio *r* and the strain rate sensitivity coefficient *m*; information about the straining behavior during the plastic deformation of the sheet. However the best way for a complete prediction of plastic instability phenomena related to complex states of deformation is given by the Forming Limit Diagram (FLD).
The FLD is created by different steps. The first stage is the virtual computerized forming-process development In this step the forming limits and grade of the steel under investigation is needed to determine the forming severity for each point on the stamping. The following operation is the design of tools and of the process. In this step the specific features of the tooling are established and again computer-validated compared to forming limits for the specific steel is repeated.
The FLD consists in a map of strains, indicating the onset of critical local necking for different strain paths, represented by major and minor strains. The limits of useful deformation and the safety region are provided by the critical strains. The safety region is represented by the points below the critical strain curves. The FLDs are experimentally determined forming flat specimens of different widths. The FLD also depends of the n-value and thickness of the material considered.
Studies about the formability of HSLA strip steels revealed the dependence of this property to the processing parameters, in particular to the coiling temperature. In Nb

HSLA steels an higher coiling temperature was found to allow a more intense precipitation of the interstitial elements from the ferritic matrix, thus enhancing the formability of the material. However the V HSLA steel grade showed the best formability properties due to the formation of the favourable texture components [148].
HSLA and DP steels are expected to have a similar formability behavior, due to comparable n value at high strain. In fig. u the experimental FLDs of a mild, HSLA and DP steel are compared. While DP and HSLA steels have substantially the same trend, the mild steel shows elevated values in the FLD because of its higher n value at high strain [149].

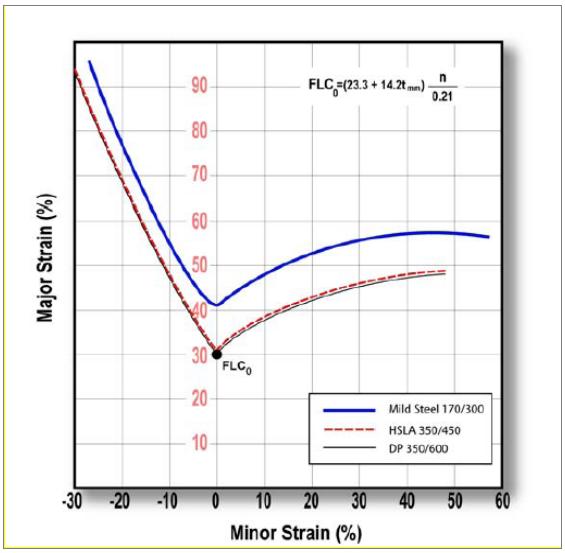

Fig. 32. Comparison between FLD of a mild steel, a HSLA and a DP steels[149]

3.3.3 Weldability

The welding properties became of fundamental importance with the growing use of HSS and AHSS especially in the automotive industry. Many studies were carried out on both welded HSLA and DP steels, however deeper knowledge and improvement are still needed. HSLA and DP steels have particular microstructural features obtained by non conventional thermal and thermo-mechanical processing. As the microstructure can be modified by following heat technological operations, the welding parameters have to been strictly controlled to not have any loss in mechanical properties. Higher heat inputs and cooling rates may strongly affected the microstructure. In this case it is normal to have martensite and/or bainite microstructures in the weld metal and in the HAZ with a consequent loss in toughness.
The weldability of most HSLA steels was found to be similar to that of mild steels. Experimental results obtained by resistant spot welding process showed that the HSLA steels can be welded with about the same current and time setting used for low carbon mild steels. However higher electrode force may be needed because of the higher strength of these steels. To limit the problems connected with the heat affected zone (HAZ) laser beam welding is suitable for HSLA steels.
The beneficial role of V in HSLA steels has been highlighted by Mitchell et al, particularly in the HAZ at slower cooling rates [150].

The DP steels can be satisfactorily welded with the suitable processes and parameters. Even for DP steels resistant spot welding and laser welding are the most used joint techniques due to their lower heat inputs if compared with other welding techniques. During resistant spot welding DP steels usually need a higher electrode force, but lower current than conventional Mild steel or HSLA as they have higher electrical resistivity (Fig. 33). Therefore, current levels for DP steels can be left constant or even reduced depending on material chemical composition.

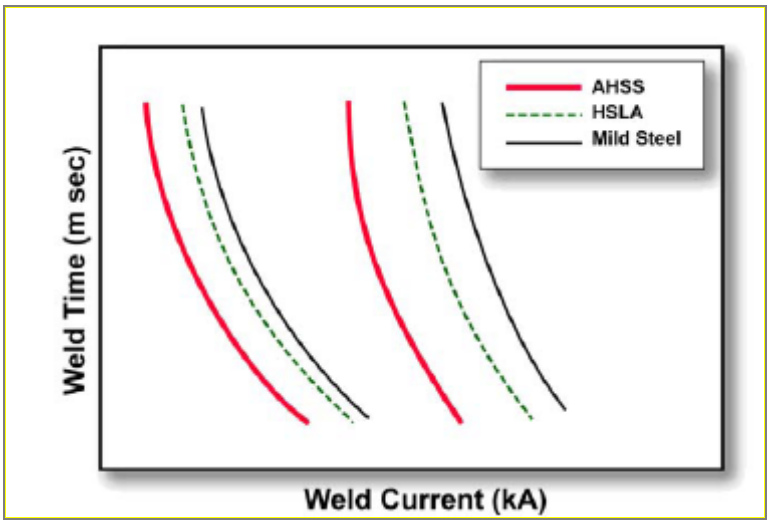

Fig. 33. Schematic weld lobes of AHSS, HSLA and Mild steel with a shift to lower currents for increased strength grades [113]

The resistant spot welding of the DP steels with different materials can negatively affect the quality and properties of the joint [151]. Moreover porosity can occur in the welded nugget of the DP steels, due to a narrower current range in the DP steels welding process compared to that of mild steels. To avoid this problem an increase of both weld force and weld time can be applied [151].

More recently laser welding of Dual Phase steels and its influence on microstructure and properties has been investigated. The importance of heat input for the martensite formation in the HAZ has been studied by Xia et al. for different grades of DP steels [152]. A martensitic structure in the fusion zone and continuous different microstructure of HAZ depending on the distance from the fusion zone have been revealed [153]. Another study compared different welding technologies applied to join DP steels, founding a substantial similarity in the microstructures of the FZ and HAZ of all the joints. Differences between the various technologies have been found connected to the width of FZ and HAZ, due to different heat inputs [154].

Brazing and Weld-brazing are of particular interest especially in zinc-coated DP steels joints.

Choosing the suitable braze materials any additional corrosion issues can be required. Moreover a lower heat input is furnished, with a beneficial effect in the HAZ (*Paper VI*, pp. 131-141).

AIMS AND BRIEF SUMMARIES OF THE PAPERS

The aim of **Paper 1** was to study the phase transformations occurring in 2507, 2205, 2304 and 2101 DSS grades during isothermal treatments in the range 750-1000°C and continuous cooling heat treatments. This was of particular importance due to the possible precipitation of secondary phases which are detrimental for both mechanical and corrosion properties. The experimental results have been compared with the Thermocalc calculations forecast. The deviation between Thermocalc calculations and experimental data was explained by the differences of ferrite and austenite phases stability of the four grades heat treated in the same critical range of temperature, thus affecting the secondary phases precipitation mechanism and kinetic.

The aim of **Paper 2** was to analyze the effects of intermetallic precipitation on toughness in two lean duplex stainless steels. The impact fracture properties and surfaces of the two steels isothermally heat treated in the range of temperature critical for secondary phase precipitation have been investigated. Different behaviors have been observed for the two steels, due to the different morphology of intermetallic phases precipitation.

The aim of **Paper 3** was to investigate the influence of cold rolling on microstructural properties and phase transformation in a lean duplex stainless steel. The application of a plastic deformation in a metastable stainless steel can induce the transformation of fcc paramagnetic austenite into bcc ferromagnetic martensite, thus potentially affecting the properties of the material. A relation between microstructure and magnetic properties such as saturation magnetic polarization, relative magnetic permeability and coercivity has been revealed, index of a possible strain-induced martensite formation occurring during cold rolling in the lean DSS considered.

The aim of **Paper 4** was the study the influence of micro-alloying elements Nb, V on microstructural properties such as grain refining and anisotropy and on mechanical strengthening in HSLA steels. To reveal the presence and distribution of micro-alloying elements carbides/nitrides and carbonitrides, transmission electron microscopy (TEM) and statistical analysis have been applied. The results was used to calculate the strengthening due to the precipitation phenomena according to Ashby-Orowan approach. A first evaluation of mechanical properties has been given by microhardness profiles along the thickness of the samples. Moreover a fractographic study has been performed on specimens failed after high cycles fatigue tests.

The aim of **Paper 5** was to determine the high cycle fatigue properties and fracture mechanisms in a Nb-V HSLA steel for forming applications. The fatigue limit and the retard to fatigue failure was related to the fine structure due to the addition of Nb and the specific thermo-mechanical processing.

The aim of **Paper 6** was to reveal the microstructural changes occurring in the interface area of a braze-welded Dual Phase steel. The influence of braze-welding parameters on microstructure and on the width of the heat affected zone (HAZ) has been investigated as well. An intermetallic Fe-Si-Cu compound layer was found at the interface between steel and filler metal. Moreover the braze-welding speed was found to

affect the width of HAZ, the thickness of the compound layer, the size of the precipitates in the filler metal and the mechanical properties.

REFERENCES

[1] M. Kobayashi, Duplex statistics 2008, www.outokumpu.com.
[2] J-C. Gagnepain, Duplex stainless steels: success story and growth perspectives, Stainless Steel World America 2008 Conference & Expo.
[3] J. Olsson, M. Liljas, 60 years of DSS applications, NACE Corrosion 94 Conference, Baltimore, MD, (1994) paper No. 395.
[4] E.C. Bain, W.E. Griffith, Trans AIME, 75 (1927) 166.
[5] R.N. Gunn, Duplex Stainless Steels: Microstructure, properties and applications. Ed. Abington Publishing, Cambridge England (1997).
[6] I. Alvarez-Armas, Duplex Stainless Steels: Brief History and Some Recent Alloys, Recent Patents on Mechanical Engineering, 1 (2008) 51-57.
[7] J. Hochmann, Revue du Nickel, 7 ,8 ,9 (1950) 53-60.
[8] R. Scherer, Journèe de la lute contre corrosion, Paris, France, (1938) 363-370.
[9] I. Colombier, J. Hochmann, Aciers inoxydables, aciers refractaries, Ed. Dunod, Paris, (1965).
[10] J. Hochmann, A. Desestret, P. Jolly, R. Mayoud, Proc. Conf. Stress corrosion cracking and hydrogen embrittlement of iron base alloys, NACE, 3 (1977) 965-1002.
[11] J. Holtzer Co., French patent (1935) 803-361.
[12] J. Charles, Proc. Conf. Duplex Stainless Steels ’91, Beaune, Les editions de physique, 1(1991) 4-48.
[13] A. Desestret, J. Charles, Les aciers inoxydables, Les editions de physique, 18, 631-678.
[14] M.G. Fontana, F.H. Beck, Alloy Casting Institute project no. 44, Report 49 and 52, January 1964 and December 1965.
[15] G.B. Holloway, J.C.M. Farrar, Welding consumables of duplex and superduplex stainless steels-optimizing properties after heat treatment, Proc. Duplex Stainless Steels ’91, Les Editions de Physique, France (1991) 571.
[16] D.S. Bergstrom, J.J. Dunn, J.F. Grubb,W.A. Pratt, US20036551420B1 (2003).
[17] E. Alfonsson, Lean duplex – the first decade of service experience, Proc. Conf. Duplex World Stainless Steels, Beaune, France (2010).
[18] G. Chai, P. Kangus, A. Sundström, M. Klockars, A. Nyström, Hyper Duplex Stainless steels, World Stainless Steel conference (2009).
[19] J. Charles, Past, present and future of the Duplex Stainless Steels, Proc. 7th Duplex 2007 Int. Conf & Expo, Grado, Italy (2007).
[20] International Molybdenum Association (IMAO), Practical Guidelines for the Fabrication of Duplex Stainless Steels, Pensylvania, USA (2001).
[21] D.S. Bergstrom, Benchmarking of Duplex Stainless Steels versus Conventional Stainless Steel Grades, Proc. 7th Duplex 2007 Int. Conf & Expo, Grado, Italy (2007).
[22] M. Holmquist, Consider duplex stainless steels for corrosive exchangers’ service, Hydrocarbon Processing (2001).
[23] D. Zuili, The Use of Duplex Stainless Steel in Oil & Gas Industry, Conf proc Duplex Stainless Steels (2010).
[24] J. Olsson, M. Snis, Duplex - A new generation of stainless steels for desalination plants. Desalination, 205 (2007) 1-3: 104-113.
[25] H. Junichi, E. Nagashima, Duplex Stainless Steel DP28WTM Enhances Safety and Economy of Urea Plant, World Stainless Steel conference (2009).

[26] A. Wensley, Duplex in the pulp and paper industry - the good, the bad, and the ugly, Conf proc Duplex Stainless Steels (2010).
[27] P-J. Cunat, Stainless steel properties for structural automotive applications, Metal Bulletin International Automotive Materials Conference, Cologne, 21st to 23rd (2000).
[28] W.T. DeLong, Ferrite in austenitic stainless steel weld metals, Weld. J., 53 (1974) 273-286.
[29] J. Charles, Why and where duplex stainless steels, Duplex Stainless Steels '97, Maastricht, Netherlands, 1 (1997) 29-42.
[30] J-O. Nilsson, Super duplex stainless steels, Materials Science and Technology, 8 (1992).
[31] H. Sieurin, "Fracture toughness properties of duplex stainless steels", Doctoral Thesis (2006).
[32] J. Charles, Composition and properties of duplex stainless steels, Weld. World (UK), 36 (1995) 43-54.
[33] J. Charles, Duplex stainless steel 91, Beaune, Francia, Les édition de physique, 3.
[34] B. Josefsson, J.O. Nilsson, A. Wilson, Phase transformations in duplex steels and the relation between continuous cooling and isothermal heat treatment, Duplex Stainless Steels '91, Beaune, France, 1 (1991) 67-78.
[35] T.H. Chen, J.R., Effects of solution treatment and continuous cooling on σ-phase precipitation in a 2205 duplex stainless steel, Mater. Sci. Eng. A, 311 (2001) 28-41.
[36] Calliari et al., Precipitation of secondary phases in super duplex stainless steel ZERON100 isothermally aged, Mater. Sci. Technol., (2010) in press.
[37] Calliari et al., Investigation of secondary phase effect on 2205 DSS fracture toughness, Mater. Sci. Technol., 26 (2010) 81-86.
[38] C.V. Roscoe, K.J. Gradwell, G.W. Lorimer, Institute of Metals book, editor. Conf. transcript, Stainless Steels (1984) 563.
[39] A.J. Strutt, G.W. Lorimer, Conf. Proc., Int. Conf. on Duplex Stainless Steel '86, The Hague (1986) 310.
[40] M. Pohl et al., Materials Characterization 58 (2007) 65–71.
[41] L. Duprez, B.C. De Cooman, N. Akdut, Redistribution of the substitutional elements during σ and χ phase formation in a duplex stainless steel, Steel research, 72 (2001) 311-316.
[42] T. H. Chen, K. L. Weng and J. R. Yang: Mater. Sci. Eng. A, A338 (2002) 259–270.
[43] L. Karlsson, L. Bengtsson, U. Rolander and S. Pak, Proc. Conf. Application stainless steel 92, Stockholm, Sweden, (1992) The Institute of Metals, 335–344.
[44] J.-O. Nilsson, A. Wilson, B. Josefsson, and T. Thovarldsson, Proc. Conf. 'Stainless steels '92', Stockholm, The Institute of Materials, 1 (1992) 280.
[45] R. Dakhalaoui, C.Braham, A. Baczmanski, S.Wronski, K.Wierbanoski, E.C.Oliver, Analyze of phase's mechanical behaviour of duplex stainless steels by X-ray and neutron diffraction. Duplex, Grado, Italy (2007).
[46] H. W. Hayedn and S. Floreen, Trans. ASM, 61 (1968) 474.
[47] M. Jacobsson, Fatigue testing of the duplex grades SAF 2304, SAF 2205 and SAF 2507, Internal Report no. 6060, Sandvik Steel, Sandviken, Sweden (1991).
[48] J. Charles, Duplex stainless steels, a review after DSS '07 held in Grado, Rev. Met. Paris, 3 (2008) 155-171.

[49] J. Stolarz, J. Foct, Specific features of two phase alloys response to cyclic deformation, Mater. Sci. Eng. A, 319-321 (2001) 501-505.
[50] J-B. Vogt, Fatigue properties of high nitrogen steels, Mater. Proc. Tech., 117 (2001) 364-369.
[51] A. Mateo, L. Llanes, N. Akdut, M. Anglada, High cycle fatigue behaviour of a standard duplex stainless steel plate and bar, Mater. Sci. Eng. A, 319-321 (2001) 516-520.
[52] J.-O. Nilsson, P. Liu, Mater. Sci. Technol., 7 (1991) 853-862.
[53] C.-G. Carlborg, A. Nilsson, and P.-A. Franklind, Proc. Conf. Duplex stainless steels '91, Les Viis, France, Les Editions de Physique 685 (1991).
[54] M. Femenia, J. Pan, C. Leygraf, Journal of the Electrochemical Society, 151, B581 (2004).
[55] S. Aoki, H. Yakuwa, K. Mitsuhashi, J. Sakai, ECS Transactions, 25 (2010) 17.
[56] S. Bernhardsson, Proc. Conf. Duplex Stainless Steels ’91, EDP Sciences, Les Ulis, (1991).
[57] L. Peguet, A. Gaugain, Localized corrosion resistance of duplex stainless steels: methodology and properties; a review paper, Proc. Conf. Duplex World Stainless Steels, Beaune, France (2010).
[58] R.F.A. Pettersson, E. Johansson, Stress corrosion resistance of duplex grades, Proc. Conf. Duplex World Stainless Steels, Beaune, France (2010).
[59] S. Bernhardsson, R. Mellström, J. Oredsson. Proc. Conf. Duplex Stainless steels 1982, ASM (1983).
[60] S.R.F. Batista and S.E. Kuri, Aspects of selective and pitting corrosion in cast duplex stainless steels, Anti-Corrosion Methods and Materials, 51 (2004) 205–208.
[61] C.M. Garzon, C.A. Serna, S.D. Brandi, A.J. Ramirez, J. Mater. Sci., 42, 9021 (2007).
[62] Z. Cvijovic´ , G. Radenkovic´, Corrosion Science 48 (2006) 3887–3906.
[63] Z. Wei , J. Laizhu, S. Hongmei, H. Jincheng, W. Zhiyu, Comparative study of mechanical property and precipitation of duplex stainless steel 2101 and 2205, Proc. Conf. Duplex World Stainless Steels, Beaune, France (2010).
[64] C. Bergqvist, J. Olsson, Machining in the new duplex grade LDX 2101® - easier than expected, Proc. Conf. Duplex 2007 International Conference and Expo, Grado, Italy (2007).
[65] Outokumpu Corrosion Handbook, Uniform corrosion testing of stainless steels using the MTI-1 procedure (2009) I:29-I36.
[66] E. Johansson, T. Prosek, NACE Corrosion 2007, paper no 07475 (2007).
[67] M. Liljas, P. Johansson, H.-P. Liu, C.-O. Olsson, Development of a lean duplex stainless steel, Steel Research International, 79 (2008) 466-473.
[68] Lihua Zhang, Yiming Jiang, Bo Deng, Wei Zhang, Juliang Xu, Jin Li, Effect of aging on the corrosion resistance of 2101 lean duplex stainless steel, Mat.Charact. 60 (20090) 1522–1528.
[69] V. Di Cocco, F. Iacoviello, O. Di Bartolomeo, D. Cipriani, Heat treatment influence on localized and selective corrosion resistance in a 21 Cr 1 Ni stainless steel, Proc. Conf. Duplex 2007 International Conference and Expo, Grado, Italy (2007).
[70] P.L. Mangonon, G. Thomas, Metall. Trans. 1 (1970) 1587.
[71] V. Seetharaman, P. Krishnan, J. Mater. Sci. 16 (1981) 523.

[72] A. Mitra, P.K. Srivastava, P.K. De, D.K. Bhattacharya, D.C. Jiles, Ferromagnetic Properties of Deformation-Induced Martensite Transformation in AISI 304 Stainless Steel, Met. Mat. Trans. A, 35A (2004) 599-605.
[73] K. Mumtaz, S. Takahashi, J. Echigoya, Y. Kamada, L.F. Zhang, H. Kikuchi, K. Ara, M. Sato, Magnetic measurements of martensitic transformation in austenitic stainless steel after room temperature rolling, Journal of Materials Science, 39 (2004) 85-97.
[74] I. Mészáros, J. Prohászka, Magnetic investigation of the effect of α'-martensite on the properties of austenitic stainless steel, Journal of Materials Processing Technology, 161 (2005) 162–168.
[75] J. Talonen, Effect of strain-induced α'-martensite transformation on mechanical properties of metastable austenitic stainless steels, Doctoral Thesis (2007).
[76] M. Baeva, S. Neov, R. Sonntag, Appearance of bcc martensite after cold deformation of austenitic Fe-Cr-Mn-N, Scripta Metallurgica et Materialia, 32 (1995) 1031-1035.
[77] P. Haušild, V. Davydov, J. Drahokoupil, M. Landa, P. Pilvin, Characterization of strain-induced martensitic transformation in a metastable austenitic stainless steel, Materials and Design, 31 (2010) 1821–1827.
[78] P.K. Chiu, K.L. Weng, S.H. Wang, J.R. Yang, Y.S. Huang, J. Fang, Low-cycle fatigue-induced martensitic transformation in SAF 2205 duplex stainless steel, Materials Science and Engineering A, 398 (2005) 349–359.
[79] S.M.M. Tavares, M.R. da Silva, J.M. Pardal, H.F.G. Abreu, A.M. Gomes, Microstructural changes produced by plastic deformation in the UNS S31803 duplex stainless steel, Journal of Materials Processing Technology, 180 (2006) 318–322.
[80] G. Fargas, N. Akdut, M. Anglada, A. Mateo, Microstructural Evolution during Industrial Rolling of a Duplex Stainless Steel, ISIJ International, 48 (2008) 1596–1602.
[81] M.R. Berrahmoune, S. Berveiller, K. Inal, E. Patoor, Materials Science and Engineering A 438–440 (2006) 262.
[82] Y.H. Kim, K.Y. Kim, Y.D. Lee, Materials and Manufacturing Processes 19 (2004)
[83] R. P. Reed, Acta Met., 10 (1962) 865.
[84] D. A. Porter, K. E. Easterling, Phase Transformation in Metals and Alloys,. Chapman and Hall, London (1992).
[85] R. F. Bunshah and R. F. Mehl, Trans. AIME 197 (1953) 1251.
[86] K.H. Lo et al., Recent developments in stainless steels, Materials Science and Engineering R 65 (2009) 39–104.
[87] I. Altenberger, B. Scholtes, U. Martin, H. Oettel, Mater. Sci. Eng. A 264 (1999) 1.
[88] C.X. Huang, G. Yang, Y.L. Gao, S.D. Wu, S.X. Li, Journal of Materials Research 22 (2007) 724.
[89] A. Das, S. Sivaprasad, M. Ghosh, P.C. Chakraborti, S. Tarafder, Materials Science and Engineering A 486 (2008) 283.
[90] N. Gey, B. Petit, M. Humbert, Metallurgical and Materials Transactions A 36 (2005) 3291–3299.
[91] M. Humbert, B. Petit, B. Bolle, N. Gey, Materials Science and Engineering A 454– 455 (2007) 508.
[92] T.-H. Lee, C.-S. Oh, S.-J. Kim, Scripta Materialia 58 (2008) 110.

[93] K. Spencer, M. Veron, K. Yu-Zhang, J.D. Embury, Materials Science and Technology 25 (2009) 7.
[94] J.-Y. Choi, W. Jin, Scripta Materialia 36 (1997) 99
[95] P. Hedström, "Deformation and Martensitic Phase Transformation in Stainless Steels", Doctoral Thesis (2007).
[96] L.E. Murr, K.P. Staudhammer, S.S. Hecker, Metallurgical Transactions A 13 (1982) 627.
[97] S.G.S. Raman, K.A. Padmanabhan, Journal of Materials Science Letters 13 (1994) 389.
[98] K.G. Farkhutdinov, R.G. Zaripova, N.A. Breikina, Materials Science and Engineering A174 (1994) 217.
[99] B. Mazza, P. Pedeferri, D. Sinigaglia, A. Cigada, .A. Fumagalli, G. Re, Corrosion Science 19 (1979) 907.
[100] S.V. Phadnis, A.K. Satpati, K.P. Muthe, J.C. Vyas, R.I. Sudaresan, Corrosion Science 45 (2003) 2467.
[101] L. Peguet et al., Corrosion Science 49 (2007) 1933–1948.
[102] Xu Chunchun, Hu Gang, Effect of deformation-induced martensite on pit propagation behaviour of 304 stainless steel, Anti-Corrosion Methods and Materials 51 (2004) 381-388.
[103] B.R. Kumar, B. Mahato, R. Singh, Influence of cold-worked structure on electrochemical properties of austenitic stainless steels, Metallurgical and Materials Transactions A 38 (2007) 2085-2094.
[104] T. Siwecki and G. Engberg, Thermo-Mechanical Processing in Theory, Modelling & Practice, Eds. Hutchinson B. et al., Stockholm, 1996, ASM Inter., 121 (1997).
[105] D.B. Santos, R.K. Bruzszek, P.C.M. Rodrigues, E.V. Pereloma, Mater Sci Eng A 346 (2003) 189.
[106] J.G. Williams, New alloy design perspectives for high strength steels", Proc. Conf. The third international conference on themomechanical processing of steels, Padua, Italy (2008).
[107] Yu. I. Matrosov, A.G. Nasibov, and I. N. Golikov, "Properties of low-pearlite steels with vanadium and niobium after controlled rolling," Metalloved. Term. Obrab° Met., No. I, 27-34 (1974).
[108] C.I. Garcia, M. Hua, K. Cho, A.J. DeArdo, On the strength of microalloyed steels-an interpretative review, Proc. Conf. The third international conference on themomechanical processing of steels, Padua, Italy (2008).
[109] M. Maruyama, R. Uemori, M. Sugiyama, Mater Sci Eng A 250 (1998) 2.
[110] S. Takaki, K. Kawasaki, Y. Kimura, J Mater Process Technol 117 (2001) 359.
[111] W.M. Rainforth, M.P. Black, R.L. Higginson, E.J. Palmiere, C.M. Sellars, I. Prabst, ISS, Columbus, OH (2002).
[112] A. Pandit, A. Murugaiyan, A. Saha Podder, A. Haldar, D. Bhattacharjee, S. Chandra et al., Scr Mater 53 (2005) 1309.
[113] Committee on automotive applications, International Iron and Steel Institute, Advanced high strength steel (AHSS), Application Guidelines (2006).
[114] G. Lovicu, M. Barloscio, M. Bottazzi, F. D'Aiuto, M. De Sanctis, A. Dimatteo, C. Federici, S. Maggi, C. Santus, R. Valentini, Hydrogen Embrittlement of advanced high strength steels for auto motive use, Proc. Conf. The second International Super-high strength steels Conference, Peschiera del Garda, Verona, Italy (2010).
[115] B. Dutta, A. Valdes, C.M. Sellars, Acta Metall. Mater., 40 (1992) 653.

[116] M. Murayama, K. Hono, Scr Mater 44 (2001) 701.
[117] E.V. Pereloma, I.B. Timokhina, K.F. Russell, M.K. Miller MK, Scr Mater 54 (2006) 471.
[118] A.J. Craven, K. He, L.A.J. Garvie, T.N. Baker, Acta Mater 48 (2000) 3869.
[119] R. Stasko, H. Adrian, A. Adrian, Mater Charact 56 (2006) 340.
[120] J.A. Wilson, A.J. Craven, Ultramicroscopy 94 (2003) 97.
[121] M. MacKenzie, A.J. Craven, C.L. Collins, Scr Mater 54 (2006) 1.
[122] L.J. Cuddy, Grain refinement of Nb steels by Control of Recrystallization During Hot Rolling, Metall. Trans., 15A (1984) 87-98.
[123] M. Cabibbo, A. Fabrizi, M. Merlin, G. L. Garagnani, J Mater Sci, 43 (2008) 6857–6865.
[124] M. Venkatraman, T. Venugopalan, Proc. Int. Conf. TMP'2004, Liege (2004) 99.
[125] A.J. DeArdo, Niobium in Modern Steels, International Materials Reviews, 48 (2203) 371-402.
[126] C. Lech, Strengthening of cold rolled HSLA steels by rapid transformation annealing (RTA), Proc. Conf. The second International Super-high strength steels Conference, Peschiera del Garda, Verona, Italy (2010).
[127] L. M. Brown, R. H. Cook, R. K. Ham, G. R. Purdy, Scripta Metallurgica, 7 (1973) 815-820.
[128] T. Gladman, D. Dulieu and I. D. McIvor, Structure-Property Relationships in High Strength Microalloyed Steel, Microalloying 75, Union Carbide Corporation, New York, NY, USA, 32-55.
[129] R. Abad et al., ISIJ International, 41 (2001) 1373-1382.
[130] S.F. Medina, A. Quispe, ISIJ International, 36 (1996) 1295-1300.
[131] R.M. Poths, W.M. Rainforth, E.J. Palmiere, Materials Science Forum, 500-501 (2005) 139-146.
[132] B. Dutta, E.J. Palmiere, and C.M. Sellars, Acta Materialia, 49 (2001) 785-794.
[133] H.S. Zurob et al., Acta Materialia, 50 (2002) 3075-3092.
[134] C.M. Sellars, E.J. Palmiere, Materials Science Forum, 500-501 (2005) 3-14.
[135] A. Kundu, C.L. Davis, M. Strangwood, Grain structure development during reheating and deformation of Niobium-microalloyed steels, Proc. Conf. The third international conference on themomechanical processing of steels, Padua, Italy (2008).
[136] R. Kuziak et al., Microstructure control of ferrite-pearlite high strength low alloy steels utilizing microalloying additions, Journal of Material Processing Technology 53 (1995) 520-532.
[137] M. MacKenzie et al., Scripta Materialia 54 (2006) 1–5.
[138] T. Siwecki et al., Proc. Int. Conf. on Microalloyng, Pittsburg PA (1995) 197.
[139] G.R. Speich, A.B. Miller, R.A. Kot and B.L. Bramfitt, editors, Fundamentals of dual-phase steels, The Metallurgical Society of AIME, New York, USA (1981) 279.
[140] T. Senuma, Physical Metallurgy of Modern High Strenght Steel Sheets, ISIJ International, 41 (2001) 520-525.
[141] S.T. Mandziej, Thermomechanical processing for dual-phase microstructure, Proc. Conf. The third international conference on themomechanical processing of steels, Padua, Italy (2008).
[142] K. Mukherjee, S.S. Hazra, M. Militzer, Metall. Mater. Trans. A (2009) 2145.
[143] M. Calcagnotto, Effect of grain refinement to 1 μm on deformation and fracture mechanisms in ferrite/martensite dual-phase steels, Proc. Conf. The second

International Super-high strength steels Conference, Peschiera del Garda, Verona, Italy (2010).
[144] A. Konieczny, Advanced High Strength Steels – Formability, Great Designs in Steel, American Iron and Steel Institute (2003). www.autosteel.org
[145] J. Bauer, V. Schwinn, K.H, Tacke, Recent developments of pipe steels using tmcp-technology, Proc. Conf. The third international conference on themomechanical processing of steels, Padua, Italy (2008).
[146] S. P. Bhat, M. E. Fine, Fatigue crack nucleation in iron and high strength low alloy steel, Material Science and Engineering A314 (2001) 90-96.
[147] M. D. Chapetti et al., Fatigue crack propagation behavior in ultra-fine grained low carbon steel, International Journal of Fatigue 27 (2005) 235-243.
[148] R. Venturini, "Effetto della tecnologia di colaggio in sottile con laminazione diretta sulle proprietà meccaniche e di formabilità di acciai HSLA", Doctoral Thesis (2006).
[149] A. Konieczny, Advanced High Strength Steels – Formability, Great Designs in Steel, American Iron and Steel Institute (2003). www.autosteel.org.
[150] P.S. Mitchell, W.B. Morrison, The manufacture and weldability of Vanadium-containing steels. www.vanitec.org
[151] S. Schreiber, S. Keitel, R. Winkler, P. Zak, Resistance welding of high strength steels combinations, Proc. Conf. The second International Super-high strength steels Conference, Peschiera del Garda, Verona, Italy (2010).
[152] M. Xia, E. Biro, Z. Tian, Y.N. Zhou, Effects of heat input and martensite on HAZ softening in laser welding of dual phase steels, ISIJ International, 48 (2008) 809.
[153] P. Rizzi, S. Bellingeri, F. Massimino, D. Baldissin, L. Battezzati, Microstructures in laser welded high strength steels, Journal of Physics, Conference Series 144 (2009) 012005.
[154] A. Tiziani, P. Ferro, R. Cervo, M. Durante, Effects of differetn welding technologies on metallurgical and mechanical properties of DP600 steel welded joints, Proc. Conf. The second International Super-high strength steels Conference, Peschiera del Garda, Verona, Italy (2010).

PART 2

PAPERS

Analysis of phase stability in Cr-Ni and Cr-Mn DSS

I.Calliari[1], M. Pellizzari[2], S. Baldo1, M. Zanellato[1] and E. Ramous[1]

[1]DPCI, University of Padova, Italy
[2]DMEIT, University of Trento, Italy

Abstract. The phase modifications in the 2205, 2507, 2304 and 2101 DSS during isothermal treatments in the range 750-1000°C and continuous cooling have been examined and compared. For all the steels considered the Thermocalc calculations forecast the sigma and chi phase precipitation. However this indication is confirmed by the experimental results for 2205 and 2507 grades only. On the contrary in the Cr-Mn grades 2305 and 2101, dangerous phases precipitation is much more sluggish and these phases are very rarely observed after isothermal aging or low rate continuous cooling. This different behavior could be justified by the differences of ferrite and austenite phases stability in the four grades, in the same temperature range of the sigma and chi precipitation, because these differences can affect the sigma phase precipitation mechanism and kinetic.

1. INTRODUCTION

Duplex stainless steels (DSS) combine attractive corrosion and mechanical properties, obtained with a balanced microstructure, having approximately equal amounts of ferrite α and austenite γ. To this end both composition and thermo-mechanical treatments of these alloys have to be properly designed and controlled. To attain the desired technological properties the composition is adjusted by adding well equilibrated amounts of Cr, Mo, Ni, Mn to the base Fe- Cr alloy. However such additions affects both the relative stability of austenite and ferrite phases, and can induce the formation of a number of χ and σ, dangerous TCP phases, in the temperature range below 1000°C, during either service and fabrication, detrimental both for corrosion and mechanical properties. Therefore thermo-mechanical treatments are always necessary, like a solution annealing followed by rapid quenching from temperature above 1000°C, both to avoid dangerous phases formation and to maintain the balanced microstructure of ferrite and austenite, stable only at temperatures above 1000°C [1-4].

These phenomena are well known and have been extensively studied, for its important practical implications, which determine both service and fabrication conditions. The study of dangerous phases formation in DSS, beside some interesting fundamentals aspects, is necessary to understand and clarify the behavior of DSS in two practical situations: the cooling from high temperatures, like the quenching after the solution annealing or after welding operations, and during long time maintenance at high temperatures, during service, for instance. To this end therefore it is necessary to study the eventual microstructure transformations occurring in the DSS both in continuous cooling tests (CCT) and in isothermal treatments (TTT) to define the mechanisms and sequence of dangerous phases formation in the two situations. Mechanisms and sequence indeed seems to be very different in DSS grades having different compositions, as the Cr-Ni and the Cr-Mn DSS [5-13].

Therefore it seems to be interesting to analyze and compare the sequence of dangerous phases formation in some between the more commonly used DSS grades: the results obtained could be useful also to correlate the differences of behaviour with the different compositions of the DSS grades examined.

2. EXPERIMENTAL

The as received material was a wrought SAF 2205, 2507, 2304 and 2101 DSS as rod and bars (30mm). Actual chemical compositions are reported in Table I.

Isothermal ageing treatments of specimens, previously solution annealed at 1020 or 1050 °C for 30 minutes, were carried out in the temperature range 650-1000°C. Both relatively short ageing times were chosen (20 -120 min) to measure low amounts of secondary phases and investigate their precipitation kinetics, and long times aging (up to about 550 hours), to investigate the behaviour of low nickel DSS steels.

Continuous cooling tests have been performed in a Setaram “Labsys TG” machine, in Argon atmosphere. Samples (diameter 6 mm, length 8 mm) were heated at 10°C/min from room temperature and solution treated (maintenance for 5 min) at temperatures of 1020°C and 1050 °C, then cooled in argon at various cooling rates in the range 0.02-0.4 °C/s.

	C	Si	Mn	Cr	Ni	Mo	Cu	W	P	S	N
2205	0.030	0.56	1.46	22.75	5.04	3.19	-	-	0.025	0.002	0.16
2507	0.030	0.43	0.54	24.48	6.36	4.0	0.67	0.72	0.020	0.008	0.263
2101	0.026	0.69	3.95	22.57	1.1	0.07	-	-	0.03	0.001	0.13
2304	0.03	0.56	1.4	23.20	4.1	0.18	-	-	0.027	0.001	0.10

Table I. Steels compositions

Different phases have been identified by SEM-BSE examination of unetched samples. The ferrite appears slightly darker than austenite, while the secondary phases are lighter. Owing to the higher content of molybdenum, in combination with the large atomic scattering factor of molybdenum χ-phase appears in brighter contrast than σ-phase [14]. On the contrary, nitrides appears as small black particles. The amount of secondary TCP phases has been determined using image analysis software on SEM-BSE micrographs (10 fields, 1000x). The chemical composition of the phases was determined by SEM- EDS on unetched samples. The volume fractions of ferrite and austenite in a solution treated sample have been measured on 3 longitudinal and 3 transversal sections (20 fields for each section) by image analysis on light micrographs at 200x, after etching with the Beraha's reagent (R.T., 10s).
Thermodinamic modelling in this work is based on the CALPHAD method (CALculation of PHAse Diagrams) [15]. The software Thermo-Calc [16] was used in connection with the thermodynamic database TCFe3. The method is based on the minimization of Gibbs free energy of the phases provided by the Fe-C-Si-Mn-Cr-Ni-Mo-N multicomponent system.

3. Equilibrium data

The microstructures obtained in the steels examined after solution annealing, isothermal aging and continuous cooling tests can be analyzed and discussed relating them to the equilibrium microstructures which can be derived from Thermocalc calculations and some equilibrium phase diagrams. The results of Thermocalc calculations for the examined steels are shown in Fig. 1: the diagrams present a rather similar general pattern but with some significant differences.

For all the grades:

1. the solidification produce a ferrite solid phase which, decreasing the temperature gradually and partially transform to austenite: therefore in all steels at 1020-1080°C, the microstructure consist of almost equivalent parts of austenite and ferrite;
2. at lowest temperatures, below 400°C, the microstructure consist mainly of ferrite, with some minor constituents as chi phase, other intermetallics and chromium carbides and nitrides; just in one case, i.e. 2101 grade, sigma phase is indicated also below this temperature.

Moreover the Thermocalc diagrams enlighten some important differences:

3. the temperature of the sigma phase formation decrease from the 2507 steel, to 2205, 2304 and 2101 steels, in the order, from about 1000°C to about 750°C;
4. only in the 2507 and 2205 grades the sigma formation occurs together with the disappearance of the ferrite which transform to sigma and secondary austenite and, at lower temperatures, the austenite partially transforms to ferrite, leaving the sigma unchanged;
5. on the contrary, in 2101 grade, the sigma formation occurs without the complete transformation of ferrite to secondary austenite; at low temperatures, as in 2507 and 2205 grades, austenite transform to ferrite;
6. the behaviour of the 2304 steel appears as intermediate: during the sigma formation ferrite partially transform to secondary austenite, therefore in this steel a significant ferrite content remains in all the considered temperature range.
7. in view of the higher Mo content, the precipitation of the chi phase is predicted for 2205 and 2507, while this is not for the 2101 and 2304 grades.

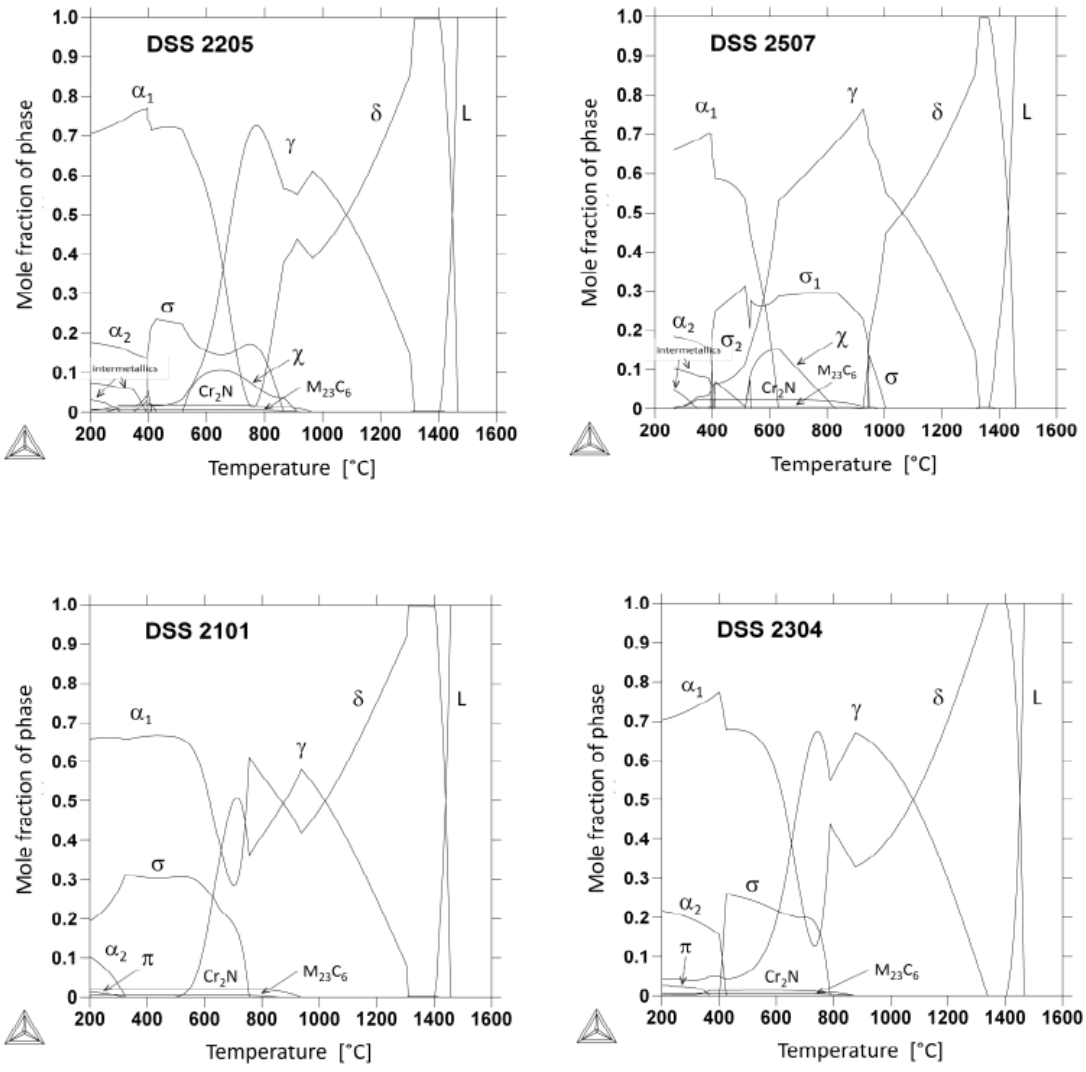

Fig. 1. Thermocalc diagrams of the four DSS

4. RESULTS AND DISCUSSION

4.1 Solution annealing

For all the steels examined, the microstructure obtained after solution annealing and quenching was typical of the DSS rolled products, in particular as concerning the ferrite/austenite ratio) The banded structure of elongated γ-phase islands was observed in the longitudinal sections, while the isotropic structure of ferrite and austenite grains was displayed on the transverse sections. The values of volume fractions of ferrite and austenite, measured on longitudinal and transverse sections, were typical of the steels considered: 50-55 % of ferrite and the remainder of austenite. The differences between transversal and longitudinal data are less than standard deviations. Therefore all the quantifications were performed on the transverse sections. Secondary phases were not detected in the annealed materials before the isothermal aging, in agreement with thermodynamic calculations (Fig.1).

4.2 2205 and 2507

4.2.1 Isothermal aging

In the 2205 grade the precipitation of secondary phases occur after ageing in the range 780-900°C (Fig.2). The precipitation sequence can be summarized as follows:

- 780 °C: the first precipitates appear after 30' ageing and become more evident after 40'. The small bright particles were identified as χ-phase by the SEM-EDS, just within the beam resolution limit.
- 850 °C**:** the χ-phase appears after about 10', while the σ-phase after about 20'; After 30' the χ-phase and the σ-phase are both present: the χ-phase is always at the boundaries γ/α and α/α. The σ-phase penetrates the ferrite or grows along the γ/α boundary.
- 900 °C: also at this temperature the first precipitating phase is the χ-phase, generally decorating the grain boundaries. By increasing the holding time, the amount of χ-phase increases and also the σ-phase appears, in the form of coarser precipitates at the γ/α boundary, but growing into the ferrite (fig.2) . Although σ particles are, at the beginning, less numerous than the χ-phase particles, they are coarser, and grow more rapidly, quickly reaching almost the same volume fraction. By increasing the holding time, σ-phase grows to large particles, moving from the boundaries into the ferrite, embedding some small χ particles. This seems to show the progressive transformation of χ-phase to σ-phase [6].

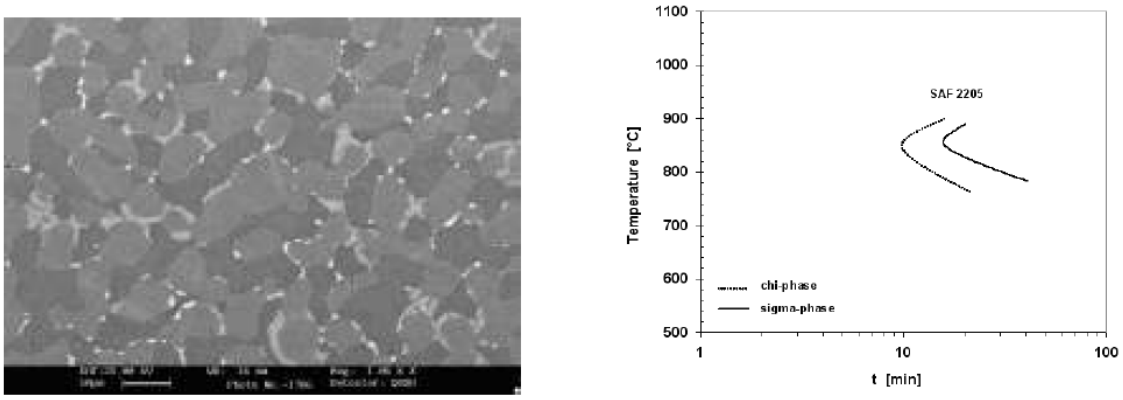

Fig. 2. 2205 isothermal aging: (left) SEM-BSE micrograph after 30 min at 900°C (right) σ and χ precipitation kinetic

In the 2507 grade the precipitation of secondary phases occur at higher temperatures than in the 2205 grade, between 850 and 1000°C [7]. The precipitation sequence is quite similar to that of the 2205 grade, and can be summarized as follows:

- 850°C: chi-phase is the only one phase to precipitate at the alfa/gamma (volume fraction <0.1%).
- 900°C: at this temperature the formation kinetic of χ-phase is favoured (Figs 3-4)
- 950°C Chi is the first phase to precipitate after 3', followed by sigma after 5' by increasing the holding time, sigma grows
- to large particles, moving from the boundaries into the ferrite, embedding some small chi particles which seems to behave as preferential sites for the sigma-phase nucleation
- -1000 °: After 5' chi and sigma are mainly at grain boundaries and a few inside the ferrite grains (about 0.5%). By increasing the time, the content of chi slowly decreases while the amount of sigma increases to its maximum value of 4% after 900s.

In all the samples treated at 900-950°C small nitrides were detected at grain boundaries.

Looking at the property diagram in fig. 1, it can be deduced that Thermocalc underestimates the precipitation temperatures of chi and sigma phases.

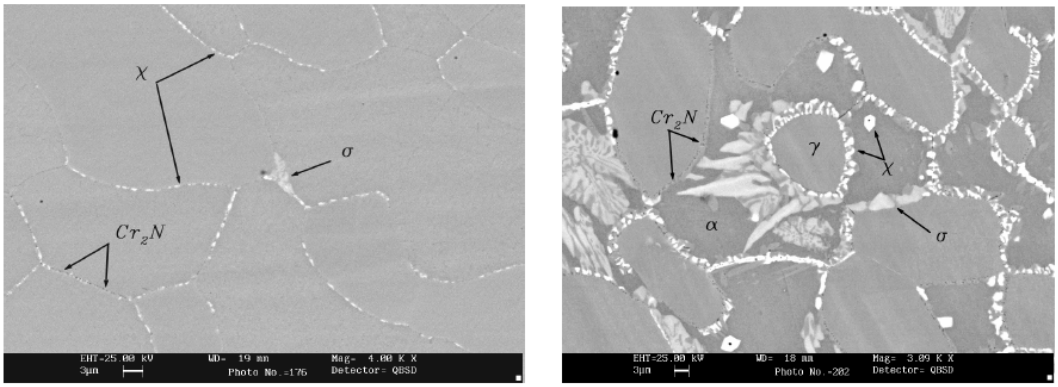

Fig. 3. BSE of 2507 5 min (left) and 40 min (right) at 900°C; nitrides and chi-phase transforming to sigma-phase

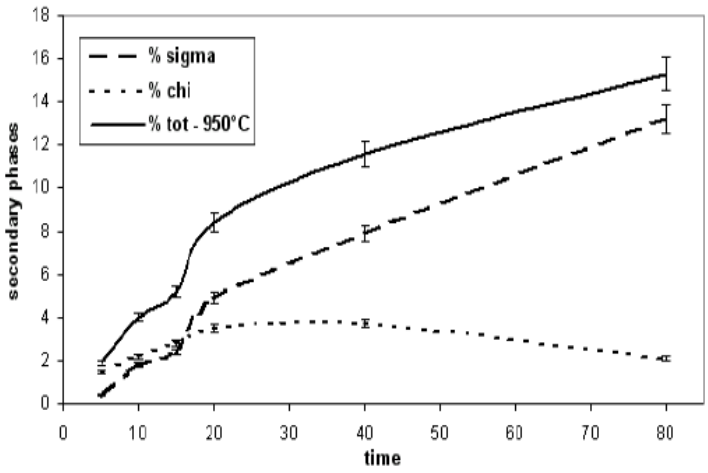

Fig. 4. Volume fractions of secondary phases in 2507 aged at 950°C

4.2.2 Continuous cooling

The morphology and localization of the secondary phases after continuous cooling are very similar to that observed in the isothermal ageing tests (the precipitation occurs at the α/γ grain boundaries and especially at the triple points), while the formation sequence of secondary phases seems to be different.

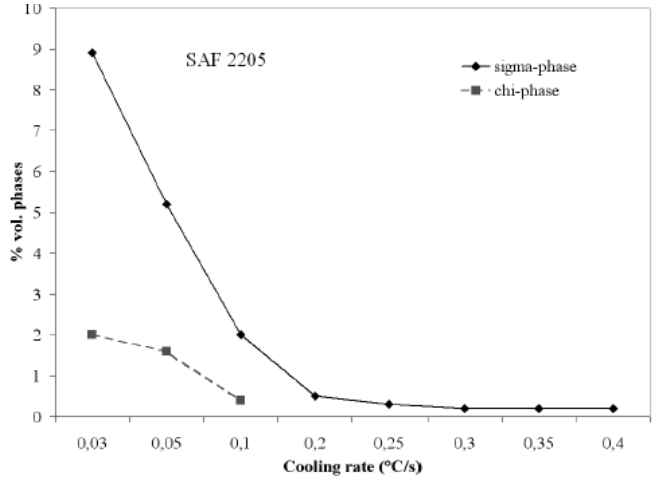

Fig. 5. Sigma and chi (% vol.) vs. cooling rate in the 2205 DSS, solution annealed at 1120°C

In the 2205 grade the total amount of secondary phases is lower for the highest solution annealing temperature, in agreement with [10], and is strongly dependent both on the cooling rates and on annealing temperature (see fig.5). At the highest cooling rates the secondary phases precipitation is completely avoided. As the cooling rate slows down, the σ-phase appears as the first phase: the critical cooling rate for σ-phase formation is 0.35 °C/s, when a final σ-phase content of 0.2 % is obtained. With a further lowering of the cooling rate, the σ-phase content gradually increases and at about 0.1-0.15 °C/s a small amount of χ-phase appears: therefore the χ-phase appears only at lower cooling rates than the σ-phase [8-9].
The sequence of precipitation during continuous cooling seems to be different from that obtained by isothermal ageing. In the latter the χ-phase is always the first precipitating phase. In the continuous cooling the same sequence occurs only at low cooling rates, and at the highest cooling rate the χ-phase formation seems to be not possible.

The effects of continuous cooling treatments in the 2507 are very similar to that of the 2205 grade and can be summarized:

- the total amount of secondary phases is slightly lower for the highest solubilisation temperature (1120°C), in agreement with the results obtained for 2205,
- the amount of secondary phases and the relative morphology are quite similar for both the solution temperatures; the secondary phases' volume fraction increases if the cooling rate decreases;
- no nitrides neither carbides are detected.

The cooling rate corresponding to the first precipitation, less than 1%, can be estimated to be 0.8-0.9°Cs-1.

4.2.3 Secondary phases composition.

Further information on the secondary phases precipitation in Ni-base DSS can be derived from the chemical composition of the phases, after the different heat treatments considered.
The compositions of χ-phase and σ-phase in the 2205 steel after isothermal ageing (table 2) and continuous cooling treatments, (tables 3 and 4) are in good agreement with the results of other investigations [1,17]. The χ-phase composition is characterized by a significant higher content of molybdenum, nearly twice the Mo content of the σ-phase. Therefore it is quite easy to distinguish these two phases through SEM-BSE imaging.

Element	σ-phase	χ-phase
Mo	7.5±0.8	13.0±0.9
Cr	26.7±1.1	24.0±0.7
Ni	1.4±0.1	3.6±0.1

Table 2. Chemical composition (wt%) of χ-phase and σ-phase after isothermal ageing

It is interesting to point out that after isothermal ageing the chemical composition of both χ-phase and σ-phase is independent from the time, the temperature

and the phase amount. Moreover the σ-phase composition is near the equilibrium phase composition [1].
On the contrary the compositions of the secondary phases from continuous cooling tests are significantly dependent on the solution annealing temperature and mainly on the cooling rates (tables 3-4). As the cooling rate decreases, in both σ and χ- phases the molybdenum and chromium contents gradually increase, approaching the values obtained in the isothermal tests.

c. rate °C/s	Solution annealing at 1020 °C			Solution annealing at 1050 °C		
	Mo	Cr	Ni	Mo	Cr	Ni
0.03	14.3	25.2	2.7	15.2	26.0	2.9
0.05	11.8	25.2	2.9	16.1	25.7	3.0
0.10	11.2	24.3	3.3	12.0	26.1	3.5

Table 3. Mo, Cr and Ni content (wt%) of χ-phase after solubilization and continuous cooling treatment

c. rate °C/s	Solution annealing at 1020 °C			Solution annealing at 1050 °C		
	Mo	Cr	Ni	Mo	Cr	Ni
0.03	8.4	28.5	3.1	7.8	28.7	2.9
0.05	7.3	27.2	3.3	8.0	28.8	3.0
0.10	7.3	27.3	3.0	7.5	25.9	3.5
0.20	7.3	27.3	3.0	7.3	27.5	3.2
0.25	6.1	25.5	3.7	8.3	26.6	3.3
0.30	6.1	25.1	4.0	6.8	27.0	3.5
0.35	5.6	25.4	3.9	7.0	26.1	3.8

Table 4. Mo, Cr and Ni content (wt%) of σ-phase after solubilization and continuous cooling treatment

The most significant variation concerns the molybdenum content. In the σ-phase Mo content varies from 4.6 %, at the highest cooling rate, to 8 % , at the lowest cooling rate. Given that the base alloy contains about 3 % Mo , the large composition variation can be justified considering that the σ-phase and χ-phase formation is strongly dependent on diffusion. At the highest cooling rates there is not sufficient time for diffusion to supply adequate molybdenum (and chromium) amounts to reach the equilibrium composition. Therefore, the highest cooling rates produce σ-phase at the lowest alloying elements content. The more evident variation of the χ-phase composition follows the same behaviour and can be justified in the same way. Owing to its high molybdenum content, the formation of the χ- phase is even more affected by the restriction of the time for diffusion. The χ-phase appears only in the precipitation conditions with the longest time allowed for diffusion: isothermal ageing and the lowest cooling rates. This behaviour could be justified because the χ- phase nucleation is favoured by smaller coherency strains than σ-phase in the ferrite lattice [3]. On the contrary the χ-phase formation need a more effective diffusion, having a higher molybdenum content. Therefore, in experimental conditions with the longest diffusion

time, i.e. isothermal aging tests and continuous cooling at low rates, the nucleation prevails and the χ-phase appears as the first precipitating phase.
Results on the composition variations of σ and χ phase in the 2507 steel are completely similar to that observed in the 2205.
These results seem to indicate the conditioning affect of diffusion on the precipitation sequence and moreover that the role of the χ-phase, as the stable σ-phase precursor in the DSS, is not a general phenomena, but depends on the steel composition (mainly on the molybdenum content) and can occur only with specific conditions of solubilization temperature or cooling rates. This, perhaps, could also justify some discrepancies between various results already reported [9,10,18,19], concerning the sequence of secondary phases formation in DDS.

4.3 2304 and 2101 DSS

The first effect of the aging treatments is the increase in the austenite content more relevant in the 2304 steel at 750 and 850°C, than in the 2101 steel. At 750°C, for example, the amount of austenite in 2304 increased to 53.1 pct after 45 minutes of aging and to 54.6 pct after 90 minutes of aging. The increase in the austenite content is due to the formation of secondary austenite.
However in both steels, the aging treatments did not produce the precipitation of χ or σ phases, as usually occurs in Ni-base conventional DSS, also for very long soaking times, over 750 hours. Instead in the 2101 steel the precipitation of small black particles (in the SEM-BSE images) at the α/α and α/γ grain boundaries was observed. In Figure 5, a schematic of the precipitation kinetics is shown. The precipitates were analyzed by EDS (close to the resolution limit), and an evident enrichment of chromium was observed. Making reference to other different experimental observations reported in the literature, such small black particles can be identified as chromium nitrides, although it cannot be excluded that some of them are chromium carbides.
In the 2304 steel, no precipitation of black particles was observed after aging at 550°C and 650°C, but a precipitation of particles was observed after 40 to 45 minutes of aging at 750°C and 850°C. The precipitation of the nitrides in this steel therefore requires higher temperatures and longer times.

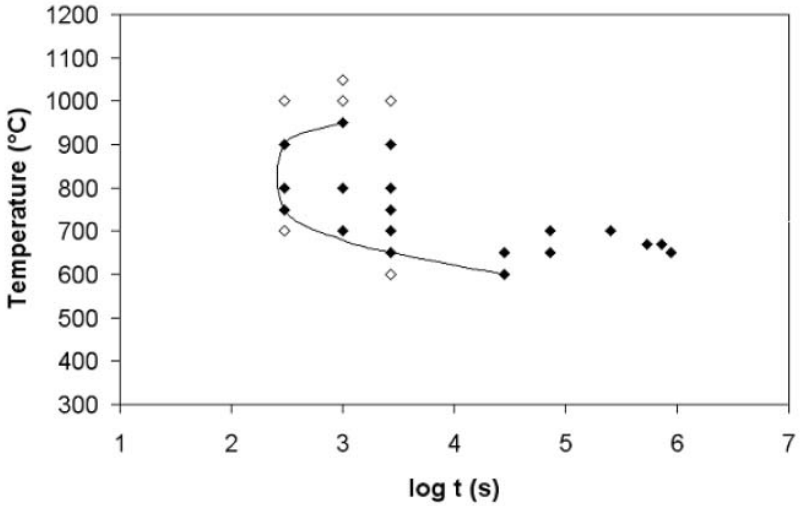

Fig. 5. Nitrides precipitation kinetic in 2101 DSS

In addition, in this steel, the precipitates are close to the α/γ grain boundaries and inside the austenitic grain. This result shows that the precipitation was followed by the formation of secondary austenite [5], as confirmed by the results of the image analysis that indicate an increase in the austenite content in the case of aging at 750°C and 850°C. The EDXS analysis shows that the concentration of Cr in the α and γ phases is around 28 and 22 pct, respectively, and its concentration in the secondary austenite is 19.2 pct. In the secondary austenite, a Cr depletion is thus observed because of the formation of the precipitates. In addition, the concentration of Ni is 3.2 and 6.5 pct in the α and c phases, respectively, and 5 pct in the secondary austenite. This means that the Cr-depleted region, as a consequence of nitrides formation, is enriched by the Ni that diffused into it from the γ phase. The formation of secondary austenite is a result of both the depletion of Cr and the enrichment of Ni. The very low Ni content in the 2101 steel therefore explains why secondary austenite was not formed in this steel and why the nitrides remain located at the grain boundaries.

4.4 Ni DSS vs. Mn DSS.

As concerning the phases transformations in Ni-base and Mn-base DSS during isothermal aging, the difference undoubtedly more evident is the lack of σ precipitation in the latter, despite the Thermocalc calculations forecast the presence of σ phase between the stable constituents in all the four DSS considered. Actually the previous experimental results indicate that during isothermal aging the dangerous intermetallic phases can form in a rather short times in the Ni-base DSS, but, on the contrary, in the Mn-base DSS the precipitation is very sluggish and significant presence of such phases cannot be detected also after very long time aging treatments. This different behavior clearly is coming from the difference in the precipitation kinetic from the metastable solid solutions obtained in the four steels by quenching from the high temperatures of the solution annealing treatment. The formation of the same intermetallic phases is rather rapid in the Ni DSS and much more slow in the Mn DSS. The different precipitation kinetics can be justified by various effect. First of all, in the Thermocalc diagrams is evident that the temperature range of formation and stability of TCP phase is lower, below 800°C, in the Mn DSS, than in the Ni DSS, below 950°C. The highest temperature of σ possible formation in the 2101, 750°C, is nearly the lowest temperature of formation of the same phase in the 2507. Obviously decreasing the precipitation temperature decrease the diffusion and precipitation rate. Moreover the Thermocalc diagrams enlighten that the TCP phases formation in the Ni DSS occur in the same temperature range of the transformation of the ferrite to the secondary austenite, with a redistribution of the alloy elements in the new phases. This allow the development of the transformation of ferrite in austenite and TCP phases (α -> γ + σ + χ) following the favourable mechanism of the eutectoid transformations, so reducing the diffusion path necessary for the alloy elements redistribution in the new phases.
The situation is completely different in the Mn DSS, where the formation of secondary austenite is more reduced, or almost absent, as in the 2101, and occur only at higher temperatures than the TCP phase formation. Therefore the formation of TCP phases could occur only independently from the secondary austenite formation and not following the more favourable path of the eutectoid transformations. This make the TCP phase formation much more dependent on the diffusion of the alloy elements, further increasing the time for the transformation.
As third effect the differences in composition have to be considered. In the Mn DSS both Ni and Mo contents are much lower than in the Ni DSS. The low Mo content

reduce, or avoid, the possible formation of the χ, the first an more rapid precipitating phase, active also as precursor of the σ-phase during aging treatments. The lower Ni content increase the ferrite stability and reduce the possible formation of secondary austenite not allowing the eutectoid formation of austenite and TCP phases.
Finally it should be considered that Thermocalc calculations indicate the equilibrium phases which should be present in the alloys at different temperatures. As concerning our experimental results, obviously the microstructures obtained after continuous cooling tests are non-equilibrium microstructures: therefore can be different from Thermocalc indications.
But also the results of our isothermal aging tests are the microstructures deriving from a particular solid state transformation: the decomposition of the metastable solid solution coming from the solution annealing treatment. Obviously the resulting microstructures are strongly affected by diffusion phenomena and kinetic peculiarities of the solid state formation of the new (equilibrium) phases. Therefore our results indicate that kinetic of the precipitation of the sigma (equilibrium) phase from the oversaturated metastable solid solution is rapid in the Cr-Ni-Mo DSS but not in the Cr-Mn DSS, where also long time treatments, about thousand hours are not sufficient for the equilibrium microstructure formation.

5. CONCLUSIONS

The results of the analysis of the TCP phases formation in four Cr-Ni and Cr-Mn DSS can be summarized:

- equilibrium data indicate the formation of TCP phases in all the DSS considered, in the range between from1000-750 to 400°C;
- in the Cr-Ni DSS both chi and sigma phases precipitation occur, according equilibrium data: in isothermal tests the chi is the first precipitating phase but in the continuous cooling tests the chi appears only at lower cooling rates than the sigma;
- in the Cr-Mn DSS the formation of sigma phase cannot be detected also after long time isothermal aging; as equilibrium phases, only the nitrides formation have been revealed;
- the different behavior of TCP formation in the four DSS could be justified by differences in kinetic and mechanism of precipitation of the new TCP phase from the metastable solid solutions obtained from the solution annealing.

References

1. J.O. Nilsson, Mat. Sci. Techn., 8 685 (1992)
2. J.O. Nilsson, T. Huhtala, L. Karlsson, Metall. Mat. Trans., 27A 2196 (1996)
3. J.O. Nilsson, Proc. Conf. “Duplex Stainless Steel 97”, KCI pub.,73 (1997)
4. J. Charles, Steel Res. Int., 79 445 (2008)
5. P. Johansson, M. Liljas: Avesta Polarit Corrosion Management and Application Engineering, 24:17 (2001)
6. I. Calliari, E. Ramous, M. Zanesco, J. Mat. Sci., 41 1615 (2006) (2205)

7. I.Calliari, M. Pellizzari, E. Ramous, Mat. Sci. Techn. (accepted for publication)

8. I. Calliari, M. Zanesco, E. Ramous, P. Bassani, JMEPEG, 16 109 (2007)

9. T.H. Chen, K.L. Weng, J.R. Yang, Mat. Sci. Eng. A338 259 (2002)

10. T.H. Chen, J.R. Yang, Mat. Sci. Eng., A311 28 (2001)

11. I. Calliari, K. Brunelli, M. Zanellato, E. Ramous, R. Bertelli, J. Mat. Sci., 44 3764 (2009)

12. S.B. Kim, K.W. Paik, Y.G. Kim, Mat. Sci. Eng., A247 (1998) 67.

13. E. Johnson, Y.J. Kim, L. Scott Chumbley, B. Gleeson, Scri. Mat., 50 (2004) 1351.

14. I. Calliari, K. Brunelli, M. Dabala, E. Ramous, JOM, 61 80 (2003)

15. L. Kaufman, H. Bernstein: Computer Calculation of Phase Diagram, Man. Labs. Inc., Cambridge, Massachussets, Academic Press New York and London (1970)

16. B. Sundman et al., CALPHAD, 9 153 (1985)

17. JU. Toor, PJ. Hyun, HS. Kwon, Corr. Sci., 50 404 (2008)

18. K.M. Lee, H.S. Cho, D.C. Choi, J. Alloys Comp., 285 156 (1999)

19. Y.S. Ahn, J.P. Kang, Mat. Sci. Techn.,16 382 (2000)

Effect of ageing on the fracture behaviour of lean duplex stainless steels

G. Straffelini[1], S. Baldo[2], I. Calliari[2], E. Ramous[2]

[1] Department of Materials Engineering and Industrial Technologies, University of Trento,
via Mesiano 77, 38100, Trento, Italy
[2] Department of Innovation in Mechanics and Managment, University of Padova, via Marzolo 9, 35131, Padova, Italy

Abstract. The influence of ageing in the range of 550°C-850°C for 5-120 minutes on the impact fracture behavior of 2101 and 2304 lean duplex stainless steels was investigated in the present study. The 2304 steel displayed ductile behavior irrespective of the ageing conditions. In contrast, the 2101 steel displayed a ductile behavior only in the case of ageing for 5 minutes at 550°C and 650°C, whereas in all other cases it fractured in a brittle manner. The brittle fracture behavior of the 2101 steel has been attributed to the precipitation of small black particles at the α/α and α/γ grain boundaries (nitrides), which form paths for easy crack propagation. In the 2304 steel, such particles precipitated at 750°C and 850°C, but they were located inside the austenitic grains because of the formation of secondary austenite. They therefore did not embrittle the steel. The larger Ni content of the 2304 steel favoured the formation of the secondary austenite that is absent in the 2101 steel.

Published in: Metallurgical and Materials Transactions A (2009) v 40A, p 2617

1. INTRODUCTION

In conventional duplex stainless steels (DSS), the alloying elements are balanced to obtain a microstructure composed of about 50% austenite and 50% ferrite. In this way, the corrosion and mechanical properties of the materials are optimized [1]. Recently, however, several investigations have been carried out with the aim of producing low nickel and molibdenum DSS, also called lean DSS, since these elements are becoming quite expensive [2-4+. In order to balance the microstructure, manganese and nitrogen are added.

In most cases, the corrosion resistance of lean DSS is lower than that of conventional DSS [5,6]. As far as mechanical properties are concerned, both yield and tensile strength increase as the concentrations of manganese and nitrogen are increased, whereas the impact fracture toughness decreases [2,5]. This effect has been attributed to the increase in the yield strength of ferrite, which favours the early occurrence of the local stress conditions required for brittle fracture.

Conventional DSS show a large decrease in corrosion resistance and fracture toughness after ageing between 300°C and 1000°C due to the precipitation of intermetallic phases, such as carbides ($M_{23}C_6$), nitrides (CrN and Cr_2N) and the sigma (σ) and chi (χ) phases, depending on the temperature and time [7-11]. In particular, the presence of the c and s phases is very undesirable, since they strongly promote localized corrosion and also display brittle fracture behavior.

The low molybdenum content in lean DSS significantly reduces the precipitation of the deleterious χ and σ phases, and some investigations have been carried out to understand the corrosion behavior of lean DSS after solution annealing and also after exposure to high temperatures.[4,12] In the present study, instrumented impact testing is used to investigate the influence of aging on the impact fracture behavior of two lean DSS in order to the evaluate the possible benefits gained by the lack of precipitation of the χ and σ phases.

2. MATERIALS AND TESTING

In Table I, the nominal chemical compositions of the two lean DSS under study are given. The samples for investigation were machined from hot-rolled bars with a diameter of 30 mm. The bars were previously solution annealed at 1050 °C for 30 minutes and then water quenched.

		Composition (Wt Pct)							
Common Name	**UNS Number**	**C**	**Si**	**Mn**	**Cr**	**Ni**	**Mo**	**S**	**N**
2101	S32101	0.026	0.69	3.95	22.57	1.1	0.07	0.001	0.12
2304	S32304	0.027	0.56	1.43	23.17	4.29	0.18	0.001	0.12

Table I. Chemical Composition of the Steels under Study

The samples were submitted to different aging treatments at four temperatures (550 °C, 650 °C, 750 °C, and 850 °C) for 5, 45, 90, and 120 minutes.

The volume fractions of austenite and ferrite in the solution-annealed samples and in the aged samples were determined on three longitudinal and three transversal sections (20

fields for each section) by image analysis on light micrographs at 200 times, after etching with Beraha's reagent.
In order to reveal the precipitates formed during aging, examinations on unetched samples were performed with scanning electron microscopy (SEM) using the backscattered electron (BSE) signal. The scanning electron microscope was operated at 29 kV, and the BSE detector was set to maximize the atomic number contrast, allowing ferrite, austenite, and precipitates to be identified. An energy-dispersive X-ray spectrometer (EDXS) was used for composition analysis of the phases and precipitates. From the treated samples, Charpy-V notched specimens (10 mm x 10 mm x 55 mm) were obtained in the L-T direction, and instrumented impact tests were carried out at room temperature. The available energy was 300 J, and the impact velocity was 5.53 m/s. The recorded load-deflection curves were partially smoothed using the moving averages method.[13,14] The reported data are the average of three tests. In order to obtain information on the fracture behavior of the materials under study, the fracture surfaces of the broken specimens were observed with SEM. In addition, cross sections of the broken samples at the notch root were observed with SEM and optical microscopy.

3. RESULTS AND DISCUSSION

A. Microstructures

The solution-annealed materials are characterized by the absence of any secondary phases and by the presence of elongated grains of both austenite and ferrite in the longitudinal rolling direction. In the transverse direction, the grains are isotropic, and the measured volume fraction of austenite is 43.4 pct in the 2304 steel and 46 pct in the 2101 steel.
The aging treatment gave rise to an increase in the austenite content in the 2304 steel at 750°C and 850 °C, whereas it had no relevant effect on the 2101 steel. At 750 °C, for example, the amount of austenite in 2304 increased to 53.14 pct after 45 minutes of aging and to 54.56 pct after 90 minutes of aging. The increase in the austenite content is due to the formation of secondary austenite, as will be shown subsequently.
As expected, in both steels, the aging treatments did not produce the precipitation of v or r phases, as usually occurs in conventional DSS. In the 2101 steel, however, the precipitation of small black particles at the α/α and α/γ grain boundaries was observed. Figure 1 shows an example of such precipitates in the case of the alloy aged at 750 °C for 45 minutes. At 550 °C, the precipitates were observed after 90 minutes of aging. At 650°C, they were observed earlier, i.e., after 40 minutes of aging. At 750 °C and 850 °C, the precipitates were already observed after 20 minutes of aging.
In Figure 2, a schematic of the precipitation kinetics is shown. The precipitates were analyzed by EDXS (close to the resolution limit), and an evident enrichment of chromium was observed.

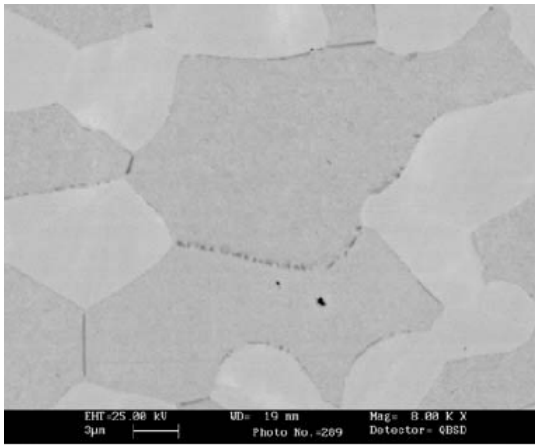

Fig. 1. SEM microstructure of the 2101 steel aged at 750 °C for 45 min. Note the presence of small black particles at the α/α and α/γ grain boundaries.

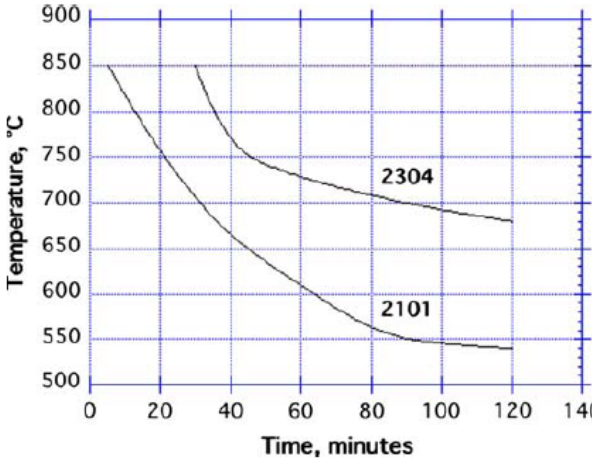

Fig. 2. Schematic representation of the precipitation kinetics in the two steels under study.

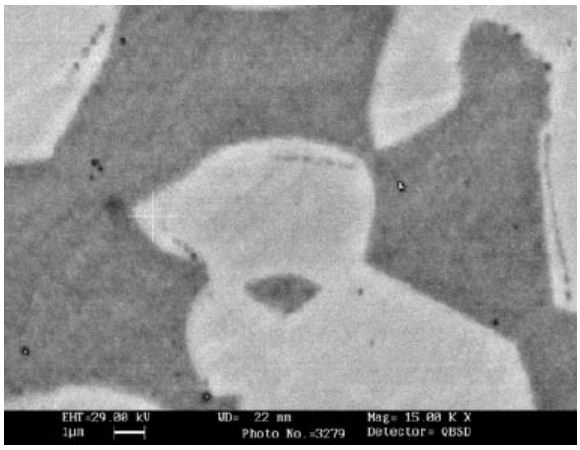

Fig. 3. SEM microstructure of the 2304 steel aged at 750 °C for 90 min. Note the presence of small black particles inside the γ grains. The region between the precipitates and the α/γ grain boundary is the secondary austenite. The composition of the secondary austenite in the region indicated by the cross (obtained by EDXS) is 19.2 pct Cr and 5.1 pct Ni.

Making reference to other different experimental observations reported in the literature, such small black particles can be identified as chromium nitrides, although it cannot be excluded that some of them are chromium carbides.[4,12,15] In the 2304 steel, no precipitation of black particles was observed after aging at 550 °C and 650 °C. As shown in Figure 2, a precipitation of particles was observed after 40 to 45 minutes of aging at 750 °C and 850 °C. The precipitation of the nitrides in this steel therefore requires higher temperatures and longer times.

This can be attributed mainly to the higher Mo content (it is more than double that in 2101), since Mo forms Mo-N cluster that decreases the diffusivity of N to the grain boundaries.[16,17] In addition, in this steel, the precipitates are close to the α/γ grain boundaries and inside the austenitic grain, as shown in Figure 3. This result shows that the precipitation was followed by the formation of secondary austenite,[12,15] as

confirmed by the results of the image analysis that indicate an increase in the austenite content in the case of aging at 750 °C and 850 °C. The EDXS analysis shows that the concentration of Cr in the α and γ phases is around 28 and 22 pct, respectively, and its concentration in the secondary austenite is 19.2 pct. In the secondary austenite, a Cr depletion is thus observed because of the formation of the precipitates. In addition, the concentration of Ni is 3.2 and 6.5 pct in the α and γ phases, respectively, and 5 pct in the secondary austenite. This means that the Cr-depleted region is enriched by the Ni that diffused into it from the γ phase. The formation of secondary austenite is a result of both the depletion of Cr and the enrichment of Ni.
The very low Ni content in the 2101 steel therefore explains why secondary austenite was not formed in this steel and why the nitrides remain located at the grain boundaries.

B. Impact Behavior

In Figure 4, the impact curve of the 2304 steel aged at 650 °C for 5 minutes is shown as an example. It should be noted that after general yielding at about 16 kN, the alloy underwent strain hardening up to a maximum load of 22 kN. At this load, the fracture crack was nucleated, [13] and the successive crack propagation took place with a large energy absorption. A similar behavior was displayed by all 2101 samples, as shown Figure 5, where the impact fracture energy of the 2304 alloy is shown as a function of aging time and temperature. In all cases, the impact energy is very high, larger than 250 J, showing that the aging treatment did not induce any embrittlement of the steel. A different behavior is displayed by the 2101 alloy.

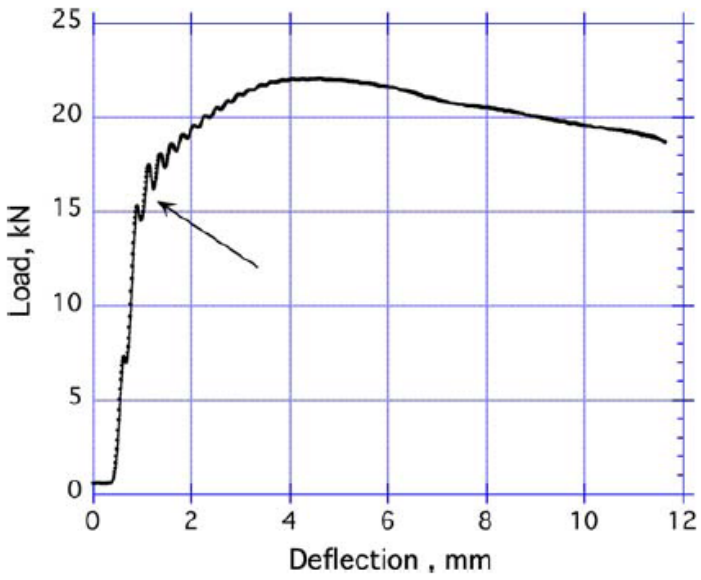

Fig. 4. Impact curve of the 2304 steel aged at 650 _C for 5 min. The arrow indicates the general yield point.

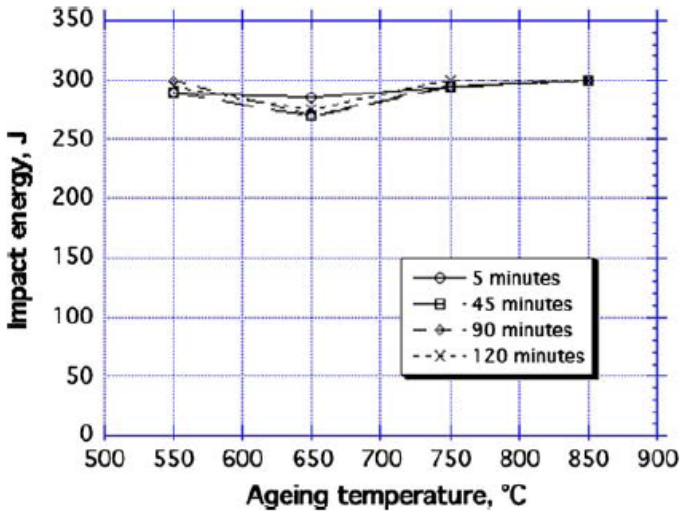

Fig. 5. Impact fracture as a function of aging temperature and time for the 2304 steel.

As shown in Figure 6, the impact energy reached 300 J (with a ductile behavior) only in the case of aging for 5 minutes at 550 °C and 650 °C. In all other cases, the impact energy was much lower, showing that aging induced a severe embrittlement of the steel.

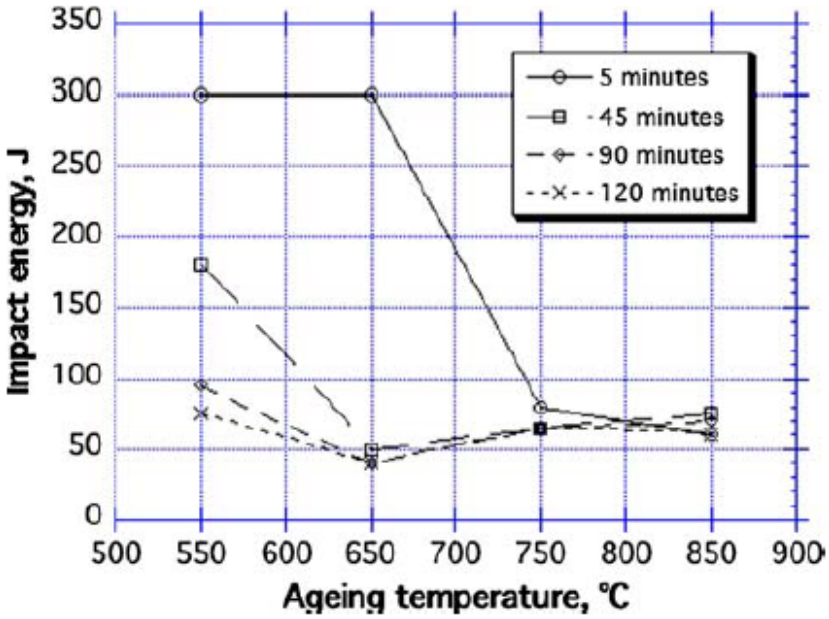

Fig. 6. Impact fracture as a function of aging temperature and time for the 2101 steel.

In Figure 7, the impact curve of the alloy aged at 750 °C for 5 minutes is shown as an example. After general yielding at about 15 kN, the alloy underwent strain hardening up to a load of about 20 kN. The fracture crack nucleated at the maximum load. In this case, however, the successive crack propagation took place with a limited absorption of

energy, although there was no abrupt drop in the absorbed energy, as observed in embrittled 2205 DSS [18].

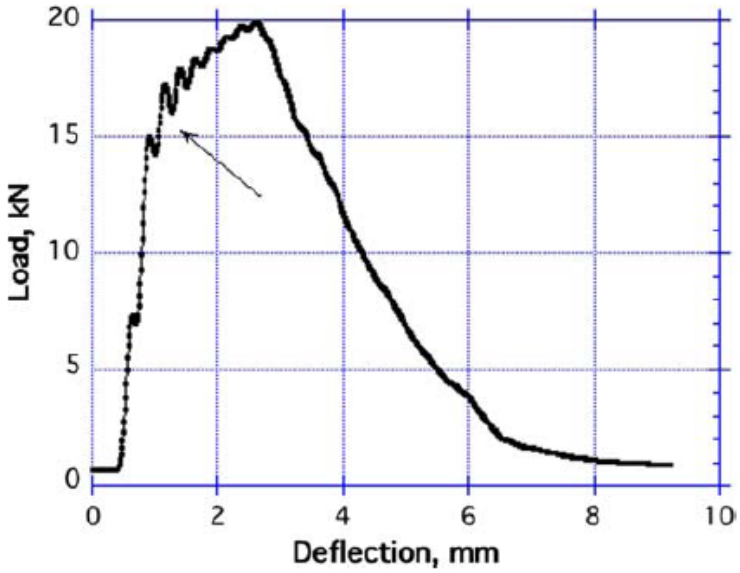

Fig. 7. Impact curve of the 2101 steel aged at 750 _C for 5 min. The arrow indicates the general yield point.

C. Fracture Behavior

The analysis of the fracture behavior initially focused on the 2101 steel, which displayed a brittle behavior following aging.

In all cases, brittle fracture was characterized by the presence of several secondary cracks on the fracture surface. An example of such cracks can be observed in Figure 8. These cracks formed during the propagation of the main fracture crack, and they were responsible for the absorption of some energy during crack propagation, as can be observed from the impact curve in Figure 7. Secondary cracks usually form when the microstructure is characterized by the presence of several weak regions (usually perpendicular to the crack propagation) that can become energetically favorable paths for crack propagation.[19,20]

Fig. 8. Fracture surface of the 2101 steel aged at 650 °C for 45 min.

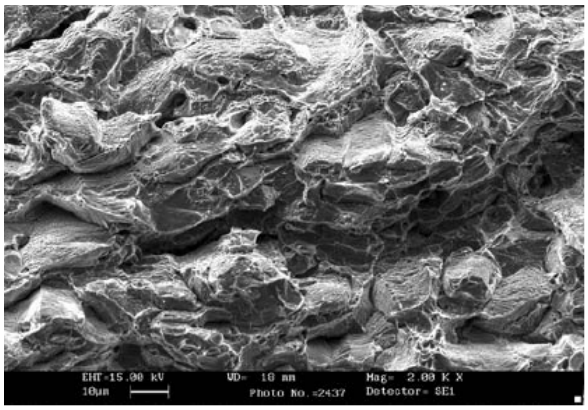

Fig. 9. Fracture appearance of the 2101 steel aged at 750 °C for 90 min.

Figure 9 shows the typical fracture morphology of the steels that underwent brittle fracture. The presence of both ductile regions with the typical dimpled morphology and brittle areas can be observed.
In addition, fracture took place without noticeable local plastic deformation, thus explaining the low amount of energy absorbed during crack propagation. Ductile fracture was mainly restricted to the grain boundaries, and the dimples are numerous but very small in dimension.
Further information on this aspect can be gleaned from the observation of the damaged microstructure below the notch. Figure 10 shows the typical microstructure at the notch root and close to the advancing crack. The crack clearly propagated along the grain boundaries where the nitrides precipitated (Figure 1). Several grain boundaries near the crack are damaged: numerous microvoids are in fact nucleated at the small precipitates. The advancing crack therefore finds an easy path for its propagation. Each secondary crack stops propagating when it is too far from the resisting section, whereas the main crack may easily produce the failure of the specimen. The nitrides are thus responsible for the brittle fracture behavior of the 2101 steel. The fracture behavior was ductile with a large amount of absorbed energy only when the aging conditions did not induce the precipitation of such particles.

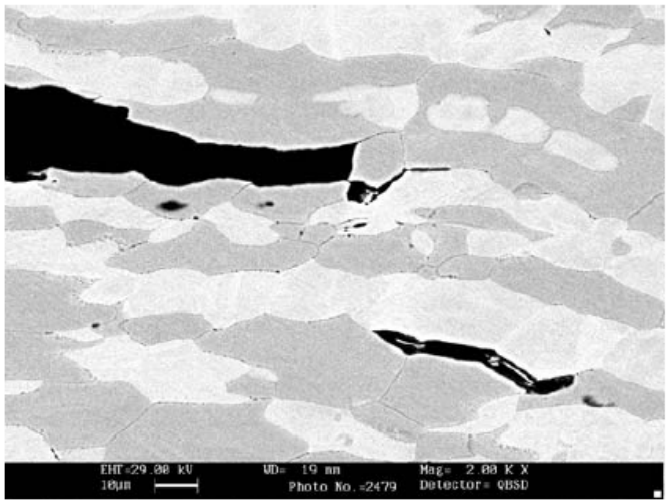

Fig. 10. Microstructure of the 2101 steel at the notch root and close to the advancing crack. The crack propagated along the grain boundaries where the dark small particles are precipitated.

As already observed in the case of an embrittled 2205 DSS,[18] the plastically deformed region below the notch root covered a large distance from the resisting section.
This is confirmed by the impact curves that show a distinct strain hardening stage after yielding and before the onset of crack propagation, and also by the presence of several regions of strain-induced martensite in the microstructure, as shown in Figure 11. Image analysis shows that in the steel aged at 550 °C for 120 minutes, the amount of martensite was about 10 pct at a distance of 80 µm from the resisting section, 9 pct between 80 and 160 µm, and 7 pct between 160 to 240 µm. Traces of martensite were observed within a distance of 1 mm from the advancing crack. Martensite regions were formed before the onset of crack propagation, and they may have helped in the brittle propagation of the fracture crack.[21,22]

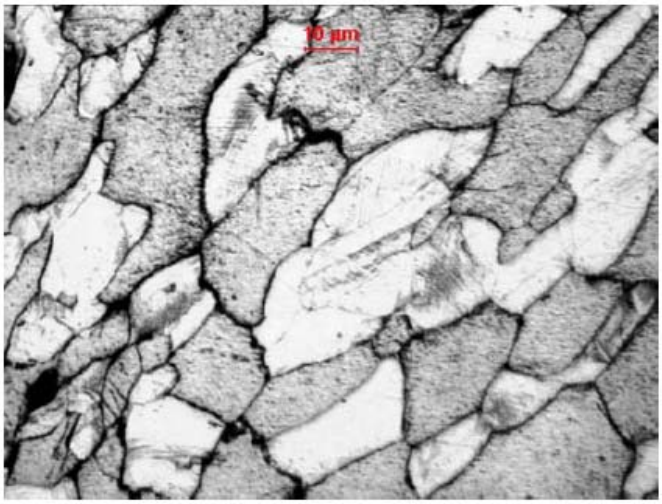

Fig. 11. Areas of strain-induced martensite close to the crack propagation region.

As already highlighted, aging did not induce any embrittlement in the 2304 steel. Irrespective of aging temperature and time, fracture was ductile, with the presence of the typical dimples on the fracture surfaces.
Figure 12 shows an example. This behavior can be attributed to the absence of precipitated particles at the grain boundaries. Where present, the precipitates were located inside the austenitic grains.

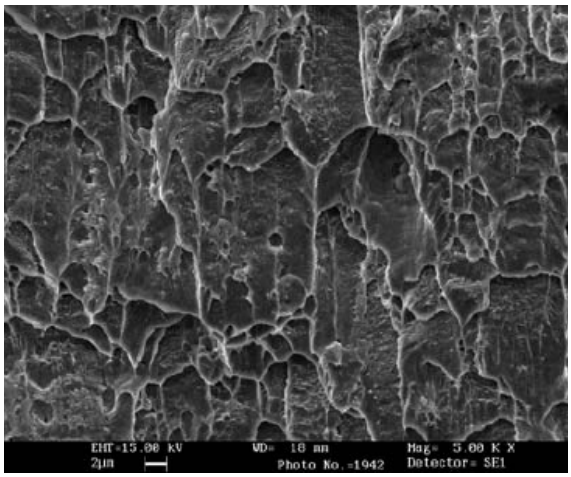

Fig. 12. Fracture appearance of the 2304 steel aged at 650 °C for 90 min.

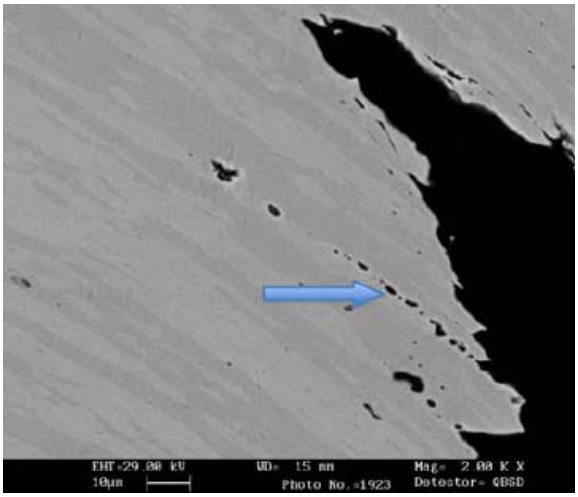

Fig. 13. Microstructure of the 2304 steel at the notch root and close to the advancing crack. The arrow shows the voids nucleated inside the austenitic phase.

As demonstrated in Figure 13, such precipitates induced the nucleation of microvoids inside these grains, and they were therefore not able to form low-energy paths for easy crack propagation.

4. CONCLUSIONS

In the 2101 lean DSS, the precipitation of small black particles (nitrides) at the α/α and α/γ grain boundaries was observed after aging in the temperature range between 550 °C and 850 °C. In the 2304 steel, no precipitation of such particles was observed after aging at 550 °C and 650 °C, whereas at 750 °C and 850 °C, only a moderate precipitation of particles was observed after 40 to 45 minutes. Such precipitates, however, were found close to the α/γ grain boundaries and inside the austenitic grains.
The 2101 steel displayed a ductile impact fracture behavior only in the case of aging for 5 minutes at 550 °C and 650 °C. In all other cases, the impact energy was much lower than 300 J, showing that aging induced severe embrittlement. The observation of the fracture surfaces highlighted the presence of several secondary cracks and of brittle and ductile regions with very limited local deformation. The ductile regions are characterized by the presence of numerous small dimples near the nitrides. On the contrary, the 2304 steel is characterized by ductile fracture with a large energy absorption during crack propagation, irrespective of the aging conditions. The results obtained in the present investigation demonstrate that the absence of the deleterious χ and σ phases in lean DSS after high-temperature aging is beneficial to the impact fracture toughness of the steels, provided that no nitrides precipitate at the grain boundaries. However, such precipitates do not deteriorate the impact fracture toughness of the lean DSS if they are located inside the austenitic grains. This can occur only if a sufficient amount of Ni is present in the steel, which favors the formation of secondary austenite.

REFERENCES

1. J. Charles: Duplex Stainless Steel ’94, Proc. Conf., TWI, Glasgow, England, 1994, paper no. K1.

2. H. Sieurin, R. Sandstrom, and E. Westin: Metall. Mater. Trans. A, 2006, vol. 37A, pp. 2975–81.

3. J. Charles: Steel Res. Int., 2008, vol. 79 (6), pp. 455–65.

4. I. Calliari, M. Dabala` , E. Ramous, and G. Straffelini: Mater. Sci. Forum, 2009, vols. 604–605, pp. 419–26.

5. S.M. Wessman, S. Hertzman, R. Pettersson, R. Lagneberg, and M. Liljas: Mater. Sci. Technol., 2009, vol. 24 (3), pp. 348–55.

6. M. Liljas, P. Johansson, H.P. Liu, and C.O.A. Olsson: Steel Res. Int., 2008, vol. 79 (6), pp. 466–73.

7. J.O. Nilsson: Mater. Sci. Technol., 1992, vol. 8, pp. 685–700.

8. J.O. Nilsson, T. Huhtala, P. Jonsson, L. Karlsson, and A. Wilson: Metall. Mater. Trans. A, 1996, vol. 27A, pp. 2196–2208.

9. X. Li, A.P. Miodownik, and N. Saunders: Mater. Sci. Technol., 2002, vol. 18, pp. 861–68.

10. J. Dobranszky, P.J. Szabo, T. Berecz, V. Hrotko, and M. Portco: Spectrochimic Acta Part B, 2004, vol. 59, pp. 1781–88.

11. H. Sieurin and R. Sandstrom: Mater. Sci. Eng. A, 2006, vol. 37A, pp. 271–76.

12. A. Bhattacharya and P.M. Singh: Corrosion, 2008, vol. 64 (6), pp. 532–40.

13. T. Kobayashi: Eng. Fract. Mech., 1984, vol. 19, pp. 49–61.

14. G. Straffelini: Metall. Mater. Trans. A, 2000, vol. 31A, pp. 1443– 51.

15. A.J. Ramirez, J.C. Lippold, and S.D. Brandi: Metall. Mater. Trans. A, 2003, vol. 34A, pp. 1575–82.

16. M. Wada, K. Hosoi, and O. Nishikawa: Acta Metall., 1982, vol. 30, pp. 1005–11.

17. M. Murayama, K. Hono, H. Hirukawa, T. Ohmura, and S. Matsuoka: Scripta Mater., 1999, vol. 41, pp. 467–73.

18. G. Straffelini, I. Calliari, and E. Ramous: Mater. Sci. Technol., 2009, in press.

19. R.W. Herzberg: Deformation and Fracture Mechanics of Engineering Materials, Wiley, New York, NY, 1989.

20. T. Otarola, S. Hollner, B. Bonnefois, M. Anglada, L. Coudreuse, and A. Mateo: Eng. Failure Analysis, 2005, vol. 12, pp. 930–41.

21. Y. Tomota, Y. Xia, and K. Inoue: Acta Mater., 1998, vol. 46, pp. 1577–87.

22. M.X. Zhang and P.M. Kelly: J. Mater. Sci., 2002, vol. 37, pp. 3603–13

Effect of cold rolling on microstructure and magnetic properties in a metastable lean duplex stainless steel

S. Baldo*, Istvan Mészáros**

* Department of Engineering's Chemical Processes (DPCI), University of Padova, Via Marzolo, 9 35131 Padova, Italy

** Department of Material Science and Engineering, Budapest University of Technology and Economics (BUTE), Budapest, Hungary

Abstract. Microstructural and magnetic properties changes of a metastable ferritic-austenitic stainless steel due to cold rolling were studied together with the possibility to develop a new ferritic-martensitic stainless steel. With the aim to reduce costs low Ni content was maintained in the lean duplex stainless steel considered, making it more susceptible to strain-induced martensitic transformation. In this work a practically complete γ→α´ transformation was found for 80% of thickness reduction, resulting a new two-phase ferritic- α´ martensitic stainless steel. To investigate the structural evolution different values of thickness reduction were applied. Light optical and scanning electron microscopy was performed to characterize the morphology and grain refining of the structure after each rolling step. Martensitic transformation and work hardening were detected and analyzed by studying of magnetic properties (saturation magnetic polarization, relative magnetic permeability, coercivity). Additionally, hardness tests were performed. The results highlighted a strong grain refining and increase of martensitic phase and hardness with increasing cold deformation. A strict relation between microstructure and magnetic properties was revealed. In particular the reciprocal of relative magnetic permeability and the coercivity increased with martensite content and the amount of cold deformation. Therefore the possible application of magnetic measurements as non destructive tests to study microstructural evolution during cold rolling was shown for the steel considered.

Published in: Journal of Materials Science (2010) v 45, p 5339-5346

1. INTRODUCTION

In the last decades the development of low cost stainless steels has been carried out to reduce the cost fluctuation of certain expensive elements like Ni and Mo. Austenitic stainless steels were partly substituted by ferritic-austenitic duplex stainless steels, characterized by comparable corrosion resistance, better mechanical properties and less content of Ni and Mo. However the requirement of high strenght steels with good corrosion resistance can be satisfied with a new type of two-phase stainless steel. Hayden and Floreen studied the influence of martensite and ferrite on the properties of a ferritic-martensitic stainless steel [1]. In their work martensite is obtained by cooling at high subzero temperatures as dispersed islands in a ferritic matrix. The results highlighted the beneficial effects of martensite on mechanical resistance and toughness. In the present work the possibility to create a new ferritic-martensitic stainless is studied. Hence cold deformation is applied on ferritic-austenitic lean duplex stainless steel to obtain a ferritic-martensitic stainless steel with strain-induced martensite in a ferritic matrix.

With the aim to improve both mechanical and surface properties for structural application, cold rolled finishes can be applied to flat products. The main effects of cold rolling are to smooth the material surface, to refine the grain structure and sometimes to induce microstructural changes. Many authors have investigated the formation of strain induced martensite due to plastic deformation mainly in AISI 301, 304 and 316 austenitic stainless steels [2-9] and common duplex stainless steels [10]. In the latest years new ferritic-austenitic duplex stainless steels were get ready [11, 12]. These new types of duplex stainless steels are characterized by a further decrease of Ni, substitued by Mn and sometimes by N, leading to a higher instability of austenitic phase that can evolve to martensite after cold deformation or heat treatment. It is well known that two types of martensite can form from metastable austenite: □ hcp paramagnetic and α′ bcc ferromagnetic martensite. The α′ is thermodynamically more stable than □ martensite. The □ phase forms before the α′ phase and increasing deformation α′ grows at the □ phase expense. Finally at high deformation α′ martensite predominates. Based on these observations the sequence of transformation γ→□+ α′ was suggested [4, 8]. The diffusionless transformation from γ-phase, paramagnetic, into α′ phase, strongly ferromagnetic, can be detected studying the magnetic properties of the deformed material.

Actually there is a growing interest in the use of magnetic measurements as non destructive evaluation (NDE) techniques for monitoring the strain-induced martensite transformation in steels characterized by metastable austenitic phase.

In the present work the microstructural changes produced by cold rolling in a ferritic-austenitic lean duplex stainless steel have been investigated. A lean duplex stainless steel with less content of metastable austenite has been chosen in order to obtain a final structure characterized only by ferrite and strain-induced martensite. The effect of cold rolling on microstructure and grain refining has been investigated through metallographic technique using light optical and scanning electron microscopy. Magnetic measurements and XRD have been performed to assess the amount of strain-induced martensite after cold rolling with different thickness reductions.

Finally Vickers microhardness and coercivity measurements have been carried out for each step of cold rolling.

2. EXPERIMENTAL

The material under investigation was a lean duplex stainless steel (chemical composition shown in Table 1) received as hot rolled plates of 8 mm in thickness, solution annealed at 1050°C for 30 minutes and then quenching in water.

C	Cr	Mn	Ni	Si	Mo	P	S	N	Cu
0.028	21.72	3.41	1.13	0.78	0.15	0.026	0.01	0.13	0.32

Table 1. Chemical composition (%wt.).

Plastic deformation of the solution annealed material was carried out by cold rolling at ambient temperature. A single stand reversing mill, with 130mm diameter rolls was used. The plates were cold rolled in one direction, through many constant passes, to gradually reduce its thickness by compression. A thickness reduction of 0.10 mm was used for each pass, in order to perform high cold deformation without strong bending. Seven cold rolled samples were obtained applying different thickness reductions in the range of 10-80%.

Metallographic samples were prepared with conventional grinding, polishing and etching with Beraha's etchant. Microstructural investigations were carried out using a light optical microscope (Leica DMRE) on etched samples and scanning electron microscopy (Stereoscan 440 SEM, Cambridge) using the backscattered electron signal on unetched samples. In particular the BSE detector was set to maximize the atomic number contrast, allowing ferrite, austenite and other phases to be detected. Quantitative metallography was performed using Leica QWin image software analysis. The volume fractions of austenite and ferrite in the solution annealed material was determined on 3 longitudinal and 3 transversal sections (20 fields for each section) on light optical micrographs at 200x, after etching with Beraha's metallographic reagent.

For the identification of the phases, X-ray diffraction was performed in a diffractometer Siemens® D500 XRD using a CrKα radiation (λ=2.2897 Å, operating at 30kV and 20mA), in step scan mode with step size of 0.025° and time per step of 5s. The diffractograms have an angular range of 50-120°.

First magnetization curve and hysteresis loops were measured in a double-yoke DC magnet-steel tester. The predecessor equipment was firstly described by Stäblein and Steinitz. Our equipment is characterized by two E-shaped soft iron yokes, opposite one another with an air-gap between each of the three pairs of transverse limbs. Equal magnetizing windings are placed on each half of the long arms of both yokes. Hence the equipment has a perfect symmetry. The introduction of a specimen in one gap causes an imbalanced symmetry, an additional flux is needed to complete the circuit mainly across the central air-gap, the flux in which is thus closely proportional to the magnetization (M) of the specimen. The apparatus for measuring the strength of the applied field H may be calibrated in any known field, and is found to give accurate readings of the value of H applied to the specimen [13]. The maximum applied external field was of 210 kA/m. The present form of the measuring setup is developed at the Department of Materials Science and Engineering of the BUTE and it applies up-to date field sensors and data acquisition apparatus. AC measurements of the minor hysteresis loops were carried out by using a specifically designed permeameter type magnetic property analyzer, with a maximum applied external field of 2450 A/m. For each cold rolled sample the relative magnetic permeability values were derived from the resulting magnetizing curves. The coercivity (H_c) of t was measured by a high-accuracy Förster

coercimeter (Type 1.093) equipment, based on the compensation of the own remnant magnetic field of the samples. The coercivity was measured magnetizing the samples along their rolling direction. Vickers hardness (HV) tests were also performed using a Buehler MMT-3 digital microhardness tester. All measurements were carried out using a load of 0.5 Kg on each sample.

3. RESULTS AND DISCUSSION

3.1. Microstructural observations

The as received material in the solution annealed condition is characterized by coarse austenitic grains in a ferritic matrix. Austenitic grains are elongated in longitudinal direction due to the previous hot rolling (Fig. 1a, Fig. 1b) and equiassic in the transversal cross section, perpendicular to rolling direction (Fig. 1c). The measured average volume fraction of austenite and ferrite is of 20.4 and 79.6 respectively.

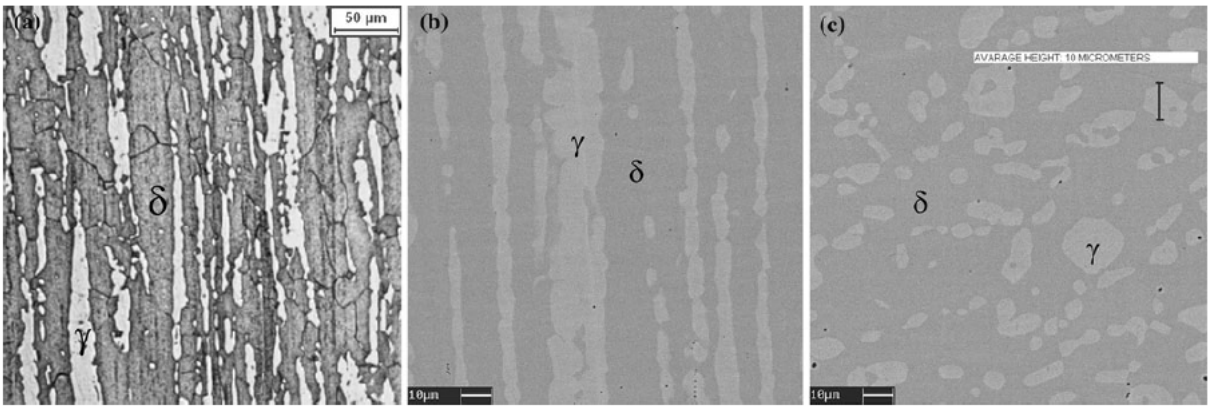

Fig. 1. As-received material of a Beraha's etching, light optical micrograph, b longitudinal section, SEM–BSE micrograph, c transversal section, SEM–BSE micrograph

The first effects obtained by cold rolling were the strong grain refining and changing in shape compared to the solution annealed sample microstructure. The grain refining is a consequence of elongation and break of grain due to deformation at room temperature. Particularly with intermediate stage of thickness reductions (Fig. 2) grain refining and flattening began to be evident in the section perpendicular to cold rolling direction, while a higher elongation and width reduction of austenitic grains were detected in the direction of cold rolling (Fig. 3).

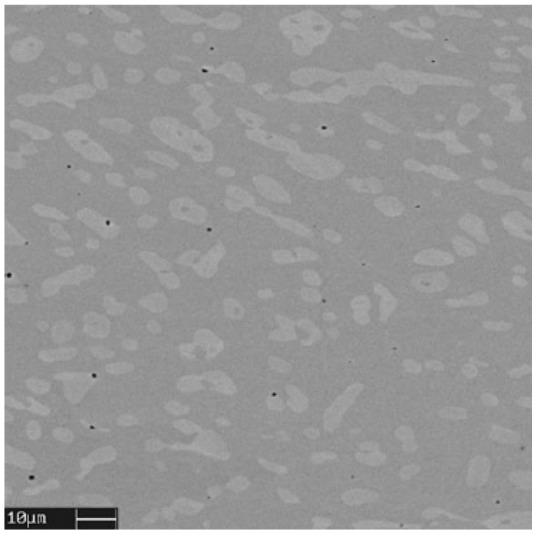

Fig. 2. Cold rolled material thickness reduction 40%, transversal section, SEM–BSE micrograph

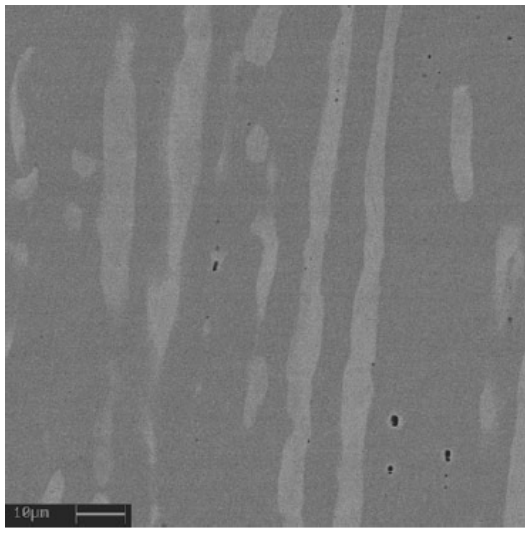

Fig. 3. Cold rolled material thickness reduction 50%, longitudinal section, SEM–BSE micrograph

By increasing strain to the maximum value considered in this work, a stronger grain refinement was revealed in all the sections of the samples (Fig. 4a, Fig. 4b). The average value of flattening in austenitic grains changed of about 80%: from a grain height of almost 10µm in the as received material to almost 2µm in the higher thickness reduction applied (Fig. 1c, Fig. 4b).

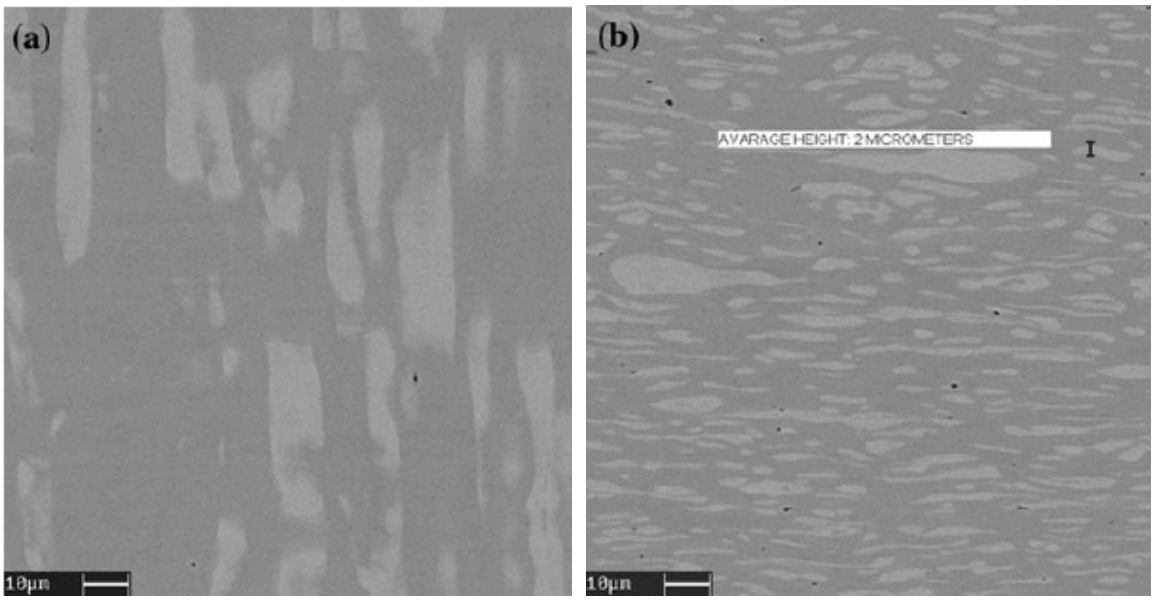

Fig. 4. Cold rolled material thickness reduction 80% of (a) longitudinal section SEM– BSE micrograph, (b) transversal section, SEM–BSE micrograph

The other important effect obtained to cold rolling is the strain induced martensitic transformation. The quantification of martensitic phase was not possible through classical metallographic technique because Beraha's etchant unequivocally was able to distinguish only the ferritic (dark) and the austenitic (light) phase.

The micrographs obtained by SEM using BSE signal highlighted some fluctuations of colour inside the austenitic grains after cold deformation, due to local differences in chemical composition but did not clearly reveal the presence of a different martensitic phase. Hence martensitic phase is believed to have almost the same chemical composition of its parent austenitic phase.

3.2. X-Ray Diffraction and Magnetic Measurements

X-ray diffraction and magnetic measurements were so performed for the identification and quantification of α′- martensite for each thickness reduction in cold rolled samples.
In Fig.5 X-ray diffractograms of solution annealed sample without cold deformation (0% Thickness Reduction) and of the strongest deformed sample (80% Thickness Reduction) are shown.

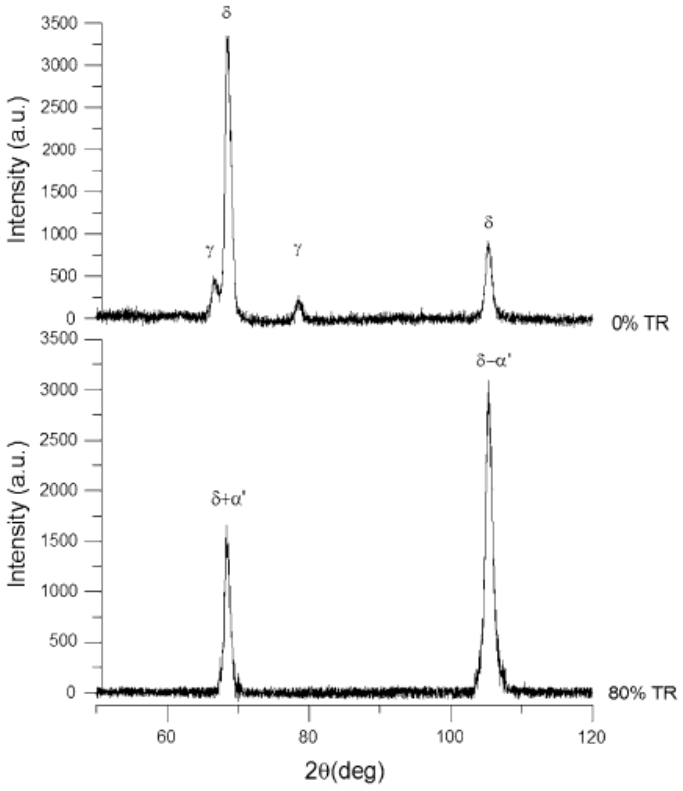

Fig. 5. X-ray diffractogram of as-received material and cold rolled material (80% thickness reduction)

In the cold rolled sample the peaks of ferrite (δ) and α′- martensite are not distinguishable as the two phases present the same reflections. Over the detection limit the peak of austenitic phase completely disappears after the maximum thickness reduction applied. Therefore it can be concluded that at this deformation condition all the austenitic phase detectable transformed into α′- martensite. This last result together with phase quantification previously performed through image analysis leads to calculate the amount of ferromagnetic α′- martensite in each cold rolled sample. The saturation magnetic polarization is in fact linearly proportional with the amount of

ferromagnetic phase. In the non-deformed condition only a ferromagnetic phase (δ – ferrite) was present in a structure characterized by 79.6% of ferrite and 20.4% of austenite. The saturation magnetic polarization in this case was $\mu_0 M_s$ (δ) = 0.752 T, and remained a constant value during cold rolling. With the application of cold deformation another ferromagnetic component was introduced because of the appearance of α´- martensite, which increased with cold deformation up to a complete detectable ferromagnetic structure made of 79.6% of ferrite, 20.4% of α´- martensite and 0% of austenite. The relation between saturation magnetic polarization $\mu_0 M_s$ and the amount of ferromagnetic phase was the following:

$\mu_0 M_s = \mu_0 M_s (\delta) + a \cdot \alpha'(\%)$,

where $\mu_0 M_s$ (δ) was the saturation magnetic polarization of ferrite and α'(%) was the amount of α´- martensite. The slope (a) of the line was determined (Fig. 6a) knowing the saturation magnetic polarization values in the non-deformed sample and in the fully ferromagnetic sample. Therefore it was possible to calculate the amount of α´- martensite, α'(%), corresponding to each value of saturation magnetic polarization and thickness reduction (Fig. 6a).

The saturation magnetic polarization ($\mu_0 M_s$) seems to be almost the same at lower thickness reduction (up to 30%) (Fig. 6b). Further increase in cold deformation has the consequence of stronger and gradual increase in saturation magnetic polarization due to the increasing presence of ferromagnetic α´- martensite, reaching the highest value of 0.94 T for the highest thickness reduction imposed (80%).

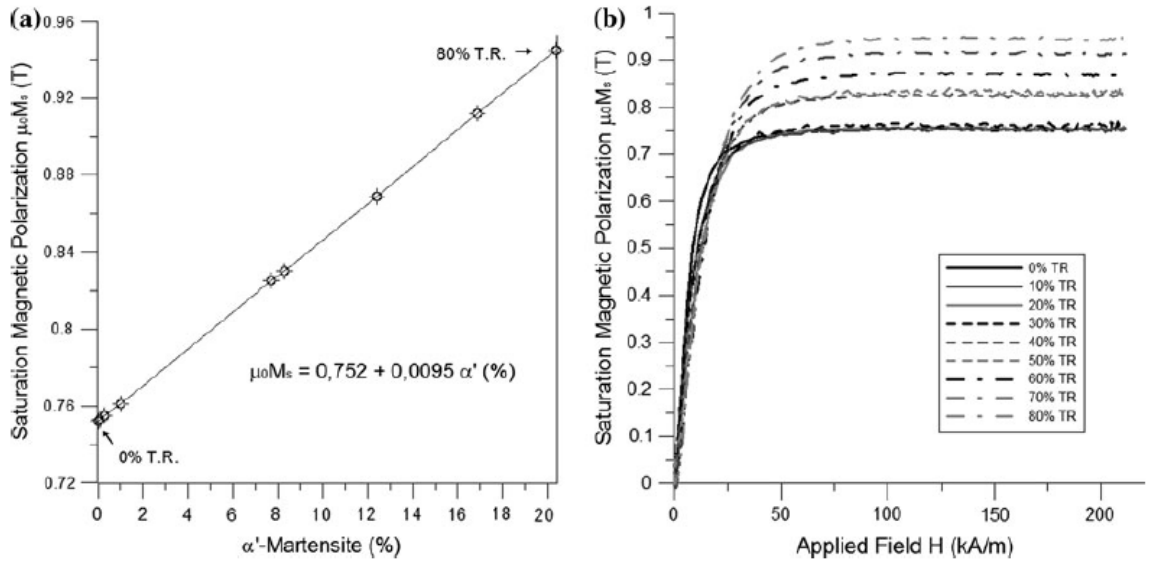

Fig. 6. (a) α'-Martensite quantification, (b) saturation magnetization curves

Relative magnetic permeability and maximal relative permeability values were derived from AC normal magnetization curves (Fig. 7a, Fig. 7b). As it is well known the normal magnetization curve is the locus of the peak points of symmetrical minor hysteresis loops and the magnetic permeability is the slope of the normal magnetization curve. Magnetic permeability is an index of how well a material concentrates the magnetic field. In austenitic stainless steels cold rolling induces an increasing of relative permeability [14], corresponding to an increase of ferromagnetic α´- martensite content. In contrast to austenitic stainless steels, the duplex stainless steel investigated in this

work shows an inverse ratio between relative permeability and cold deformation. Probably this is due to the appearance of ferromagnetic strain induced martensite and to the interaction between dislocations introduced by cold rolling and magnetic domain walls in the ferritic phase [15]. Therefore the results show a relationship between the reciprocal of maximum relative magnetic permeability and the presence of strain induced martensite, making relative magnetic permeability a possible non destructive measurement to detect martensitic transformation in the duplex stainless steel considered.

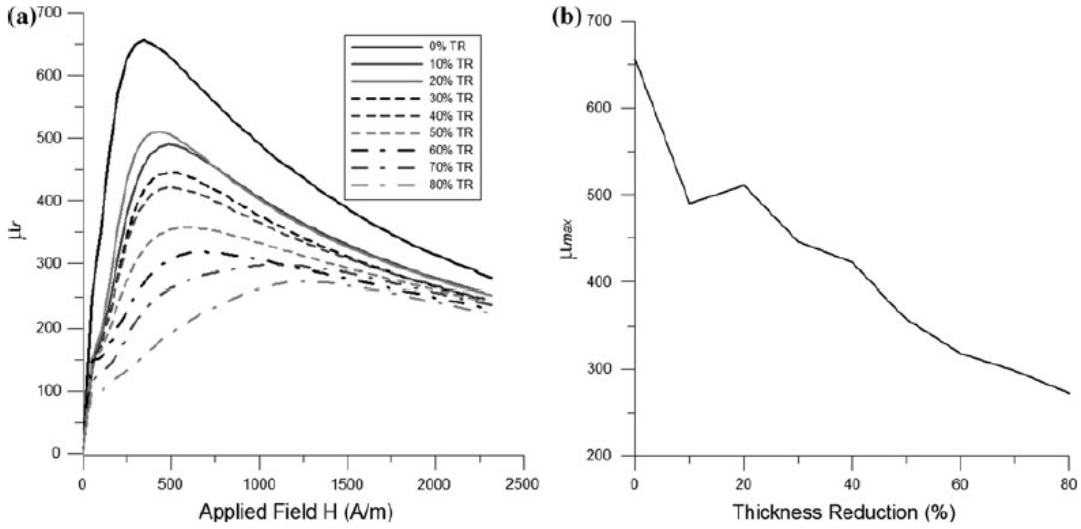

Fig. 7. (a) Relative magnetic permeability, (b) relation between maximum relative magnetic permeability and thickness reduction

3.3. Vickers Hardness and Coercivity measurements

The results of Vickers hardness and coercivity H_c are plotted together with the thickness reduction of the samples in Fig. 8. Both Vickers hardness and H_c linearly increase with cold deformation, but with different trends.

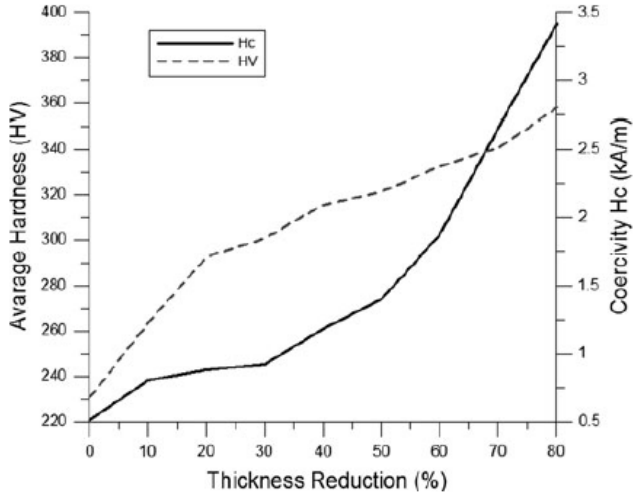

Fig. 8. Relation among vickers hardness, coercivity, and thickness reduction

According to saturation magnetic polarization values the principal phenomenon at low strain rates is strain hardening so Vickers hardness rapidly increases up to 20% of thickness reduction. For further deformations martensitic transformation takes place, reflecting a slight decrease of the slope of hardness curve and strong increase of H_c.
H_c is an extrinsic property of materials, sensitive to microstructural conditions and it usually increases with the dislocation density and the reciprocal of grain size [16].
Some authors [17, 18] have studied the variation of coercivity H_c due to cold deformation in metastable austenitic stainless steels, finding different connections revealing different mechanism of ferromagnetism in dependence of low and high content of α′- martensite. In some studies H_c reaches a saturation value after cold deformation [18], in other works H_c decreases continuously with strain [17]. In particular in cold deformed austenitic stainless steels H_c seems to be mainly affected by the average size and distance of α′- martensite. After low plastic deformation low amount of α′- martensite small particles is uniformly distributed in austenitic paramagnetic grains and the distance between the ferromagnetic phases is very high. Increasing strain rate the small martensitic ferromagnetic particles form clusters and finally martensitic islands in austenitic matrix. Martenisitc particles, clusters and islands act as small ferromagnets and are magnetized when an external magnetic field is applied, influencing the magnetic properties of the material. In this way in order to reach saturation magnetic polarization and to obtain H_c value a high applied magnetic field is needed to overcome the internal demagnetization field.
In the first stage of deformation when the size of the martensitic clusters is small and the distance between them is high weak intercluster exchange interactions take place. Increasing the sizes of clusters, all the volume of the material is subjected to domain wall movement, being possible intercluster exchange interaction. The movement of domain wall is here affected by grain boundaries and defects present in the material. When the clustering size is relatively high the distance between clusters becomes more important, with important consequences on coercivity. The maximum value of coercivity is reached with quite high clustering size with strong exchange interaction over longer range than cluster size. On the contrary if the clusters are closer the grain boundaries reduce, leading to less pinning effect which causes a decrease in the coercivity [17].
In this work metastable paramagnetic austenitic phase evolved into ferromagnetic α′-martensite in a ferromagnetic ferritic matrix after cold rolling. The difference between the two matrixes in which martensitic particles nucleate and grow: paramagnetic austenitic matrix in austenitic stainless steels and ferromagnetic ferritic matrix in the duplex stainless steel considered in this work, can affect in different way the coercivity. In the duplex stainless steel neither saturation of H_c, nor continuous decreasing was detected. H_c always linearly increased with thickness reduction applied, but with different slope. The trend seems to be strongly influenced by the presence and amount of strain-induced martensite. Up to 10% of thickness reduction H_c increased because of the high dislocation density. At the first appearance of α′- martensite, 10-30% of thickness reduction, H_c continued to increase but slowly. At higher thickness reduction rates H_c showed a continuous faster increase due to the high increase of α′- martensite at such strain rates. The relationship between H_c and martensite amount is plotted in Fig. 9.

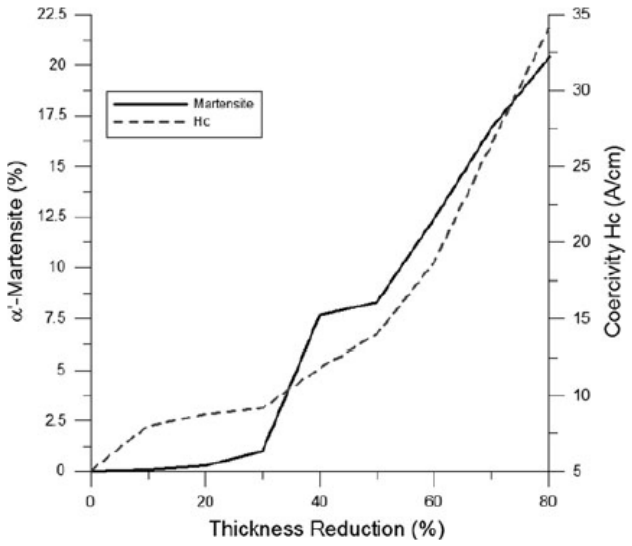

Fig. 9. Relation between coercivity, α'-martensite amount, and thickness reduction

The strongly deformed structure, the hardening of ferritic phase, the high refining with the creation of new grain boundaries due to the different deformation feature between ferrite and the parent austenitic grains are all defects with pinning effect to domain growth and wall movements, those can help to increase H_c.
In the lean duplex stainless steel investigated in the present work a strong dependence between coercivity and α´- martensite content has been highlighted. Hence coercivity measurements may be used as a non-destructive method for useful indication of deformation-induced martensite amount in this type of steel.

4. CONCLUSIONS

This paper concerns with the possibility to obtain a ferritic-martensitic structure in a lean ferritic-austenitic stainless steel by the application of cold deformation inducing martensitic transformation.
Microstructural evolution occurring in a lean duplex stainless steel cold rolled in a range of 0-80% of applied thickness reduction was investigated. The results obtained can be summarized in the following conclusions.

- A strong grain refining is noticeable increasing the strain value to the maximum considered in the present work, leading to grains characterized by few micrometers size.
- A practically complete ferritic - α´ martensitic structure can be obtained at 80% of applied thickness reduction.
- The presence of ferromagnetic strain induced martensite was detected by saturation magnetic polarization measurements, and quantified by the same technique on the basis of X-ray diffraction results.
- The saturation magnetic polarization seems to be not affected by cold rolling up to 30% of thickness reduction, while further increase in cold deformation lead to an increase in saturation magnetic polarization reaching the highest value of 0.94 T for the highest thickness reduction imposed (80%).

- AC magnetic results reveal an inverse ratio between derived relative permeability and cold deformation at low applied external field. Also a strong dependence between coercivity and α´- martensite content has been highlighted.
- The reciprocal of maximum relative magnetic permeability and coercivity were found to be useful parameters for non-destructive quantitative measurements of the amount of deformation-induced martensite amount in the type of steel considered.
- Both Vickers hardness and coercivity linearly increase with cold deformation.

ACKNOWLEDGEMENTS

The authors acknowledge Acciaieria Valbruna S.p.a. for the furniture of the material and G. Fassina for the experimental contribution to this research. This work as partially supported by the Hungarian Research Project OTKA 80173CK.

REFERENCES

1. Hayden HW, Floreen S (1970) The influence of martensite and ferrite on the properties of two-phase stainless steels having microduplex structure. Metall Trans 1:1955-1959

2. Tavares SSM, Neto JM, Da Silva MR, Vasconcelos IF, Abreu HFG (2008) Magnetic properties and α′martensite quantification in an AISI 301LN stainless steel deformed by cold rolling. Mater Charact 59:901–904

3. Mangonon PL, Thomas G (1970) The martensite phases in 304 stainless steel. Metall Trans 1:1577–86

4. Milad M, Zreiba N, Elhalouani F, Baradai C (2008) The effect of cold work on structure and properties of AISI 304 stainless steel. J Mater Process Technol 203:80–85

5. Mészáros I, Prohászka J (2005) Magnetic investigation of the effect of α´-martensite on the properties of austenitic stainless steel. J Mater Process Technol 161:162–168

6. Choi JY, Jin W (1997) Strain induced martensite formation and its effect on strain hardening behavior in the cold drawn 304 austenitic stainless steels. Scr Mater 36:99-104

7. Seetharaman V, Krishnan P (1981) Influence of martensite transformations on the deformation behaviour of an AISI 316 stainless steel at low temperature. J Mater Sci 16:523–30

8. Baeva M, Neov S, Sonntag R (1995) Appearance of bcc martensite after cold deformation of austenitic Fe-Cr-Mn-N steels. Scr Metall Mater 32:1031-1035

9. Güler E, Kirindi T, Aktas H (2007) Comparison of thermally induced and deformation induced martensite in Fe-29% Ni-2% Mn alloy. J Alloys Compd 440:168-172

10. Tavares SSM, Da Silva MR, Pardal JM, Abreu HFG, Gomes AM (2006) Microstructural changes produced by plastic deformation in the UNS S31803 duplex stainless steel. J Mater Process Technol 180:318–322

11. Liljas M, Johansson P, Liu HP, Olsson CO (2008) Development of a lean duplex stainless steel. Steel Res Int 79:466-473

12. Zhang L, Jiang Y, Deng B, Zhang W, Xu J, Li J (2009) Effect of aging on the corrosion resistance of 2101 lean duplex stainless steel. Mater Charact 60:1522-1528

13. C. E. Webb, Soft Magnetic Materials and Magnetic Measurements, Experimental electricity and magnetism 3 227-234

14. Vértesy G, Mészáros I, Tomás I (2005), Nondestructive indication of plastic deformation of cold-rolled stainless steel by magnetic minor hysteresis loops measurement. J Magn Magn Mater 285:335–342

15. Baudouin P, Houbaert Y (2002) The study of a uniaxial deformation effect on the magnetic properties of a non-oriented electrical steel using acoustic emission characterization. J Magn Magn Mater 246:247–253

16. Kronmüller H, Fähnle M (2003) Micromagnetism and the Microstructure of Ferromagnetic Solids. Cambridge University Press

17. Zhang L, Takahashi S, Kamada Y, Kikuchi H, Ara K, Sato M, Tsukada T (2005) Magnetic properties of SUS 304 austenitic stainless steel after tensile deformation at elevated temperatures. J Mater Sci 40:2709-2711

18. Mitra A, Srivastava PK, De PK, Bhattacharya DK, Jile DC (2004) Ferromagnetic Properties of Deformation-Induced Martensite Transformation in AISI 304 Stainless Steel. Metall Mater Trans A 35A:599-605

Effect of micro-alloying elements Nb and V on microstructural and mechanical properties of HSLA forming steels

M. Merlin[1], S. Baldo[2], G.L. Garagnani[1]

[1] Engineering Department, University of Ferrara
[2] DIMEG, University of Padova

Abstract. In the present work the experimental results obtained by different characterizations on two High Strenght Low Alloy (HSLA) steels are discussed. Metallographic samples were prepared and analyzed along the three spatial directions to evaluate the effect of micro-alloying elements on grain refining and anisotropy. Transmission electron microscopy (TEM) and statistical analysis have been applied to study the morphology and distribution of precipitates in both the two types of steels considered. Hence the strengthening due to the precipitation phenomena was calculated through Ashby-Orowan approach. A first evaluation of mechanical properties has been given by microhardness profiles along the thickness of the samples. Moreover a fractographic study was performed on specimens failed after high cycles fatigue tests. In particular the morphology and the effect of micro-alloying elements on crack nucleation areas were analyzed.

Proceedings of 32° AIM National Conference, Ferrara, Italia (2008)
(translated in English)

1. INTRODUCTION

HSLA steels are a category of steels characterized by good mechanical properties, weldability, lightness and competitive costs of production processes. The combination of such properties was obtained through the addition of small amounts of micro-alloying elements like Nb and V and suitable thermomechanical treatments [1,2]. The reduction of carbon content and the presence of microalloying elements, which precipitate as nitride, carbide and carbide-nitride in austenitic phase during specific rolling process, permitted to control ferrite re-crystallization and ferrite grain growth. Thus the optimal microstructure, characterized by very fine grains, was achieved permitting to obtain the required mechanical properties.

Many studies highlighted the role of Vanadium on the increase of mechanical properties through precipitation hardening mechanism. In particular V induced the precipitation of V(C,N) nanoparticles into ferrite during cooling after hot rolling [3,4]. While Niobium was found to act on the strengthening of the material mainly through a different mechanism. In fact Nb is more stable at higher temperatures than V, leading to a stronger effect on grain refining and, consequently, an increase of both mechanical resistance and toughness [5-7]. The synergistic effect of Nb and V, operating at different temperature range, showed the most innovative and interesting solution. The nano-precipitated particles hinder dislocations path enhancing the work hardening of the material but potentially decreasing the ductility and the formability typical of traditional mild low carbon steel sheets [8].

The increase of mechanical properties, due to the micro-alloying combined with the controlled rolling process, is associated with different strengthening mechanisms. Grain refining has been revealed to be the most advantageous mechanism. A large area of austenitic grain boundary per volume during $\gamma \rightarrow \alpha$ transformation is required to maximize the ferritic grain refining. This was possible using a specific technological process for strips production: the controlled rolling [9,10]. The nitrides, carbides and carbide-nitrides formed by the micro-alloying elements limit the growth of austenitic grain during heating and retard the austenitic grain re-crystallization during rolling [11]. This allows a higher austenitic grain stretching, offering an elevated number of ferrite nucleation sites, with a final refine structure. The most important and easy to adjust parameter during the technological process is the coiling temperature. Therefore through the micro-alloying elements content and the process parameter just mentioned, the re-crystallization, phase transformation and crystallographic texture phenomena can be optimized [12]. The HSLA steels considered in this work were produced by the Thin Slab Direct Rolling (TSDR) process. It consisted in a continuous process including a direct casting with a following controlled rolling [13,14]. The fatigue behavior of the material is direct related to the ultimate tensile strength and to the toughness, which increased with the cooling rate after rolling. Comparing with the traditional mild steels, the HSLA steels showed a stronger influence of slip bands than grain boundaries during the fatigue crack nucleation. The role of the precipitates to promote the crack nucleation and propagation close to slip bands seemed to be the main mechanism in the initial stage of the fatigue fracture. Some authors found a transgranular mechanism of fracture for both the HSLA steel containing V and the one alloyed with Nb-V, differently from the traditional carbon forming steels, in which fatigue crack started both in a trangranular and intergranular ways. In classical carbon steels the ferritic grains close to the transgranular fracture area is elongated along the load direction. Moreover they are characterized by few and coarse slip bands with a more homogeneous deformation in comparison to HSLA steels [17]. Other studies stated that the average diameters of

ferritic grains influenced the initiation of fatigue crack. In particular refine structure was believed to retard the formation of fatigue fracture since grain boundaries acted as effective barrier to cracks propagation [19,20].
In this paper two types of HSLA steels are considered: a first HSLA steel alloyed with only V and a second one alloyed with Nb-V, compared to a traditional mild low carbon steel. Traditional metallographic preparation and following observations through optical (OM) microscope were performed on the three spatial directions. Image analysis was used on the micrographs to determine the grain size and the anisotropy of the material. Statistical analysis was applied on transmission electron micrographs to evaluate morphology, amount, distribution of V and Nb-V precipitates and finally the contribution of precipitation reinforcement on the total strength. Microhardness profiles were taken for both the HSLA steels and the mild steel. Moreover high cycles fatigue tests were performed to study the failure of the considered materials. Hence fracture morphology, mainly dealing with crack initiation, was studied through optical microscope (OM) and scanning electron microscope (SEM) observations.

2. MATERIALS AND METHODS

The materials under investigation were a traditional mild steel, taken as reference material, and two HSLA steels. The materials, whose chemical compositions and coiling temperatures are reported in the table I, were supplied as strips 1.5 mm thick.

Acciaio	C	Mn	Si	P	S	Al	Nb	V	N	T_{aspo} [°C]
Riferimento	0.04	0.19	0.03	0.005	0.001	0.042	-	-	0.009	690
V	0.044	0.48	0.02	0.006	0.001	0.039	-	0.039	0.009	680
Nb-V	0.05	0.51	0.07	0.006	0.001	0.051	0.015	0.0025	0.009	680

Table I. Chemical composition (wt %) and coiling temperature of the steels under investigation

With the aim to give a complete microstructural characterization, metallographic samples were cut along each of the three main spatial direction. The following designation was given: “P” (parallel) to indicate the sample cut along the direction parallel to the rolling direction, “L” (longitudinal) for the sample taken along the rolling direction and finally for the sample whose surface is perpendicular to rolling direction was used the letter “T” (transversal). Metallographic samples were prepared by traditional technique and observed after Nital 2 chemical etching at the optical microscope LEICA MEF4M. Grain size and morphology were determined through Leica QWin image analysis software. TEM observations were performed in order to reveal the presence of V and Nb carbide-nitride to study the morphology of the nano-precipitates by meaning of average diameter, volume fraction and distance. TEM samples were cut from thin foils punched in disks 3 mm diameter large. Thin foils were made thin from the original coil firstly by manual grinding and polishing till 70 μm of thickness, then by mechanical automatic polishing using a Dimple Grinder equipment till 15 μm of thickness and finally Precision Ion Polishing System-PIPS was applied till the suitable thickness. TEM analysis were performed at the Università Politecnica delle Marche using a Philips™ CM200 TEM operating at 200 kV and equipped with double tilt. TEM observations were done in bright field mode, tilting the samples to better

reveal the presence and distribution of the nanoprecipitates. Statistical analysis was applied on at least five micrographs in a range of magnitude between 38 and 88 kX for each experimental condition. The local thickness of the sample was measured by Kossel fringes method.
Samples for fatigue test were cut according to ASTM E 466 standard and along the rolling direction. The high cycles fatigue tests were performed in air, at room temperature, through an ItalSigma® apparatus. A stress ratio of R=0.1 and a load application frequency of 16 Hz were chosen for the fatigue tests, while the maximum load applied was set in order to not exceed the yield load determined by previous static tensile tests.
Samples failed after high cycles fatigue tests were studied at low magnitude microscope to reveal the general morphology of the fracture. For detailed observations a Cambridge Stereoscan® S-360 SEM was used on the same samples. Finally the cross section close to the fatigue crack initiation was metallographic prepared, etched and analyzed by OM.

3. RESULTS AND DISCUSSION

3.1 Grain size and morphology evaluation

The most interesting parameters calculated by image analysis software were the average equivalent diameter of ferritic grain and the aspect ratio, that is the ratio between the length and the width of the ferritic grain.
In fig. 1 the graph about the average grain diameter along the three spatial directions is reported. A strong grain refinement is noticeable in the HSLA steels compared to the traditional carbon steel. Moreover the HSLA steel alloyed with only V showed grain diameter about 5 μm larger than HSLA steel alloyed with Nb and V.

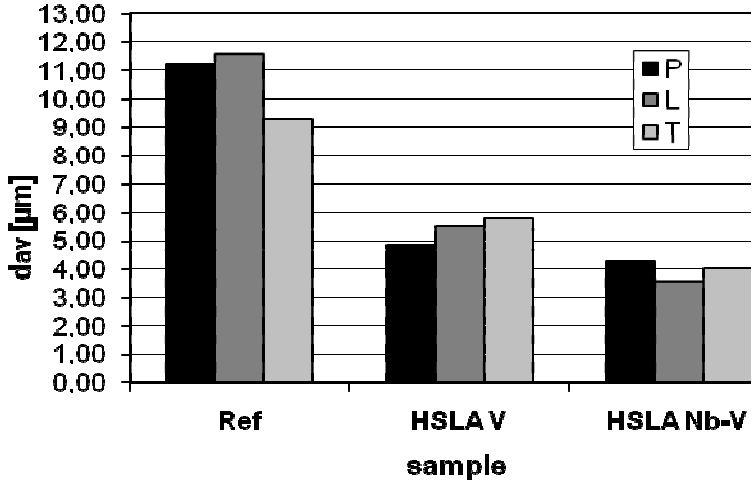

Fig. 1. Grain average diameter values along the three spatial directions of the steels considered

The aspect ratio values are reported in Fig. 2. In this case the values are more homogeneous. In particular for the “P” samples the average value is about 1.7, for the “L” samples the average value is about 2.05 while “T” samples of HSLA steel containing V had higher aspect ratio than HSLA steel containing both Nb and V.

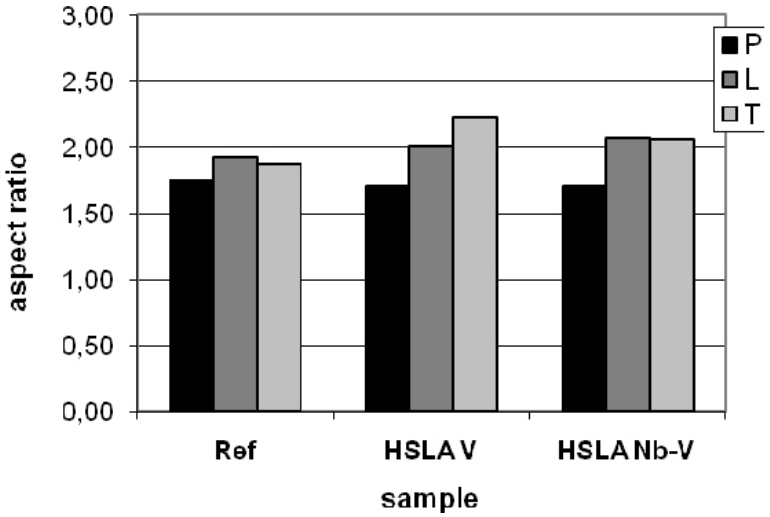

Fig. 2. Average aspect ratio values along the three spatial directions of the steels considered

3.2 Amount, distribution and morphology evaluation of nanoprecipitates

TEM bright field observations revealed the presence of nanoprecipitates of Nb and V as small black particles random distributed in the volume of the samples. Larger aluminum nitrides were also revealed in both HSLA steels and reference material. The parameters and quantities used in the statistical analysis are summarized in table 2. The collected data were organized in N classes of fixed amplitude.

Symbols and formulae	Meanings
N	- Class
Δ	- Class Amplitude: function of range and classes number
$n(j)$	- Number of the precipitates for each class
M_i	- Magnitude of "i-" micrograph
$\sum n(j)$	- Total number of the precipitates
$A_{tot} = \sum A_i / M_i^2$	- Total surface area of the precipitates
$N_A(j) = n(j)/A_{tot}$	- Precipitates density vs surface area for each class
$N_V(j)$	- Volume density of the precipitates for each class
$N_{V(av)} = \sum N_V(j) / \sum n(j)$	- Average volume density
$V_V = (\pi/6) \cdot 3\Delta^3 \cdot \sum N_V(j)(j - 1/2)^3$	- Volume fraction of the precipitates
$\lambda = (1 - V_V) / (\pi/4 \cdot N_{V(av)} \cdot d_{eq(av)}^2$	- Average particles spacing
$d_{eq(av)} = \left[\Delta \cdot \sum n(j)\right] / \sum \left[n(j)/(j - 1/2)\right]$	- Average equivalent diameter
$\tau = (G_b / 2\pi\lambda) \ln(\lambda / d_{eq(av)})$	- Taylor factor
$\sigma_{Orowan} = 3\tau$	- Ashby-Orowan strengthening

Table 2. Quantities and equations used in statistical analysis

The results about the average equivalent diameter ($d_{eq(av)}$) and about the volume fraction (V_v%) of the precipitates were in good agreement with literature data [21], especially concerning HSLA steel alloyed with only V. While in reference carbon steel

only coarse aluminum nitrides were detected, in HSLA steels a finer size and more homogeneous distribution of Nb,V(C,N) precipitates (Table 3). HSLA steels containing only V as microalloying elements seemed to have precipitates characterized by the smaller size and distance between them compared to the other steels investigated. The precipitation strengthening, derived from Ashby-Orowan formulation and on the basis of the results obtained by statistical analysis, is higher in the HSLA steel alloyed with only V, then in the HSLA steel alloyed with Nb and V and finally in the mild steel. As expected, the contribution of precipitation reinforcement on total strength is definitively higher in HSLA steels than in the reference mild steel.

Steel	**deq(av)** [nm]	**Vv** %	**λ** [nm]
Ref	14.065	0.019370	246.710
V	3.314	0.007588	68.396
Nb-V	4.957	0.003812	90.641

Table 3. Average equivalent diameter ($d_{eq(av)}$), volume fraction (Vv%) and precipitates spacing (λ) in HSLA samples and AlN precipitates in the traditional steel

The values of precipitation reinforcing calculated by Ashby-Orowan formula is reported in table 4 together with the total amount of strength derived from tensile tests [21,22].

Steel	**E** [GPa]	**YS** [MPa]	**UTS** [MPa]	**σOrowan** [MPa]
Ref	180	272	355	154
V	190	393	466	364
Nb-V	193	421	484	327

Table 4. Precipitation strengthening values resulted from statistical analysis

The microhardness profiles performed along the transversal section in the steels considered are shown in Fig. 3. In all the cases a decrease in hardness from the surface to the middle of the sample is noticeable, due to the surface hardening during the rolling process. As expected, the hardness in both the HSLA steels reached higher values in comparison to the traditional mild steel, because of the reinforcement mechanism created by the precipitation of (Nb-V)CN. Moreover Nb-V microalloyed HSLA steel presented more homogeneous and higher values of hardness than V microalloyed HSLA steel which had a stronger hardness drop from the surface to the centre of the strip thickness.

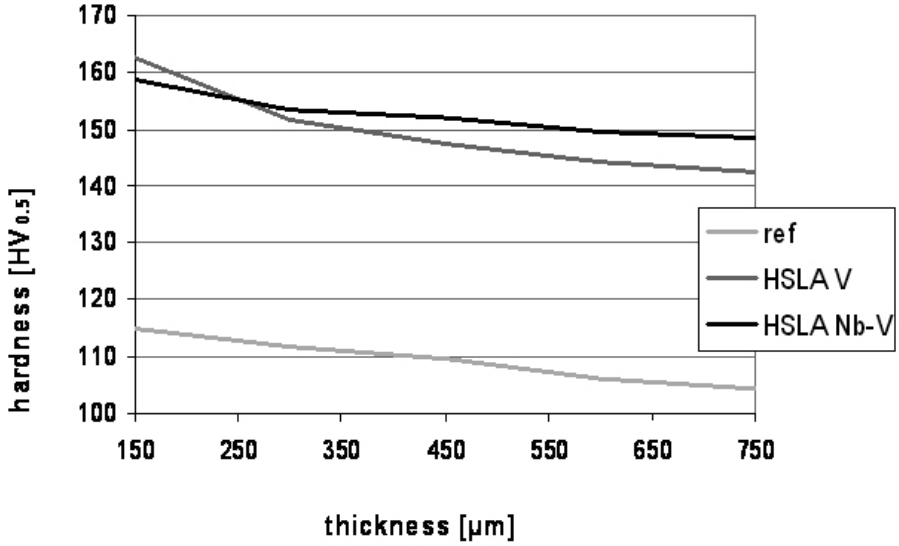

Fig. 3. Microharndess profile on the transversal section of the strips

3.3 Fractographic analysis

The fractographic analysis was carried out on samples failed after high cycle fatigue tests. Besides the common fracture morphology characterized by fatigue striations, the investigation focused on crack nucleation and initial growth areas. A mixed way of fracture, both transgranular and integranular, was revealed in the mild steel, assisted by the presence of carbide and the elongation of ferritic grains in the maximum applied load (Fig. 4). Only few ferritic grains also presented coarse slip bands in the area of crack initiation (Fig. 5).

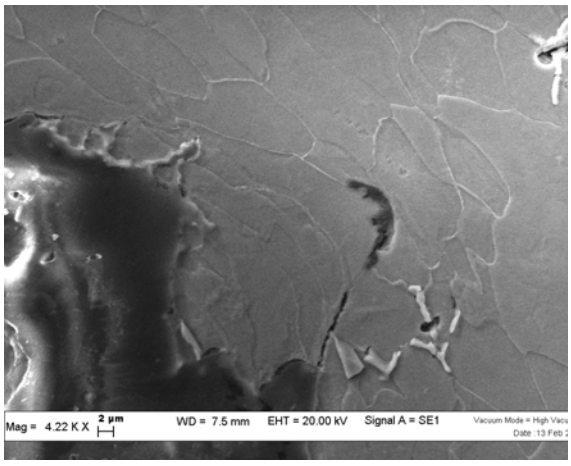

Fig. 4. Traditional forming steel, transgranular and intergranular fracture

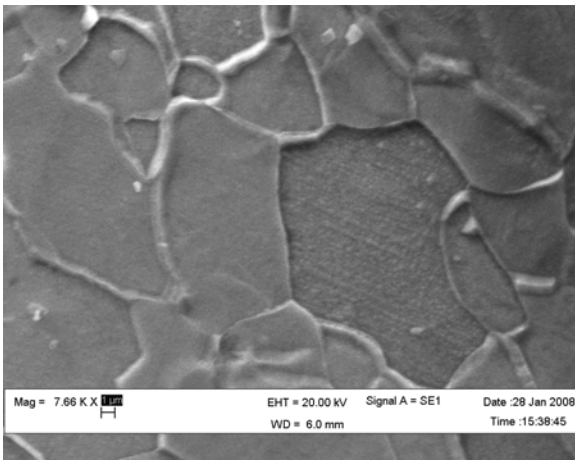

Fig. 5. Traditional forming steel, few coarse slip bands, area of crack nucleation

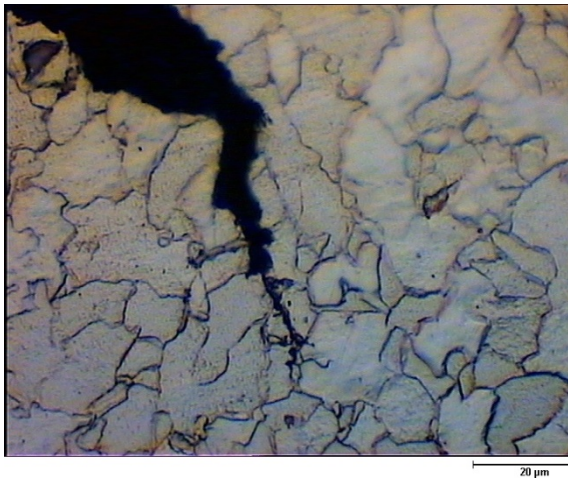

Fig. 6. V HSLA steel, transgranular growth of fatigue crack

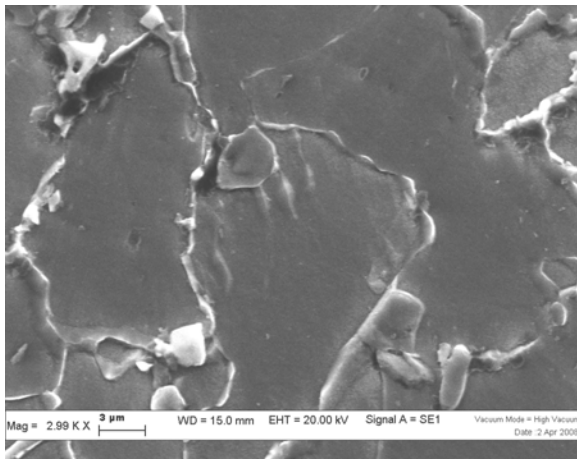

Fig. 7. V HSLA steel, area close to crack nucleation

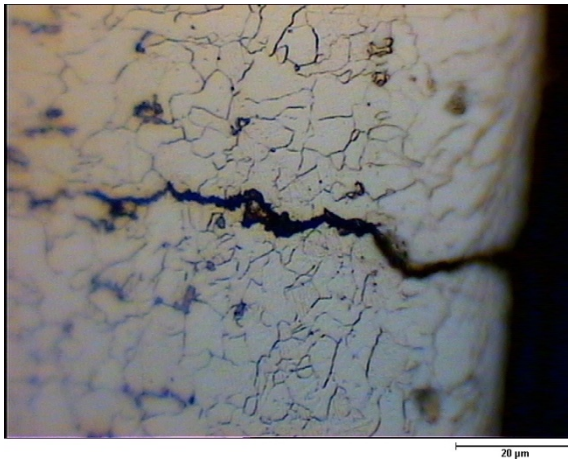

Fig. 8. Nb-V HSLA steel, transgranular growth of fatigue crack

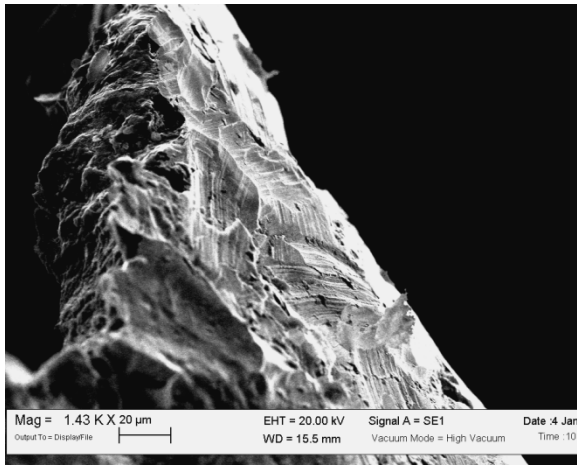

Fig. 9. Nb-V HSLA steel, slip bands in the area close to crack nucleation

In both the HSLA steels the fatigue fracture was transgranular. SEM micrographs revealed the presence of a large number of grains characterized by slip bands (Fig. 9), while OM micrographs (Fig. 6 and Fig. 8) highlighted the grain refining in the HSLA steels, larger in the Nb-V microalloyed steel. The close grain boundaries net seemed to stop and to deviate the fatigue micro-cracks, slowing down the fatigue fracture in the early stage of damage.

CONCLUSIONS

The results of the study presented in this paper can be summarized as follow:

- HSLA steels, especially the Nb-V micro alloyed steel, revealed a stronger grain refining in comparison to a traditional mild low carbon steel;
- The aspect ratio was uniform along the rolling direction for both the HSLA steels, while it decreased along the direction perpendicular to rolling one in the Nb-V HSLA steel;

- The precipitation reinforcement contribution, according to Ashby-Orowan approach, was higher in the V HSLA steel, due to the smaller size of the precipitates and the shorter distance between them; while in Nb-V HSLA steel the grain refining reinforcement component seemed to prevail;
- Both HSLA steels were characterized by definitively higher hardness than traditional carbon steel, in particular the Nb-V HSLA steel showed higher average microhardness values than V HSLA steel;
- Fractographic analysis on samples failed after high cycles fatigue tests revealed a mixed transgranular and intergranular fracture path in the mild steel, assisted by the presence of carbides at grain boundaries; while the way of fracture was mainly transgranular in the HSLA steels, characterized by slip bands in the area of fatigue crack nucleation. The grain refining, especially in the Nb-V HSLA steel, seemed to slowing down the fatigue fracture in the early stage of damage.

ACKNOWLEDGEMENTS

This work was developed in the MIUR-PRIN2005 project contest, with the collaboration of the Politecnico di Milano and the Università degli Studi di Brescia. The authors thanks Acciaierie Arvedi for the collaboration and the material supplied. The authors are also grateful to Prof. M. Cabibbo, Università Politecnica delle Marche, for the cooperation in TEM analysis.

REFERENCES

1. A.GHOSH et al., “Infuence of thermo-mechanical processing and different post-cooling techniques on structure and properties of an ultra low carbon Cu bearing HSLA forging”, Material Science and Engineering A348 (2003) p.299-388

2. T. SENUMA, “Physical metallurgy of modern high strength steel sheets”, ISIJ International 41 (2001) p.520-532

3. T. GLADMAN, “The Physical metallurgy of Microalloyed Steels”, The Institute of Materials, London (1997), p.81-185

4. R. KUZIAK et al., “Microstructure control of ferrite-pearlite high strnght low alloy steels utilizing microalloying additions”, Journal of Material Processing Technology 53 (1995) p.520-532

5. T. SIWECKI et al., Proc. Int. Conf. on Microalloyng, Pittsburg PA (1995), p.197

6. N. MARUYAMA et al., “The role of niobium in the retardation of the early stage of austenite recovery in hot-deformed steels”, Material Science and Engineering A250 (1998) p.2-7

7. J. K. PATEL and B. WILSHIRE, “The challenge to produce consistent mechanical properties in Nb-HSLA strip steels”, Journal of Material Processing Technology 120 (2002) p.316-321

8. G. ARVEDI et al., Stahl und Eisen 17-3 (2003) p.57-69

9. S. ZAJAK et al., Metall. Trans. 22A (1991), p.2681

10. T. SIWECKI et al., Conf. Proc. TMS-AIME, Warrendale, USA (1982), p.163

11. S. YANNACOPOULOS and M. C. CHATURVEDI, Can. Metall. Q. 27 (1988) p.163

12. Y. SHUNFA et al., "HSLA steel metallurgy and applications", Int. Conf. on HSLA Steels, ASM, Metals Park OH (1986), p.213

13. Y. KANG et al., "Morphology and precipitation kinetics of AlN in hot strip of low carbon strip produced by compact strip production", Material Science and Engineering A351 (2003) p.265-271

14. R. WECHSLER, "The status of twin-roll casting technology", Scandinavian Journal of Metallurgy 32 (2003) p.58-63

15. O. UMEZAWA and K. NAGAI, "Subsurface crack generation in high cycle-fatigue for high strength low alloys", ISIJ International 37 (1997) p.1170-1179

16. D. Y. WEI et al., "Fatigue behaviour of 1500 MPa bainite/martensite duplex-phase high strength steel", International Journal of Fatigue 26 (2004) p.437-442

17. Y. H. KIM and M. E. FINE, "Fatigue crack initiation and strain-controlled fatigue of some high strength low alloy steels", Metallurgical Transaction A 13A (1982) p.59-72

18. S. P. BHAT and M. E. FINE, "Fatigue crack nucleation in iron and high strength low alloy steel", Material Science and Engineering A314 (2001) p.90-96

19. M. D. CHAPETTI et al., "Fatigue crack propagation behavior in ultra-fine grained low carbon steel", International Journal of Fatigue 27 (2005) p.235-243

20. M. ZHANG et al., "Micromechanism of fatigue crack nucleation and short crack growth in a low carbon steel under low cycle impact fatigue loading", International Journal of fatigue 21 (1999) p.823-830

21. R. VENTURINI, "Effetto della tecnologia di colaggio in sottile con laminazione diretta sulle proprietà meccaniche e di deformabilità di acciai HSLA", PhD Thesis, Politecnico di Milano, Italy, AA 2005-06

22. Y. W. CHUNG and W. J. LEE, "Cyclic plastic strain energy as a damage criterion and environmental effect in niobium-bearing high strength low alloy steel", Material Science and Engineering A394 (2005) p.126-131

Fatigue characterization and fractographic analysis of a Nb-V HSLA sheet steel

S. Baldo[1], M. Merlin[2]

[1]DPCI, University of Padua
[2]Engineering Dept., University of Ferrara

Abstract. There is a growing interest in the use of high strength low alloy (HSLA) steels for forming operations. The addition of microalloying elements and the introduction of thin slab casting and controlled rolling permit to obtain a good combination of mechanical properties, weldability and lightness at competitive production costs.
The recrystallization and coarsening of the ferrite grains phenomena are controlled by the precipitation of carbide/nitride/carbonitride of the microalloying elements during deformation cycles at established temperatures. This leads to a reinforced material with a particularly fine microstructure and high mechanical properties. The synergic addition of small quantities of Niobium and Vanadium, acting in a different precipitation range of temperature, makes Nb-V HSLA steels of strategic interest.
In the present work the high cycle fatigue behavior and the morphology of fracture surface of a Nb-V HSLA strip steel have been studied. With this purpose light optical and electronic microscopy was applied. Moreover chemical analysis on eventual inclusions in the fatigue fracture areas was carried out through energy dispersive X-ray spectroscopy (EDS).

Proceedings of IGF Workshop, Forni di Sopra (Udine), Italy (2009)
(translated in English)

1. INTRODUCTION

The HSLA steels in sheet and strip forms found large applications due to the addition of microalloying elements like Nb and V, together with specific thermo-mechanical processing such as thin slab casting and controlled rolling. This led to obtain high mechanical properties, weldability and a certain toughness with low cost raw materials and high productivity technological processing. Therefore the substitution of more expensive high strength steels with low alloyed ones was possible without any loss in mechanical properties.

The Nb-V microalloyed steels received particular attention thanks to the increase in mechanical properties due to the synergic effects of these two elements that precipitate in carbide/nitride/carbonitride forms at different ranges of temperature during controlled rolling [1,2]. As reported in literature [3], V precipitates as V(C,N) nanoparticles dispersed in the ferritic matrix during cooling after controlled rolling. Thus the main contribution to the total strength of the material was given by V addition through a precipitation hardening mechanism of V(C,N) nano-precipitates. On the contrary Nb was found to act mainly as a grain refiner, being more stable at higher range of temperatures. The grain refinement produced by Nb addition enhances both strength and toughness of the steel [4].

The grain refinement reinforcement is more evident if the surface area/volume ratio of the prior austenitic grain is higher in the $\gamma \rightarrow \alpha$ transformation during controlled rolling cycles. The precipitation of carbides/nitrides/carbonitrides of the alloying elements limits the austenite grain coarsening and retards the recrytallization phenomenon. The favourable elongated shape of the austenitic grains leads to a higher number of ferrite nucleation sites during the following cooling. As consequence the resulting material is characterized by very fine microstructure and high mechanical properties [5].

The specific processing applied to the steel under investigation is the thin slab direct rolling (TSDR). The TSDR consists in a first casting and rolling step in which the steel is transformed in thin slabs. In a following stage the thin slabs, still containing a liquid core, are directly rolled at high temperature to obtain a product characterized by homogeneous structure. The hot rolled products obtained through TSDR have thickness typical reductions, shape, surface quality and planarity similar to cold rolled ones. Moreover the mechanical properties have almost the same values along all the length of the strip, as highlighted by anisotropy studies [6]. Through the direct production of low thick and ultra-low thick strips, the following post treatment such as cold rolling, can be avoided thus reflecting in a global costs saving of this class of steels [7]. Relatively few informations are available in literature about the fatigue behavior and fatigue fracture mechanisms of Nb-V HSLA steels. Some authors [8,9] observed a fatigue crack nucleation mainly dominated by the presence of slip bands if compared to traditional mild low carbon steels where the early stage of fatigue fracture was strongly influenced by the grain boundaries. In other works the average ferritic grain diameter was related to the initial stage of the fatigue fracture. In particular it was found that a more refined grain structure, with its larger extension of grain boundaries, retards the formation of fatigue cracks, as the grain boundaries acts as a barrier to microcrack propagation [10,11,12]. Also a different routes of crack propagation was revealed for the HSLA steels in comparison to mild steels. In the HSLA steels the way of fatigue fracture was revealed to be principally transgranular whereas the traditional low carbon steels are typically characterized by a mixed way of fracture, both transgranular and intergranular, in the early stage of crack propagation [13].

2. EXPERIMENTAL PROCEDURES

The material under investigation is a Nb-V HSLA steel, here named AS32NBV. The chemical composition of the steel considered in this work is reported in Tab.1.

	Chemical Composition (wt%)								
	C	Mn	Si	P	S	Al	Nb	V	N
AS32NBV	0.05	0.51	0.07	0.006	0.001	0.051	0.015	0.025	0.009

Table 1. Chemical Composition.

High cycle fatigue tests were performed on 17 specimens drawn from a 1.5 mm thick strip, according to ASTM E 466 standard, which imposes a bend radius value of 8 times the specimen thickness value between the gauge length and the fatigue machine grips. The area of the gauge part has to be between 1.94 and 645 mm^2, while the height of the gauge part and the specimen thickness ratio has to be between 2 and 6.
The axial fatigue tests were carried out through an ITALSIGMA® equipment on specimens along the rolling direction of the strip. The tests were conducted in air, at room temperature, with a load ratio of R=0.1 to avoid any instability phenomenon, and a frequency of 16 Hz. The stop of the tests was set at $2 \cdot 10^6$ cycle. The specimens failed after fatigue tests were observed at LEICA MEF4M® light optical microscope (LOM). The LEICA QWIN image analysis software was used to evaluate the grain size of the samples. Then a detailed analysis of the fracture surface was performed using a scanning electron microscope (SEM) Cambridge Stereoscan® S-360. The chemical composition of eventual inclusions was evaluated through EDS.

3. RESULTS AND DISCUSSION

The results about yield strength and the ultimate tensile strength obtained from tensile tests conducted in a previous work (σ_s = 421 MPa, σ_R = 484 MPa) [6] together with the estimated fatigue limit values for a similar steel were used to set the stress amplitude levels to be applied. Therefore the specimens were subjected to different levels of stress amplitude spaced by a constant quantity *d*. To give a more precise evaluation of the fatigue limit, *d* was fixed at 5 MPa.
The specimens were tested to the chosen levels of stress amplitude till a number of cycles of $N=2 \cdot 10^6$, according to the "stair case" method (UNI 3964). This method states that if a specimen subjected to a certain stress level failed, the following specimen has to be tested at the stress level just lower. On the contrary, if the specimen at certain stress level does not fail, the following specimen has to be tested at a stress level just higher. This method is repeated till all the specimen under investigation are tested.

The levels of stress amplitude and the results of each test is noticeable in Tab.2

Δσ [MPa]	σa [MPa]	σm [MPa]	N
400	200	244.4	358770
400	200	244.4	385941
390	195	238.3	337329
390	195	238.3	384656
390	195	238.3	835581
390	195	238.3	Run – out
390	195	238.3	Run – out
380	190	232.2	219161
380	190	232.2	479410
380	190	232.2	Run – out
380	190	232.2	Run – out
380	190	232.2	Run – out
380	190	232.2	Run – out
370	185	226.1	Run – out
370	185	226.1	Run – out
370	185	226.1	Run – out
360	180	220	Run – out

Table 2. Stress levels applied and results of each fatigue test, R=0.1.

In Tab. 3 the sequence of the results are reported. According to the common designation, X means the failure of the specimen, whereas 0 is used for the surviving specimens. Moreover the parameters used in the statistical analysis for the fatigue limit calculation is below explained.

σa [MPa]																	X	0	i	n	n·i	n·i²
200											X		X					2	0	4	2	8	32
195				X				X		0		0		X				3	2	3	3	9	27
190			0		X		0		0						X		0	2	4	2	2	4	8
185		0				0										0		0	3	1	0	0	0
180 σ0	0																	0	1	0	0	0	0
																		7	10		7	21	67
																					N	A	B

Table 3. Stair-case method.

The less frequent event between failure and not failure has to be considered. In this case the less frequent event consists in the failure one. The stress amplitude corresponding to 50% of survival probability (σ_D) is determined as follows:

$$\sigma_{D(50\%)} = \sigma_0 + d \cdot \left(\frac{A}{N} \pm 0.5 \right) = 192.5 \text{ [MPa]}, \qquad (1)$$

where σ_0 is the lowest level of stress amplitude. In this case the minus sign is used as the less frequent event is the failure.
The standard deviation is :

$$s = 1.62 \cdot d \cdot \left(\frac{N \cdot B - A^2}{N^2} + 0.029 \right) = 4.86 \text{ [MPa]}. \quad (2)$$

The following conditions have to be respected for the validity of the method applied:

$$\frac{\mathrm{N} \cdot \mathrm{B} - \mathrm{A}^2}{\mathrm{N}^2} = 0.571 > 0.3\,; \quad (3)$$

$$0.6 < \mathrm{d/s} = 0.97 < 1.5. \quad (4)$$

In the case considered in this work the two conditions were respected, as it can be easily verified.

The stress amplitude values corresponding to survival probabilities of 90%, 50%, 10% respectively can be derived from the fatigue limit amplitude $\sigma_{D(50\%)}$ through the formula:

$$\sigma_{D(10\%)} = \sigma_{D(50\%)} + 1.28 \cdot s = 198.7 \ MPa \quad (5)$$

$$\sigma_{D(90\%)} = \sigma_{D(50\%)} - 1.28 \cdot s = 186.3 \ MPa \quad (6)$$

As regards to maximum stress, it can be noticed that the fatigue limit corresponding to the a stress amplitude of $\sigma_{D(50\%)}$ at $2 \cdot 10^6$ number of cycles is comparable to the yield stress of the material.

Traditional metallographic preparation and chemical etching with Nital 2 were applied to the samples before the observation through LOM and image analysis. The resulting microstructure consisted in ferrite, with average grain diameter values between $3.5 \div 4.2$ μm.
The analysis of the fracture surfaces (Fig. 1) of specimens failed during fatigue tests reveals that the fracture has started from the edge surface close to the minimum cross section of the specimen (Fig. 2). Then the fracture develops in a trasgranular way along the specimen (Fig. 3).

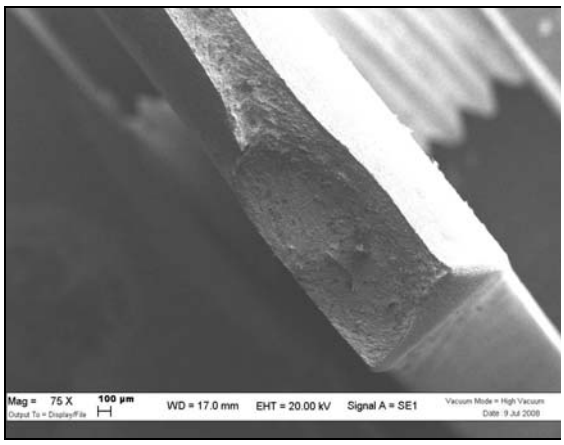

Fig. 1. Fracture surface.

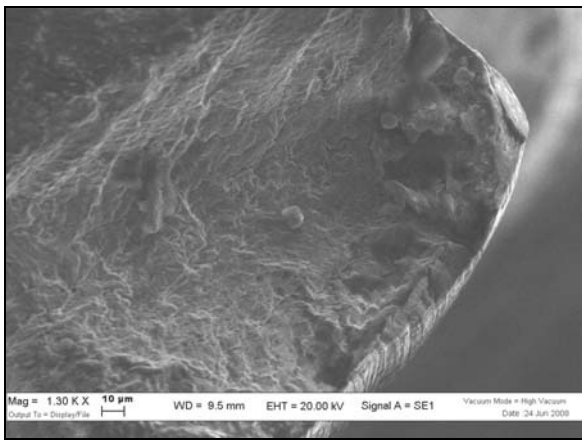

Fig. 2. Crack nucleation closet to the edge.

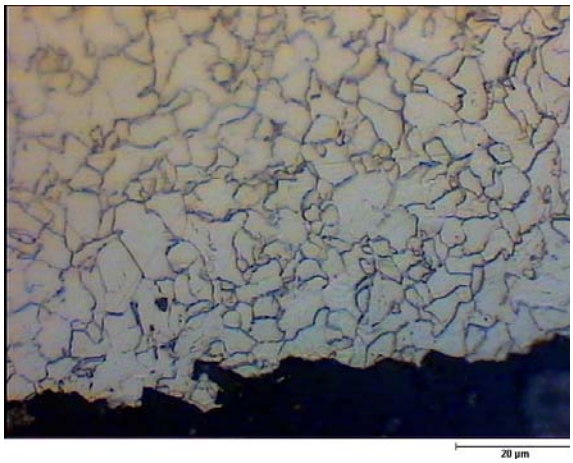

Fig. 3. Transgranular way of fracture.

Fig. 4.Transgranular fracture with microvoids and local plastic deformation.

Close to the fracture surface a plastic deformation area, characterized by several microvoids and stretched ferritic grains, can be observed (Fig.4).
In the zone of rapid failure surface, many dimples have been found as a sign of the ductility of the material.

Two general paths of fracture can be distinguished. In the area where the origin of the fatigue fracture took place the crack propagates with an orientation of 45° to the load direction for few micrometers as the microstructural effects prevail. Afterwards the propagation of the fracture is perpendicular to load application, as the mechanical component becomes predominant (Fig.5).
As well known from several works available in literature [14], the fracture nucleation and the early stage of crack propagation play an important role in the fatigue resistance of the material. In this stage of fracture (Microstructural Fracture Mechanism, MFM) microstructure is the main factor influencing the mechanism of fracture (Stage I, Mode II). The crack nucleates and grows through shear micro-mechanism, covering an area of size comparable to that of the grains structure. Such generation of shear micro-mechanisms, 45° oriented to the load direction, is due to the presence of thick shear bands oriented in the same direction (Fig. 6).

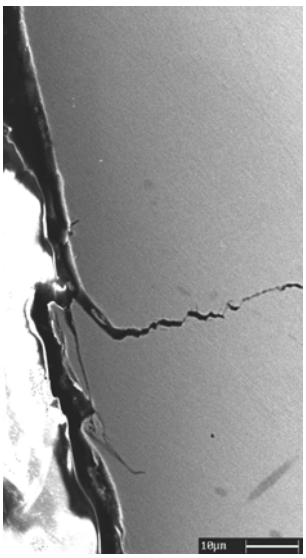

Fig. 5. Fracture behavior.

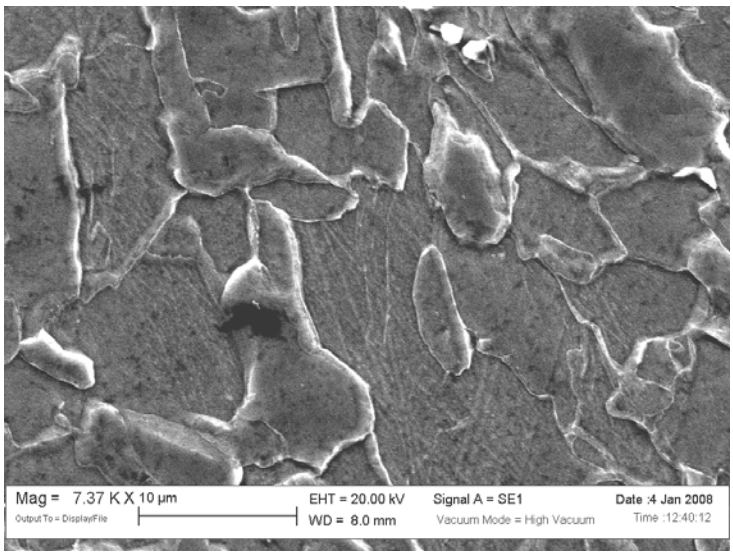

Fig. 6. Slip bands.

A strong increase of fatigue limit value of the material can be achieved maintaining the microcracks as smaller as possible, enhancing the microstructural "barriers", such as a larger grain boundaries web [14].
The SEM micrographs (fig. 8) show, next to the main crack, the presence of many secondary microcracks, developed again from the surface of the sample. However these microcracks stop at few micrometers from their nucleation. This is probably due to the obstacle introduced by the fine microstructure mainly obtained from the addition of Nb during controlled rolling.

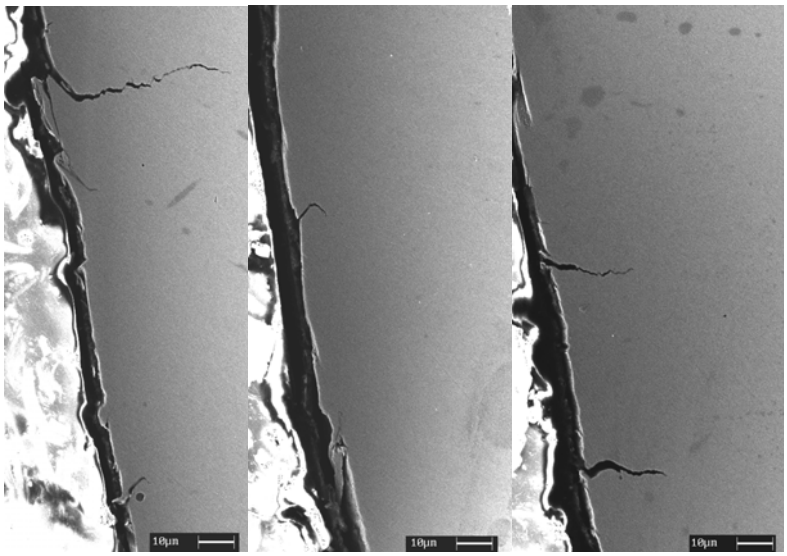

Fig. 7. Microcracks.

The presence and size of inclusions are important because of their different hardness and mechanical behavior, that can affect the fatigue fracture of the material.
In the rapid fracture surface area some inclusions have been detected inside the dimples. Qualitative chemical analysis, performed through EDS, revealed that such inclusions contain Al and Ca, deriving from the deoxidizing and desulphuring processes of the steel, Mg due to the probable interaction of the steel with the refractory material, and S which is often present in the metal charge. The inclusions, probably Calcium sulphides, Magnesium oxides and Calcium aluminates, have a spheroidal form and a size between 1-5 μm. In Fig. 7 and Fig. 8 some spectra obtained by elements chemical analysis are noticeable. Due to the small size of the inclusions also part of the metal matrix is analyzed.

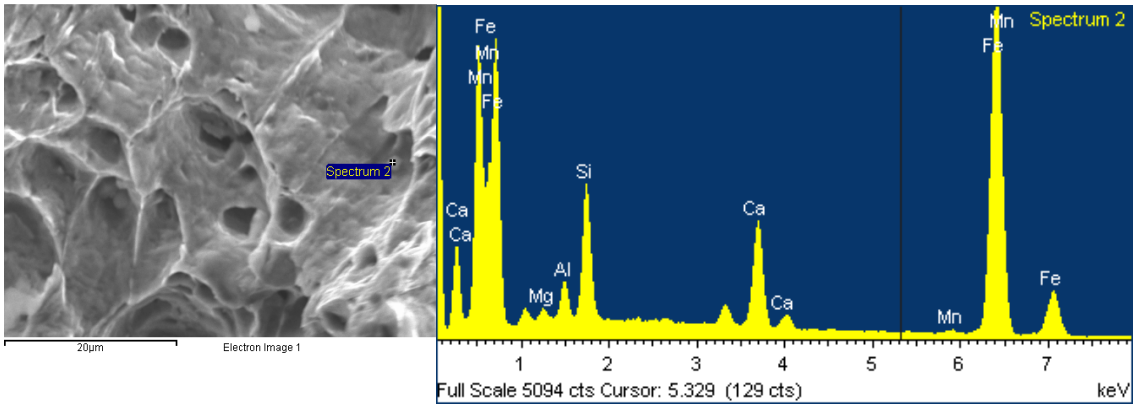

Fig. 8. Inclusions-EDS spectrum.

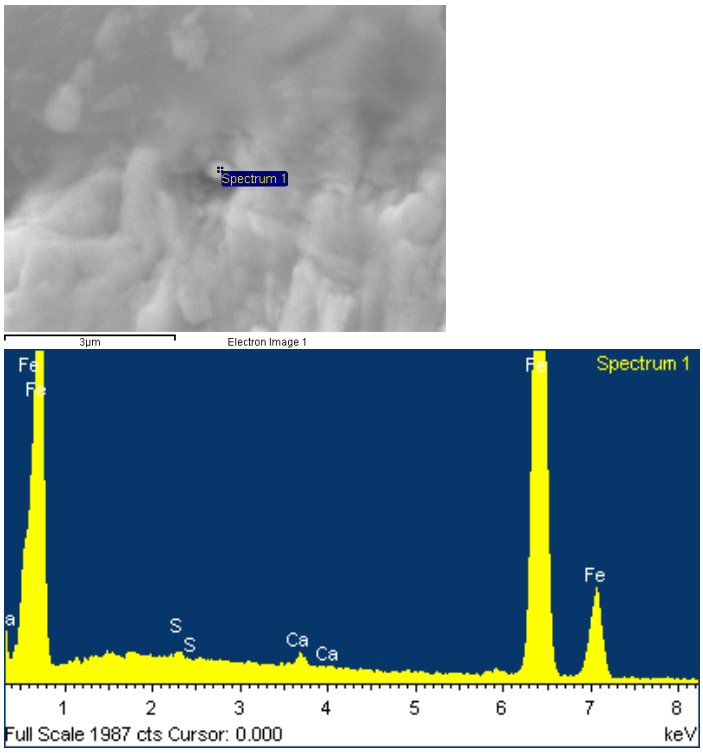

Fig. 9. Inclusions (CaS)-EDS spectrum.

4. CONCLUSIONS

The present work was aimed to characterize the high cycle fatigue behavior of a Nb-V HSLA steel together with the analysis of the fracture surfaces obtained after fatigue failure. The results obtained can be summarized as follows:

- The stress cyclic amplitude under which the material does not fail after $2 \cdot 10^6$ of cycles has been found to be of 192,5 MPa, thus close to the yield strength of the material. This was calculated applying the “stair case” method with a survive probability of 50%;

- The fatigue cracks nucleate at the surface of the tested specimens, usually in correspondence to edge of the minimum cross section; the fatigue fracture develops in a transgranular way;
- Light optical and scanning electron microscopy revealed areas of plastic deformation occurring during fatigue fracture;
- In the area close to the fracture origin, the fatigue crack propagation is oriented of 45° to the load direction; in particular the fatigue cracks in this region seem to assume the same orientation of the slip bands observed through SEM;
- A number of secondary microcracks next to the main crack have been detected; however such microcracks were not able to grow during fatigue tests thanks to a "barrier" effect caused by the dense web of grain boundaries introduced by the grain refinement connected to the addition of Nb in the steel considered;
- The rapid fatigue fracture is mainly ductile, made easier by the presence of several inclusions inside the material.

ACKNOWLEDGEMENT

The authors are greateful to Acciaieria Arvedi for the supplied materials. The authors wish also to thank Prof. Gian Luca Garagnani for the scientific support and Daniele Casari for his help in the experimental part.

REFERENCES

1. A. GHOSH et al., "Influence of thermo-mechanical processing and different post-cooling techniques on structure and properties of an ultra low carbon Cu bearing HSLA forging", Material Science and Engineering A348 (2003) p.299-388

2. T. SENUMA, "Physical metallurgy of modern high strength steel sheets", ISIJ International 41 (2001) p.520-532

3. T. GLADMAN, "The Physical metallurgy of Microalloyed Steels", The Institute of Materials, London (1997), p.81-185

4. N. MARUYAMA et al., "The role of niobium in the retardation of the early stage of austenite recovery in hot-deformed steels", Material Science and Engineering A250 (1998) p.2-7

5. M. CABIBBO et al., "Effect of thermo-mechanical treatments on the microstructure of micro-alloyed low-carbon steels", J. Mater. Sci., 2008, 43, 6857-6865;

6. R. VENTURINI, "Effetto della tecnologia di colaggio in sottile con laminazione diretta sulle proprietà meccaniche e di deformabilità di acciai HSLA", PhD Thesis, Politecnico di Milano, Italy, AA 2005-06

7. Y. Li et al., "The evolution of microstructure during thin slab direct rolling processing in vanadium microalloyed steels"

8. O. UMEZAWA and K. NAGAI, “Subsurface crack generation in high cycle-fatigue for high strength low alloys”, ISIJ International 37 (1997) p.1170-1179

9. S. P. BHAT and M. E. FINE, “Fatigue crack nucleation in iron and high strength low alloy steel”, Material Science and Engineering A314 (2001) p.90-96

10. M. D. CHAPETTI et al., “Fatigue crack propagation behavior in ultra-fine grained low carbon steel”, International Journal of Fatigue 27 (2005) p.235-243

11. M. ZHANG et al., “Micromechanism of fatigue crack nucleation and short crack growth in a low carbon steel under low cycle impact fatigue loading”, International Journal of fatigue 21 (1999) p.823-830

12. M. MERLIN et al., “Effetto degli elementi microalliganti Nb e V sulle proprietà microstrutturali e meccaniche di acciai HSLA da stampaggio”, 32 Convegno Nazionale AIM, oral section

13. Y. H. KIM and M. E. FINE, “Fatigue crack initiation and strain-controlled fatigue of some high strength low alloy steels”, Metallurgical Transaction A 13A (1982) p.59-72

14. K. J. MILLER, “The two thresholds of fatigue behaviour”, Fatigue Fract. Eng. Mater. Struct. (1993), 16:931-9

The effect of braze-welding speed on the microsturcture and mechanical properties of a Dual Phase Steel

[1]I. Rampin, [1]M. Piazza, [1]S. Baldo, [1]A.F. Miranda Perez, [1]K. Brunelli,[1] I. Calliari , [2]F.A. Reyes Valdès

[1] Università di Padova, Italy
[2] Corporación Mexicana de Investigación en Materiales, Saltillo, México.

Abstract. The attention towards high strength dual-phase steels increased significantly in the last years. Especially the automotive industry has shown a great interest in DP steels due to the possibility to reduce weight of vehicles and to increase the passenger safety at a very competitive cost. Automotive manufacturers require optimized weld schedules that meet the customer quality requirements to obtain the best weld performance during the life vehicle. The variation of welding parameters (voltage, current and speed of welding) affects weld performance and mechanical, metallurgical and corrosion steel properties. The CMT (Cold Metal Transfer) braze welding is a recent brazing technique: it is a modified metal inert gas welding process based on short-circuit transfer process. It allows to reduce the heat required for welding and permits higher joining speeds. The aim of this work is to study the interfacial microstructures and intermetallic compounds produced by cold metal transfer welding of two plates of galvanized DP600 dual phase steel with $CuSi_3$ as the filler metal. The study was performed by applying a CMT braze welding with three different joining speeds. Microstructural investigations were performed through both light optical and scanning electron microscope. Vickers microhardness and shear tensile tests were used to determine mechanical properties. The results obtained were related to the process conditions of braze-welding. A small ZTA, constituted by martensite, bainite and coarse ferrite grains, has been highlighted. Moreover, an intermetallic Fe-Si-Cu compound layer formed at the interface between steel and filler metal. It was found that joining speed influenced the size of ZTA since the heat input Q affects the phase transformation in the weld and heat affected zone. This parameter also affects influences the thickness of the compound layer and the size of precipitates in the filler metal.
The mechanical characteristics are affected by the different speed too. The fracture starts at the interface steel-copper where intermetallic compounds formed.

1. INTRODUCTION

The AHSS (Advanced High Strength Steels) have been newly achieved the same properties as traditional steels in auto-making sector instead with less weight [1]. The Dual Phase Steel has a structure formed with a ferritic matrix containing a hard martensitic second phase in the form of islands. The ferritic matrix gives a good workability while the martensite represents the hard phase that guaranty a high mechanical strength. [2]

The steel production requires a hot or cold lamination, followed of a continuous tempering. For obtaining ferritic grain, the transformation of γ to α comes on high temperature, subsequently it colds abruptly to prevent the bainitic and perlite formation. [1]

Brazing is a welding method that melts and joins metals (different type) with fed filler, keeping intact the boundary of the obtained join [3,4]. The cold metal transfer is a modified MIG welding process; it is described as a series of steps leading to the transfer of a drop of molten metal at a time.

Every time the short circuit occurs, the digital process control both interrupts the power supply and controls the retraction of the wire. The wire retraction motion assists droplet detachment during the short circuit thus the metal can transfer into the welding poll without the aid of electromagnetic force. One of the characteristic is the reduction of spatter and also the lowest heat input that it is required for the joint. [5-7]

The aim of this article is to examine the metallographic characteristics of zinc-coated steel by CMT process at the changing of welding rate. The microstructure of the joint and the tensile strength of the joint were investigated to evaluate the best parameters to use in this process.

2. EXPERIMENTAL PROCEDURES

The experimental materials were galvanized DP600 steel plates of 119x130x1,2 mm, whose composition is shown in table 1. The filler metal was ER CuSi-A. The wire diameter is 1 mm and the composition of the filler metal is listed in table 2. The filler metal is yellow-brown and two dark bands, approximately of amplitude 3 mm, extend along the sides, probably generated by the arc power required by the CMT process.

Wt.%	C	Mn	Si	P	S	N	Al	Ti	Nb	V	B	Cu	Cr	Ni	Mo	Sn
DP	.115	1.55	.186	.026	.005	.0032	.035	.002	.003	.002	.0003	.012	.347	.026	.110	.003

Table 1. Composition of the base metal

Wt.%	Mn	Si	Other	Cu
ERCuSi-A	0,75-0,95	2,80-2,95	Max. 0,5	Balance

Table 2. Composition of ER CuSi-A

The welding process was carried out using the CTM method with the following parameters: V=10,4 V and I=115 A. The varying parameter considered in this study is the welding rate and three different speed were considered. In table 3 there are the

joining rate and the heat input calculated by the formula $H_n = \frac{f_1 \cdot VI}{v}$, where f_1 is the efficiency of heat exchange.

	DPWB9	DPWB3	DPWB16
v (mm/s)	700	800	900
$\mathbf{H_n}$ (J/mm)	100,3	87,75	78

Table 3. Welding rate parameter during brazing and heat input.

The cross section of specimens was included in epoxid resin and polished by metallographic procedures. The microstructures of welded joints were examined by light microscopy, scanning electron microscopy (Cambridge Stereoscan 440 SEM) equipped with an energy dispersive X-ray spectrometer. The hardness profiles were performed by a Leitz micro-hardness tester with a load of 100 g. Microhardness testing procedures followed the UNI EN ISO 6507-1 standard test method [8]. The tensile strength of welded joints was evaluated by Galdabini Sun 2500 testing machine.
For tensile test actually does not exist a guideline for these kinds of samples, furthermore the ISO 14273:2000 [9] was used approaching to those for tensile shear test.

3. RESULTS AND DISCUSSION

3.1 Microstructure

Fig. 1 shows the cross-section OM of base material along the longitudinal section (Fig. 1a) and on the transversal side (Fig. 1b): it is constituted by ferritic matrix, whose grains are elongated along the rolling direction, and by martensitic phase dispersed in parallel bands distributed in the same direction.

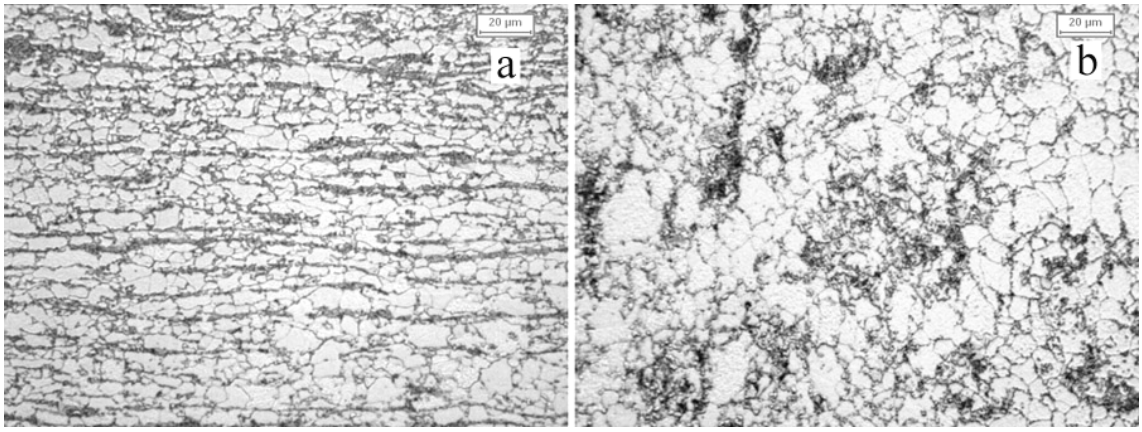

Fig. 1. Microstructure of base metal, DP600 steel, along the longitudinal section of the plate (a), on the transversal side of the plate (b).

Fig. 2 shows the microstructure of the plates in the Heat Affected Zone (HAZ) starting from the farthest (Fig. 2a) to the closest (Fig. 2d) area to the fusion zone for both the upper and the lower plates (Fig. 2e-f). The HAZ adjacent to the unaffected area is constituted by coarse ferritic grains (Fig. 2a), confirmed by SEM observation and

microhardness values. Moving toward the HAZ martensite and bainite phases were observed, which are typical for the AHSS welded (Fig. 2b) [10]. The line of transition between the base metal microstructure and fine grain zone is quite well distinguishable. Continuing in the HAZ of the upper plate a completely martensitic structure is observed with strips of martensite that are more developed near the fusion zone (Fig. 2d).

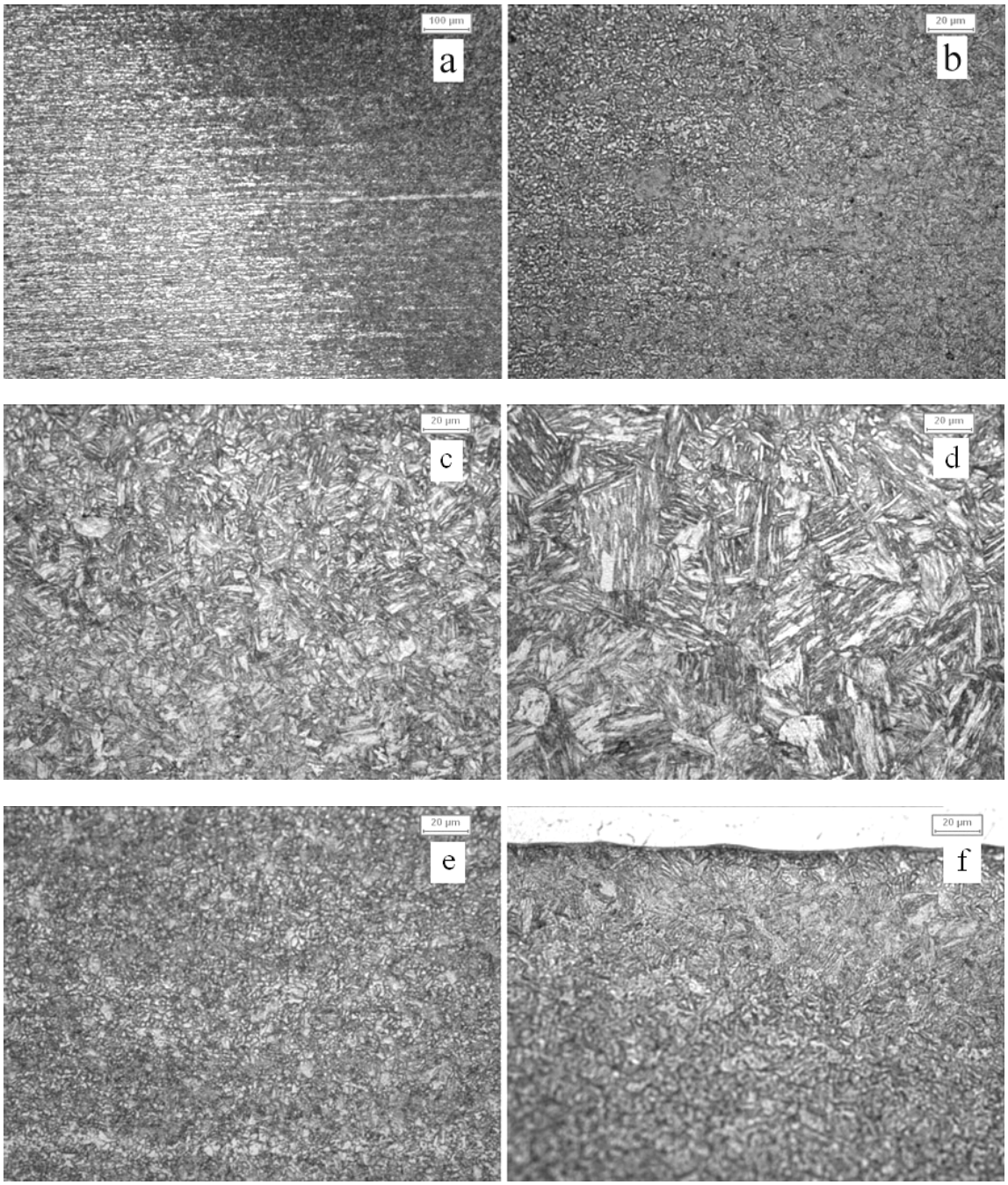

Fig. 2. Microstructure of HAZ in the upper plate (a-d) and in the lower plate (e-f). OM, Nital etching.

In the lower and in the upper plate the microstructure is similar: a coarse grain area has been detected in the unaffected-affected transition zone and a fine bainitic-martensitic structure in the heat affected zone (Fig. 2e). As it can be observed in Fig. 2f, in the lower plate the size and the amount of martensite increase in the area close to the upper plate: the more developed martensite areas are always near to the upper plate.

This microstructural sequence was investigated in all the three samples considered in this work. The differences due to welding rate are the size and quantity of martensitic phase. Considering the same areas in different samples, the sample brazed at higher *v* has more martensite grains. Figure 3 shows the scheme of the Heat Affected Zone in the upper and lower plates of welded samples and in Table 4 the measurements of HAZ width of all the samples are summarized.

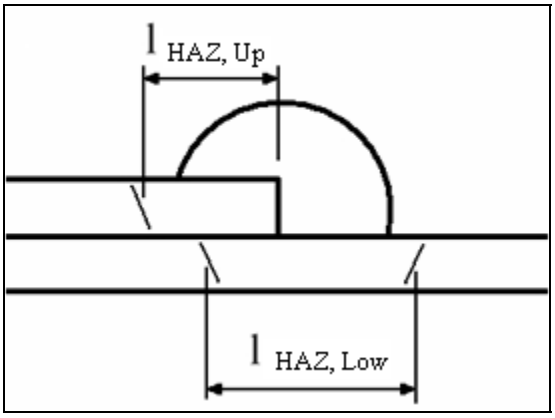

Fig. 3. Scheme of the HAZ

	DPWB9 (mm)	**DPWB3 (mm)**	**DPWB16 (mm)**
$l_{HAZ, Up}$	3,75	2,50	3,25
$l_{HAZ, Low}$	7,00	5,75	6,00

Table 4: Values of the length of HAZ in the samples

The length of HAZ is correlated to the welding rate parameter, in fact at the increasing of welding rate the affected zone becomes smaller because the heat input is lower. Moreover, increasing the welding speed, the cooling rate is higher so that the sample DP16 shows a larger martensitic area.

The scanning electron microscope analysis reveals that at the interface base metal steel-fusion zone a layer of intermetallic compounds forms. This layer is not uniform along the whole section: there are compact layers (Fig. 4a) alternate with thicker inhomogeneous zones (Fig. 4b). The compact zone has an uniform thickness of about 3 μm and it is divided into two layers (I and II). The composition of the layers I and II are shown in Table 5 for the three samples.

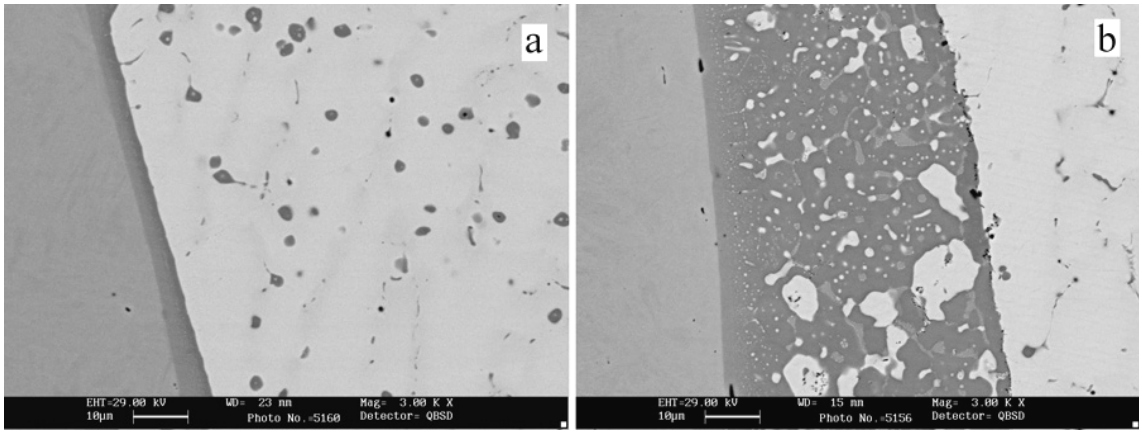

Fig. 4. Intermetallic compounds at steel-fusion zone interface: compact layer (a); irregular layer (b).

		Si (wt.%)	Mn (wt.%)	Fe (wt.%)	Cu (wt.%)
DPWB9	I	6,1	1,2	88,0	4,7
	II	10,8	1,5	74,9	12,8
DPWB3	I	8,2	1,2	84,6	6,0
	II	11,5	1,7	76,1	10,7
DPWB16	I	7,0	1,3	86,3	5,4
	II	11,8	1,2	78,7	8,3

Table 5. Composition of the compound layers

As it can be seen in Table 5, ternary Fe-Cu- Si compounds formed. The proportions between the three elements are different in I and II layers. The following proportions can be identified: I layer: $Fe_{7,26}$-$Cu_{0,34}$-Si; II layer: $Fe_{3,48}$-$Cu_{0,52}$-Si.
The layer of non homogeneous intermetallic compounds is rich in Fe and Si and their concentration increased towards the fusion zone. This layer contains zones with high concentrations of Cu, Fe and Si and gray areas with higher concentrations of Cu. The same areas are enclosed by small precipitates rich in Cu.
The thickness of the inhomogeneous compounds is higher in DPWB9 (about 40 µm) than in DPWB16 (15 µm): the nucleation and growth of compound layer are favored by higher heat input.
As it can be seen in Fig. 4, some intermetallic compounds are observed in the copper filler zone due to the strong stirring force of the arc that fragments the stick-like compounds at the interface solid/liquid so that many particles can be swept into the filler zone and grow by an Ostwald ripening mechanism [11,12].

3.2 Microhardness Test $HV_{0,3}$

The results of microhardness tests performed on three samples are summarized in Fig. 5. Increasing the welding rate the size of areas with martensitic hardness (375 to 450 HV0, 3) increases; in particular DPWB3 and DPWB16's hardness is greater than 425 HV0,3. It can also be noted that at higher *v* the heat affected zone has a smaller size and

a stronger increase of microhardness. Finally, it can be seen that the profiles made at 150 μm from the upper surface of the plates, have markedly higher hardness values, in particular on the lower plate. This confirms the optical microscope observation that points out a greater concentration of martensite in these areas.

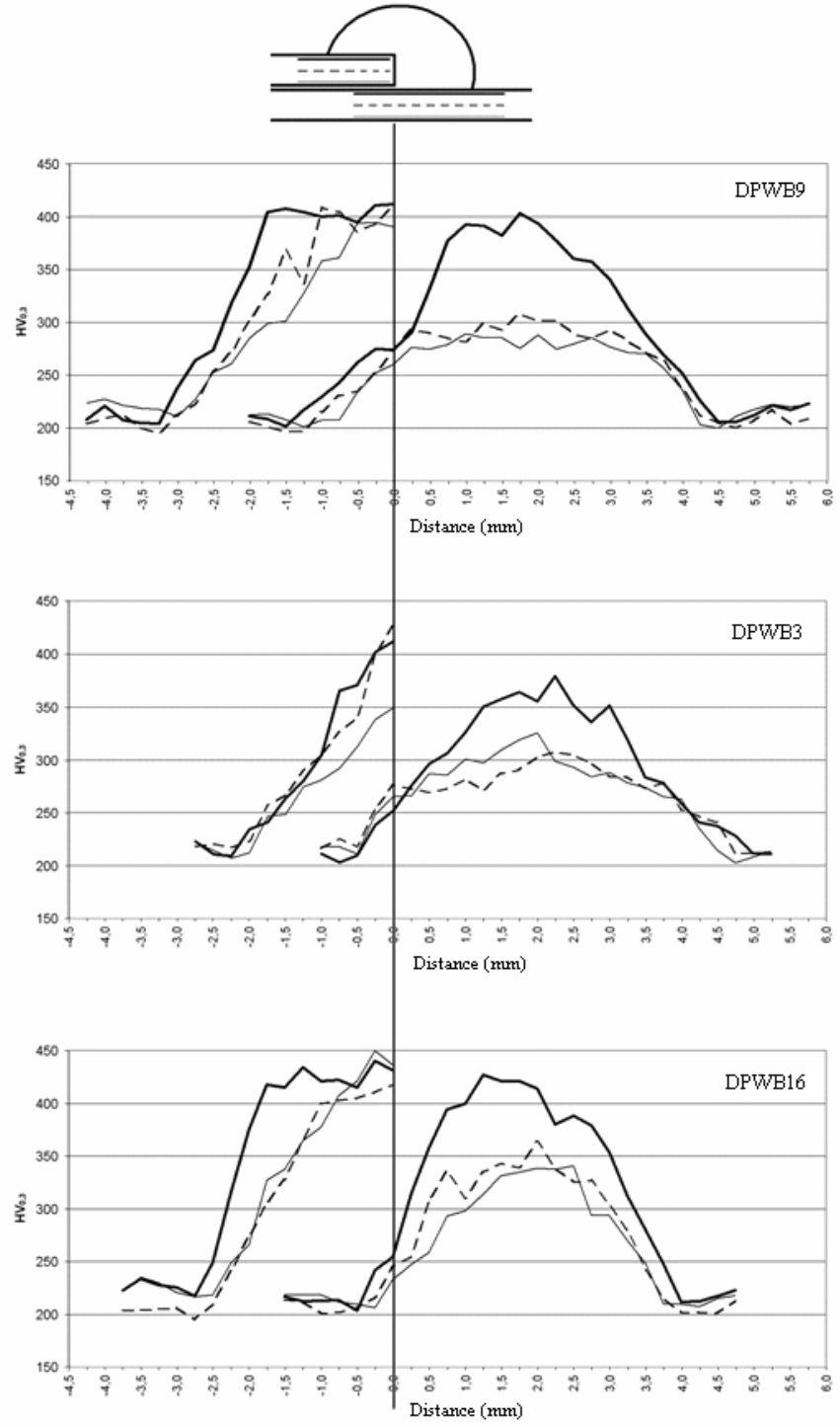

Fig. 5. Vickers microhardness profiles

3.3 Fractographic Study.

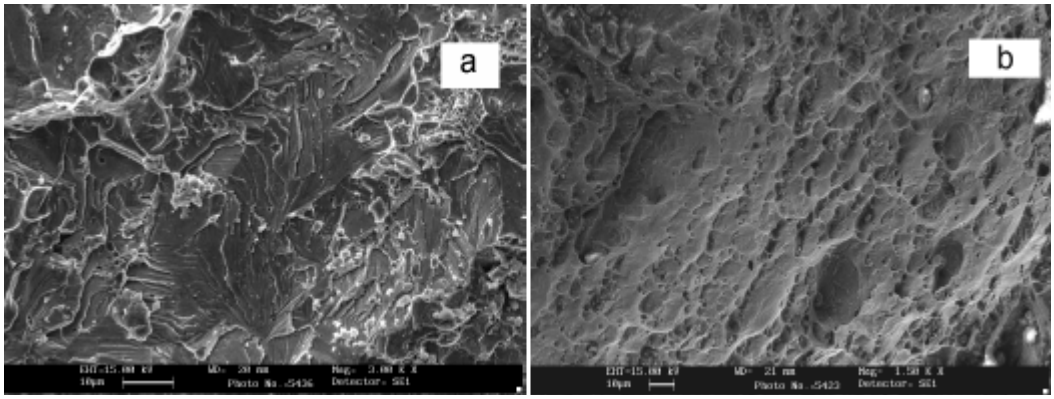

Fig. 6. Brittle fracture in the intermetallic layer (a); ductile fracture in the fusion zone (b).

A fractographic study has been carried out on the samples failed after shear tensile test in order to investigate the effect of the intermetallic layer on the fracture mechanism.
The presence of intermetallic compounds at the plate-filler interface has an embrittlement effect, causing the fracture of the joint. Subsequently, the fracture propagates in a ductile way until failure. Fig. 6a highlights the typical brittle mechanism of fracture, characterized by cleavage planes, in the intermetallic layer area while Fig. 6b refers to the fracture of the fusion zone. In this case the mechanism is ductile, characterized by small dimples.
Considering the brazing design, it comes up that the "L" edge of the upper plate covered by the filler metal increases the stress in the vertical edge of the upper plate.

4. Conclusions

This study reveals that the Heat Affected Zone is relatively small (max. 7 mm). The microstructure of HAZ is constituted by an area with coarse grains, followed by a fine grain area (bainitic and ferritic phases). Approaching the fusion zone, the quantity and size of martensitic grain increase, in the area next to the joint the microstructure is markedly martensitic. The microhardness values confirm the structure observed by the optical microscope, showing higher hardness in the areas with more martensite. At the interface steel plates-Cu filler metal an intermetallic compound layer formed. Along the interface there are zones where the intermetallic layer is uniform, compact with 3 μm thickness and others where the layer is inhomogeneous with a maximum thickness of 40 μm. Little round or elongated intermetallic precipitates formed in the Cu-filler near the interface with steel plates. In all the cases the compounds are ternary Fe-Cu-Si intermetallic phases, whose composition, calculated on the two layers of compact zones, are Fe7,26-Cu0,34-Si and Fe3,48-Cu0,52-Si.

The variation of speed in brazing affects the width of HAZ that decreases at the increasing of the welding rate, but the size and amount of martensite phase found in this area increases. The SEM and microhardness analysis show the effects of the coalescence in the heart of plates, probably due to the difference between the cooling rate on the surface and the inner zone of the plates.

The welding rate also affects the thickness of the inhomogeneous intermetallic zones: these areas are smaller when the process is quicker. Moreover, increasing the welding rate the copper concentration in the intermetallic layer decreases due to the minor diffusion time.

In the samples where the input H is minor, the penetration of molten copper between the plates is reduced, as well as the capillary diffusion of Cu and the formation of intermetallic compounds, these factors adversely affects the mechanical strength of the joint. Moreover, the fractographic study of the samples failed after shear tensile revealed an embrittlement effect of the intermetallic layer.

References

1. T. Senuma, “Physical Metallurgy of Modern High Strenght Steel Sheets”, ISIJ International, Vol. 41 (2001), No. 6, pp. 520-525.

2. D.Palmeri, “Gli acciai dual phase”, Subfornitura News, aprile 2009, pp. 50-51

3. M. M. Schwartz, “Brazing”, ASM International, Metals Park, Ohio 44073 (1987), pp. 4-10.

4. Metals Handbook Ninth Edition, American Society for Metals, Metals Park, Ohio 44073 (1983), Vol.6, pp.55, 154-155.

5. H.T. Zhang, J.C. Feng, P. He, B.B. Zhang, J.M. Chen, L. Wang, “The arc characteristics and metal transfer behaviour of cold metal transfer and its use in joining aluminium to zinc-coated steel”, Materials Science and Engineering A 499 (2009), pp. 111-113.

6. M. M. Schwartz, “Brazing”, ASM International, Metals Park, Ohio 44073 (1987), pp. 413-415

7. H.T. Zhang, J.C. Feng, P. He, “Interfacial phenomena of CMT welding of zinc coated steel wrought aluminium”, Material Science and Technology, Vol. 24 No.11 (2008), pp.1347.

8. Norma italiana UNI EN ISO 6507-1 : 1999, “Prova di durezza Vickers, Metodo di prova”.

9. Norma ISO 14273:2000 (E), ”Specimen dimensions and procedure for shear testing resistance spot, seam and embossed projection welds”.

10. E. Keehan, L. Karlsson, H.O. Andren, H.K.D.H. Bhadeshia, “New developments with C-Mn-Ni High-Strenght Steel Weld Metals, Part A – Microstructure”, Welding Journal, September 2006, pp.200-210.

11. Y. Zhi-shui, L. Rui-feng, Q. Kai, “Growth behaviour of interfacial compounds in galvanized steel joints with CuSi3 filler under arc brazing”, Trans. Nonferrous Met. Soc. China 16(2006) 1391-1396.ù

12. L. Fenggui, L. Bifeng, T. Xinhua, Y. Shun, “Study on influencing factors and joint performance of laser brazing on zinc-coated steel plate”, Int J Adv Manuf Tecnol (2008) 37, pp. 961.